

ALLEGHENY COLLEGE

Faculty Scholarship Collection

The faculty at Allegheny College has made this scholarly article openly available through the Faculty Scholarship Collection (FSC).

HOW TO GET A COPY OF THIS ARTICLE:
Students, faculty, and staff at Allegheny College may obtain a copy of this article at: https://onlinelibrary.wiley.com/doi/full/10.1002/pcr2.10039.

Article Title	Recent progress in block copolymer crystallization
Author(s)	Ryan M. Van Horn, Maxwell R. Steffen, Dana O'Connor
Journal Title	*Polymer Crystallization*
Citation	Van Horn, RM, Steffen, MR, O'Connor, D. Recent progress in block copolymer crystallization. Polymer Crystallization. 2018; 1:e10039. https://doi.org/10.1002/pcr2.10039
Link to article on publisher's website	https://onlinelibrary.wiley.com/doi/full/10.1002/pcr2.10039
Version of article in FSC	Postprint
Link to this article through FSC	https://dspace.allegheny.edu/handle/10456/48419
Date article added to FSC	April 4, 2019
Terms of Use	This is the peer reviewed version of the following article: Van Horn, RM, Steffen, MR, O'Connor, D. Recent progress in block copolymer crystallization. Polymer Crystallization. 2018; 1:e10039. https://doi.org/10.1002/pcr2.10039, which has been published in final form at https://doi.org/10.1002/pcr2.10039. This article may be used for non-commercial purposes in accordance with Wiley Terms and Conditions for Use of Self-Archived Versions."

Information about Allegheny's Open Access Policy is available at http://sites.allegheny.edu/scholarlycommunication/
For additional articles from this collection, visit https://dspace.allegheny.edu/handle/10456/34250

Recent Progress in Block Copolymer Crystallization

Ryan M. Van Horn,[1,2] Maxwell R. Steffen,[1] and Dana O'Connor[1]

[1]Department of Chemistry, Allegheny College, 520 N. Main St., Meadville, PA, USA 16335

[2]Current Address: Chemical and Biomolecular Engineering Department, Lafayette College, 730 High St., Easton, PA, USA 18045

Correspondence to: R.M. Van Horn (E-mail: vanhorrm@lafayette.edu)

ABSTRACT

Block copolymers (BCPs) are important for technological advances in numerous industries, including but not limited to, electronics, biomedical, optics, environmental, and infrastructure. Because of their ubiquity, it is important to understand their hierarchical phase behavior to tune their macroscopic properties for efficient use. These macroscopic properties are derived from the microscopic self-assembled structures. One unique form of hierarchical assembly exists when one or more of the polymeric blocks form lamellar crystals. These crystals are integral to understanding and predicting the macroscopic behavior. This review reports on recent advances in crystallization of BCPs, including bulk and solution assembly. Reports highlighting development in fundamental processes regarding crystallization mechanisms and behavior as well as for the design of practical applications are included.

KEYWORDS block copolymers, phase behavior, self-assembly

AUTHOR BIOGRAPHIES



Ryan M. Van Horn received his Ph.D. in polymer science from the University of Akron in 2009 where he studied solution crystallization of diblock copolymers under the direction of Dr. Stephen Z. D. Cheng. He recently joined Lafayette College as an associate professor of chemical and biomolecular engineering. From 2010-2018, he worked in the department of chemistry at Allegheny College. His research interests are focused on the thermodynamics and crystallization of multicomponent polymer systems.



Maxwell R. Steffen is a senior undergraduate biochemistry major at Allegheny College in Meadville, PA. Max performed undergraduate research in the lab of Dr. Ryan M. Van Horn for 2 years. His work focused on crystallization of PEO-*b*-PCL copolymers and their application in the biomedical field.



Dana O'Connor is a senior undergraduate chemistry major at Allegheny College in Meadville, PA. Dana performed undergraduate research in the lab of Dr. Ryan M. Van Horn for 1.5 years where she studied the melting behavior of PEO-*b*-PCL copolymer films cast from different solvents.

Abbreviations

BCP, block copolymer; gAC, glassy amorphous-crystalline block copolymer; rAC, rubbery amorphous-crystalline block copolymer; CC, crystalline-crystalline block copolymer; T_{ODT}, order-disorder temperature; T_c, crystallization temperature; T_g, glass transition temperature; T_{c1}, crystallization temperature of first crystallizing block; T_{c2}, crystallization temperature of second crystallizing block; M_n, number-average molecular weight; *w*, weight fraction; *k*, 1000 g/mol; CDSA, crystallization-driven self-assembly; PLLA, poly(L-lactic acid); PDLA, poly(D-lactic acid); PE, polyethylene; PP, polypropylene; PEO or PEG, poly(ethylene oxide); PCL, poly(ε-caprolactone); PDMAEMA, poly(2-dimethylaminoethyl methacrylate); P*t*BA, poly(*t*-butyl acrylate); P2EHA, poly(2-ethylhexyl acrylate); DSC, differential scanning calorimetry; PTMC, poly(trimethylene carbonate); *G*, spherulitic growth rate; POM, polarized optical microscopy; PB, poly(butadiene); T_a, annealing temperature; SAXS, small-angle X-ray scattering; *n*, Avrami index; WAXD, wide-angle X-ray diffraction; PA11, polyamide 11; *s*PP, sydiotactic polypropylene; PPL, poly(β-propriolactone); P4VP, poly(4-vinylpyridine); *h*PMB, poly(methyl butylene); *h*PHFAN, poly(hexafluoroisopropanol norbornene); *h*PN, poly(norbornene); *s*PPMS, syndiotactic poly(*p*-methylstyrene); AAO, anodic aluminum oxide; TEM, transmission electron microscopy; PI, polyisoprene; SAED, selected-area electron diffraction; 3Ph, *p*-terphenyl; *a*P3HB, atactic poly(3-hydroxybutyrate); PFS, poly(ferrocenyldimethylsilane); DMF, dimethylformamide; THF, tetrahydrofuran; PAA, poly(acrylic acid); PM, polymethylene; PNIPAM, poly(N-isopropylacrylamide); P4AM, poly(4-acryloyl morpholine); PDMA, poly(*N*,*N*-dimethylacrylamide); P2VP, poly(2-vinyl pyridine); PMVS, poly(methylvinylsiloxane); *it*-PPO, isotactic polypropylene oxide; PVDF, poly(vinylidene fluoride); *f*, volume fraction; PBT, poly(butylene terephthalate); PDMS, poly(dimethylsiloxane); PBC, poly(butylene carbonate); GIWAXS, grazing-incidence wide-angle x-ray scattering; P*n*BA, poly(*n*-butyl acrylate); hc, homochiral; sc, stereocomplex; LC, liquid crystalline; P3HT, poly(3-hexylthiophene); P3EHT, poly(3-(2′-ethyl)hexylthiophene); P3BT, poly(3-butylthiophene); P3DDT, poly(3-dodecylthiophene); PPP, poly(2,5-dihexyloxy-*p*-phenylene); P3HHT, poly(3-(6-hydroxy)hexylthiophene); PT, poly(thiophene); XRD, X-ray diffraction; PMA, poly(methyl acrylate); PHIC, poly(*n*-hexyl isocyanate); ΔH_f, heat of fusion; PMPCS, poly(2,5-bis[4-methoxyphenyl]oxycarbonyl)styrene); *q*PDM/MO, poly(quaternized 2-(dimethylamino)ethyl methacrylate/methyl orange); HRTEM, high resolution TEM; AOT, bis(2-ethylhexyl) sulfosuccinate sodium salt; PFA-C_8, poly(perfluorooctylethyl acrylate); TOBPA, 2-(3′,4′,5′-tris(octyloxy)benzamido)propanoic acid; PMMAzo, poly(6-(4-(4-methoxyphenylazo)-phenoxy)hexyl methacrylate); PGA, poly(glycerol adipate); BBCP, bottlebrush block copolymers; *hb*PG, hyperbranched polyglycerol; POxM poly(oxymethylene); SPBCP, supramolecular pseudoblock copolymer; PDGC, poly(α-D-glucose carbonate); PF, poly(1-*O*-acryloyl-D-fructopyranose); P(F-*co*-BMDO), poly(1-*O*-acryloyl-D-fructopyranose-*co*-(5,6-benzo-2-methylene-1,3-dioxepane); AAL, average arm length; pNdc, poly(*N*-decylglycine); pNte, poly(*N*-2-(2-(2-methoxyethoxy)ethoxy)ethylglycine); pNp, poly(*N*-(*n*-propyl)glycine), pNm, poly(*N*-methylglycine); Th-Try, thymine-2,4-diaminotriazine; UPy-UPy, 2-ureido-

4[1*H*]-pyrimidinone-2-ureido-4[1*H*]-pyrimidinone; PIB, poly(isobutylene); PVL, poly(δ-valerolactone); PEB, poly(ethylene-*co*-butene); PPDL, poly(pentadecalactone); HDPE, high density poly(ethylene); LLDPE, linear low density polyethylene; SEM, scanning electron microscopy; $t_{1/2}$, crystallization half time; DMA, dynamic mechanical analysis; PE/E$_E$, poly(ethylene-*co*-ethylethylene); $\langle n \rangle$, average number of connected triblock copolymers; ε_b, strain at break; PEP, poly(ethylene-*alt*-propylene); DOX, doxorubicin; DLC, drug loading capacity; CHR, chrysin; MCT, medium chain triglyceride; OCM, oil-containing micelles; PMy, polymyrcene; HPMC, hydroxypropyl methylcellulose; PMVL, poly(β-methyl-δ-valerolactone); PFMA, poly(2-perfluorooctyl ethyl methacrylate; ALD, atomic layer deposition; PTcbp, poly{3-[10-(4'-cyanobiphenyloxy)decyl]thiophene}

INTRODUCTION

Block copolymers have become a staple in polymer science since their proposal in the early 1950's by Dunn and Melville[1] and Herman Mark[2] (with a note to Dr. G.F. Tuckett) and proposed controlled synthesis by Szwarc and coworkers[3] in 1956. Over the past 68 years, synthetic techniques have improved the range of viable monomers for copolymerization and the control over molecular weight, molecular weight distribution, and architecture. Because of these advances, BCPs are now one of the most technologically-relevant polymer materials. By utilizing their unique self-assembly behavior, periodic features on the order of nano-to-micrometers are possible.[4] There is still much work to be done in understanding ways to control this phase behavior, including large scale orientation; however, advances are made every year in developing new materials for specific applications in the biomedical or electronics industry and sustainability efforts or in controlling the assembly of more traditional polymers, such as polyolefins or polyesters.

There has been significant literature on the microphase separation of BCPs starting with the fundamental breakthroughs from the seminal works by Leibler[5] and Bates (for example, Ref. 6-9). As available block copolymer materials have proliferated, additional assembly properties, often referred to as hierarchical assembly, have diversified the field. One specific type of hierarchical assembly is crystallization. Crystallization occurs in numerous polymers, though it is not universal based on the chemical structure of the backbone, functional groups, side-chain branching, or copolymer content. In BCPs, crystallization can be used to facilitate phase separation or can occur subsequent to microphase separation from the bulk homogeneous melt. Numerous reviews have been written on the topic of block copolymer crystallization where the role of transition temperature in glassy (relative to crystallization temperature) amorphous-crystalline (gAC), rubbery amorphous-crystalline (rAC), and crystalline-crystalline (CC) block copolymers as well as each permutation of triblock copolymers was discussed in detail.[10-16] A brief overview of the mechanism for crystallization in BCPs is described here.

Crystallization mechanisms in BCPs are driven fundamentally by the relative transition temperatures including T_{ODT}, T_g for the amorphous block(s), and T_c for the crystalline block(s). Table 1 summarizes all possible combinations for crystallization in gAC, rAC, or CC diblock copolymers. In short, the stability of the homogeneous melt (low T_{ODT}), metastability of the amorphous block (high T_g), or metastability of crystals (high T_c) in the crystalline block determine the order of the phase behavior and final morphological features of the material. When crystallization is the driving force for phase separation ($T_c > T_{ODT}$) or crystal growth is kinetically favored over the microphase separated state ($T_c > T_g$), then, the morphology is dominated by polycrystalline lamellar crystals. When the phase-separated state is stabilized by the glassy component ($T_c < T_g < T_{ODT}$), crystallization occurs in the microdomains of the

block copolymer in a restricted fashion – often resulting in non-polycrystalline morphologies - depending on whether the crystalline component is the minority (spheres, cylinders), majority (matrix), or equal (lamellar) volume fraction. In the case where $T_g < T_c < T_{ODT}$ but there is very strong segregation between the blocks, crystallization will occur in the phase-separated state. In CC diblock copolymers, the relative T_cs determine the crystallization order, and their relation to T_{ODT} determines whether crystallization occurs from the homogeneous melt or in the phase-separated domains. If the crystallization temperatures are largely different ($T_{c1} > T_{c2}$), then crystallization occurs in a sequential manner as the system is cooled. Depending on the operating temperature, the second block could remain amorphous. If the crystallization temperatures are similar ($T_{c1} \approx T_{c2}$), then coincident, or nearly simultaneous, crystallization occurs. Here, T_c represents the actual measured crystallization temperature for each block, where molecular weight (M_n) and weight fraction (w) of the blocks has been taken into account. For this review, values for M_n will be abbreviated using the "k-convention" to represent 1,000 g/mol, i.e. 2,000 g/mol = 2k.

More recently, crystallization in BCPs has been described as the primary self-assembly process for bulk materials[16] as well as in solution.[16-18] When crystallization is the driving force for separation, the morphological features are reflective of the crystallization process. In the bulk, lamellar morphologies of alternating crystalline-amorphous (AC copolymers) or crystalline-crystalline (CC copolymers) structures are formed irrespective of the crystalline block's volume fraction. In solution, crystallization-driven self-assembly (CDSA) occurs following one of two possible mechanisms. One is the formation of single-layer (or multi-layer due to screw dislocations in the crystal growth) single crystals that exhibit polygonal morphologies reflective of the crystalline block's unit cell. These crystals have high crystallinity, close to 98%, with regular fold surfaces. The other is the formation of micelle-like morphologies (spheres, cylinders, bilayers) that contain a crystallized core. In both instances, the non-crystalline block is relegated to the crystal surface forming a corona-like shell around the crystalline block. For single crystals, the crystal growth surfaces due not contain non-crystalline block chains; however, the material on the basal surface of the crystal can bend or stretch over the growth edge to shield the growth surface.[18] In micelle-like crystals, the outer layer may resemble more closely the corona of a micelle where the entire surface is covered with non-crystalline chains, which typically means the crystallinity and metastability of the core is poorer than the single crystal counterparts.[17] For traditional micelle morphologies, the formation mechanism can occur through CDSA or through typical solvophobic interactions followed by crystallization in the non- or weakly-solvated core.

Whether block copolymer crystallization occurs from the miscible bulk, through CDSA in solution, or within microdomains, these systems provide novel structures to study fundamental behavior, such as nucleation and growth,[12-13] thermodynamic stability,[14-15] growth kinetics,[10,12-13] crystallization in confinement,[20-22] etc., where there still are many unanswered questions in the area of polymer crystallization.[23] These include nucleation and growth mechanisms and the role of junction or tethering points in these processes, thermodynamics (energetics) of crystal size, domain size, and non-crystallized block chain structure, finding universal parameters to predict crystallization behavior by deconvoluting BCP composition (mass or volume fraction), local environment (concentration, confinement, etc), and chain dynamic effects, and controlled assembly and disassembly of BCPs or crystallized BCPs in multi-component systems. The use of block copolymers provides an opportunity to design unique systems to help probe the questions still remaining. Additionally, the rational design of crystalline block copolymer materials has significant technological implications. As such, many polymer scientists have focused their research efforts in this field.

Since there are numerous reviews regarding block copolymer assembly and crystallization therein, this review aims to highlight recent progress in this area over the last five years.[10-21] There is still a large volume of work because of the utility of block copolymers and the advantages of materials that assemble with crystalline moieties. The review is organized as follows. The first section describes current literature in diblock copolymers with one or two crystallizable blocks of more traditional materials (polyolefins, polyesters, etc.), focusing on bulk behavior as well as solution behavior. The second section has a similar organization but for triblock copolymers and a brief discussion of multiblock copolymers. Third, stereocomplex crystallization of PLLA/PDLA in BCPs will be given its own section due to the robustness and volume of work in this field. Fourth, block copolymer systems with unique chemical features, such as (a) rod-coil or rod-rod chain structures, (b) branched systems, including graft and hyper-branched, and (c) components with novel chemical structures for either one of the blocks or with supramolecular junctions. Finally, some literature highlighting the applicability of these materials will be discussed.

TABLE 1 Crystallization in Diblock Copolymers According to Relative Transition Temperatures

Type of Copolymer	Relative Transition Temperatures	Segregation Strength (Immiscible)	Crystallization Mechanism
Amorphous – Crystalline	$T_{ODT} > T_g > T_C$	Weak or Strong	Crystallization in microphase-separated domains (hard confinement), possibility of breakout crystallization when segregation strength is weak
	$T_{ODT} > T_c > T_g$	Weak	Breakout crystallization, destroys microphase-separated structure, alternating lamellar crystal and amorphous layers
		Strong	Crystallization in microphase-separated domains (soft confinement), possibility of breakout crystallization depending on segregation strength
	$T_c > T_{ODT} > T_g$	Miscible melt	Crystallization from homogeneous melt, alternating lamellar crystal and amorphous layers
Crystalline-Crystalline	$T_{ODT} > T_{c1} > T_{c2}$[a]	Weak or Strong	Sequential crystallization in microphase-separated domains, possible to have non-crystallized Block B depending on final temperature (similar to hard confinement)
	$T_{ODT} > T_{c1} \approx T_{C2}$	Weak or Strong	Coincident crystallization in microphase-separated domains (similar to soft confinement)
	$T_{c1} > T_{c2} > T_{ODT}$	Miscible melt	Sequential crystallization from homogeneous melt, alternating lamellar crystals of each block, similar to hard confinement of $T_g > T_c$, possible to have non-crystallized Block B depending on final temperature
	$T_{c1} \approx T_{c2} > T_{ODT}$	Miscible melt	Coincident crystallization from homogeneous melt, alternating lamellar crystals of each block

[a] T_{c1} – experimental crystallization temperature of block A, T_{c2} – experimental crystallization temperature of block B

CONVENTIONAL CRYSTALLIZABLE DIBLOCK COPOLYMERS

Systems containing more traditional crystallizable blocks, such as polyethylene (PE), poly(propylene) (PP), poly(ethylene oxide) (PEO or PEG), poly(ε-caprolactone) (PCL), and both enantiomers of poly(lactic acid) (PLLA and PDLA) are still prevalent in the literature. BCPs with amorphous second blocks or those where two crystallizable blocks are incorporated have presented interesting challenges in understanding crystallization behavior. These include confinement and anchoring effects on nucleation and crystal orientation, thermodynamic stability of crystals with amorphous (stretched) tethers, and kinetics of the growth mechanism. Solution assembly and crystallization provides another route to evaluating these properties while demonstrating a niche for individual particles with narrow polydispersity and tunable structure.

Bulk Crystallization Behavior

Even with the volumes of research regarding BCPs with crystalline components, there is still much work to be done to fully understand the fundamental thermodynamics and kinetics of these systems. As new chemistries are developed, as well as new analytical techniques, stronger foundations in BCP crystallization are needed to evaluate and predict structure-property relationships. This initial section covers some of the primary work in BCP phase behavior and accompanying crystallization analysis including, but not limited to, rAC ($T_g < T_c$) or gAC ($T_g > T_c$) copolymers,[24-42] CC copolymers,[43-60] thin films,[25,27-28,46,48,56] confined crystallization,[30-41,56-58] and new chain architectures.[43,59-60] With this diversity of topics in mind, research in BCP crystallization and other areas of polymer crystallization are still thriving over 60 years later.

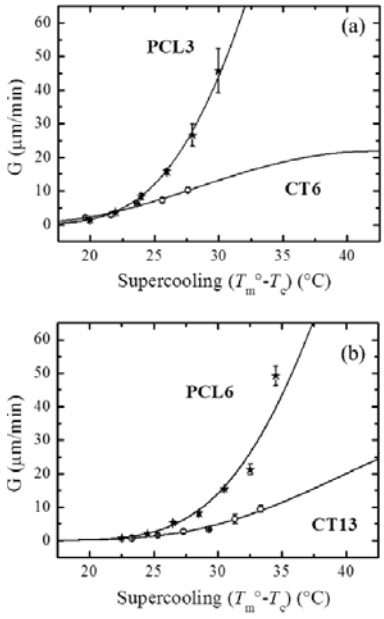

FIGURE 1 Spherulitic growth rates of homopolymer PCL (PCL3 and PCL6) compared to PTMC-*b*-PCL (CT6 and CT13) grouped by comparable M_n^{PCL}, (a) PCL3 and CT6 and (b) PCL6 and CT13 (b). Solid lines are fits to Lauritzen-Hoffman theory. (Reproduced from [29] with permission from Elsevier.)

As mentioned, research in the area of AC diblock copolymers is prolific; therefore, combinations used recently to study fundamental crystallization in confinement[27,30-41] or with unique architectures[42] are discussed separately. The few remaining works, where thermal properties are studied primarily, are discussed here. Acrylate-based copolymers were studied with PLLA crystalline blocks.[24-25,28] Boissé *et al.*[25] studied BCPs of poly(2-dimethylaminoethyl methacrylate) (PDMAEMA) and PLLA. The $T_g^{PDMAEMA}$ was near room temperature; therefore, these were rAC-type copolymers. The samples were miscible to partially miscible depending on molecular weight.[24-25] PDMAEMA retarded the PLLA local and overall crystallization rate. This effect increased with $M_n^{PDMAEMA}$. Other acrylate-based copolymers, such as glassy PMMA (dependent on weight fraction of PLLA, w_{PLLA}), rubbery poly(*t*-butyl acrylate) (P*t*BA), and rubbery poly(2-ethylhexyl acrylate) (P2EHA), showed similar results based on differential scanning calorimetry (DSC) analysis with crystallization being completely suppressed due to w_{PLLA} or glassy amorphous blocks in some samples.[28] A PCL-*b*-poly(trimethylene carbonate) (PTMC-*b*-PCL) material was compared to homopolymer PCL to elucidate the effect of PTMC on PCL crystallization.[29] It was determined that these blocks were weakly-segregated and above T_g^{PTMC}; therefore, PCL breakout crystallization was observed. PTMC did act as a diluent to decrease T_c^{PCL} slightly compared to the homopolymer. The spherulitic growth rate (G) measured with polarized optical microscopy (POM) was slowed as well due to the presence of PTMC as shown in Figure 1. It should be noted that the observed crystallization behavior was somewhat dependent on w_{PCL}. The authors also evaluated the role of chain architecture (diblock, ABA triblock, and BAB triblock) on PCL crystallization. It was found that the BAB architecture decreased the T_m^{PCL} and spherulitic growth rate due to the restriction of PCL middle-block chains. For AB and ABA, differences in nucleation reduced the kinetics of crystallization.

One unique study focused on the annealing of PEO crystals in poly(butadiene)-*b*-PEO (PB-b-PEO). Hölzer *et al.*[26] studied the thermodynamic behavior of both the microphase-separated domains and PEO crystal thickening during annealing at different temperatures (T_a) following the self-nucleation method.[61-62] Since the PB block provides soft confinement, the PEO chains were mobile enough to demonstrate crystal thickening along the *c*-axis. It was found that there were three distinct annealing regimes based on DSC and small-angle x-ray scattering (SAXS) analysis. In the first regime, at 42ºC < T_a < 46ºC, PEO crystals thickened via defect healing whereby PEO crystal stems lengthened and decreased the number of folds. Between 46ºC and 50ºC, similar long periods (PEO + PB) were found for all T_a; however, a second melting endotherm was observed in DSC. These observations combined indicated that thermal fractionation occurred in the PEO domain and that two different crystal thicknesses were formed. For both ranges, the long period increased with longer annealing time, demonstrating the mobility of the PB phase to accommodate PEO thickening. Finally, above T_a = 52ºC, sufficient melting of the original crystals was found. This study confirmed that control of crystal thickness in a diblock copolymer was dependent upon the BCP composition and annealing conditions.

For CC copolymers, the relative sequence of crystallization is important as the crystallization of the first block (Block 1) is influenced by the composition, while the second block (Block 2) is further restricted by the marked immobility of Block 1 in its crystal (similar to a glassy block) and possible confinement due to the lamellar spacing of Block 1 (Table 1).[10-16] In contrast, it also has been observed that the Block 1 crystallization may act as a nucleating agent (stretching or stiffening of Block 2 chains) for the second crystallization. The effects are more complicated when coincident crystallization ($T_{c1} \approx T_{c2}$) dominates.

Monte Carlo simulations of relatively short-chain diblock copolymers by Kundu and Dasmahapatra[43-44] showed that the segregation strength determined the crystallinity of Block 2. Stronger

segregation resulted in greater Block 2 chain stretching and a reduction in the development of crystal growth. For two-step cooling, sequential crystallization occurred (Block 1 crystals only at T_1) with Block 1 crystallinity being larger than Block 2's and increasing from T_1 to T_2. When sufficient cooling was used to induce coincident crystallization (one-step quenching), Block 1's crystallinity was decreased compared to two-step, while Block 2's remained constant for both methods. The decrease in Block 1 crystallinity indicated that the simultaneous crystallization of Block 2 limited the ability of Block 1 to grow. This holds for symmetric[43] and asymmetric[44] systems. There were some limitations in the model since it only applies to strongly-segregated experimental systems without breakout crystallization (Avrami index, $n \leq 1$). Miscible PEO-*b*-PLLA copolymers are good experimental examples of these systems ($T_c^{PLLA} > T_c^{PEO}$).[45-48] Generally, PEO crystallinity (M_n^{PEO} = 2k or 5k) was diminished in BCP samples. For moderate w_{PEO}, PEO exhibited fractionated crystallization (interlamellar and interfibrillar regions of PLLA) depending on isothermal crystallization temperature of PLLA.[45,47] Additionally, PEO crystallization was shown to influence the crystal form of PLLA.[45] For isothermal T_c^{PLLA}, both α′- and α-form crystals appear, as determined by Fourier transform infrared spectroscopy (FTIR) shown in Figure 2. In FTIR, bands at 1776, 1759, and 1749 cm^{-1} indicate α-form crystals, whereas one wide band at 1759 cm^{-1} indicates α′-form crystals. Bands at 1210 and 1135 cm^{-1} are correlated with the chain conformations, where the α-form is more ordered than the α′-form (increase in absorbance for α-form crystals). After cooling and subsequent PEO crystallization, all crystals transformed to α-form (also confirmed by wide-angle x-ray diffraction, WAXD). Thermal properties and crystallinity of other BCPs with different T_cs, namely polyamide 11-*b*-PLLA (PA11-*b*-PLLA) and PA11-*b*-PDLA[49] and PCL-*b*-PLLA,[50-51] were monitored using similar techniques. Morphological studies of a series of PCL-*b*-PLLA copolymers showed that banded and non-banded spherulites were formed depending on T_c^{PLLA}, w_{PLLA}, G, and lamellar thickness.[51] Only w_{PLLA} = 0.75 exhibited banded spherulites. At high T_c^{PLLA}, G decreases and lamellar thickness increases, making lamellar twist difficult. This results in a banded-to-non-banded transition around 125°C.

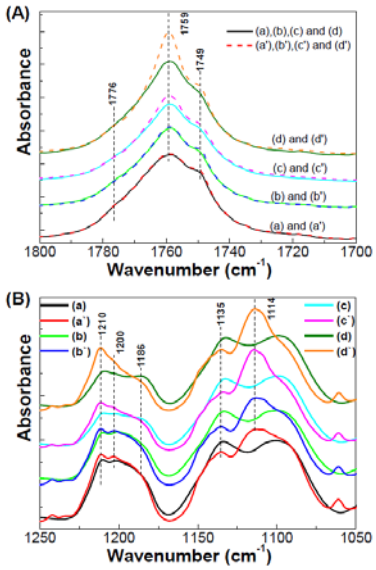

FIGURE 2 FTIR spectra of PEO-*b*-PLLA in the (A) 1700 cm^{-1} range (C=O of PLLA) and (B) 1100 – 1250 cm^{-1} range (C-CO-O and CH_3) before (a-d) and after (a′-d′) PEO crystallization. T_c^{PLLA} = 70°C (a), 90°C (b), 100°C (c), and 110°C (d). Spectra have been shifted for clarity. (Reproduced from [46] with permission from Elsevier.)

There have been a couple examples of work done in the past five years on CC copolymers with similar T_cs as well. De Rosa *et al*.[56] synthesized highly-controlled, moderate molecular weight syndiotactic PP-*b*-PE (*s*PP-*b*-PE) copolymers with w_{PE} = 0.27 and 0.49. *Via* DSC, broad, overlapping thermal transitions were observed, indicating coincident crystallization for these samples in the bulk. WAXD data showed that PE crystallized first at $T \approx 130^oC$. Homopolymer *s*PP crystallizes at 144ºC. The T_c^{sPP} for the BCP was decreased to such a degree that coincident crystallization occurred even with high *s*PP content. This is one of few examples where the expected behavior of $T_{c1} > T_{c2}$ is changed to $T_{c1} \approx T_{c2}$ due to the BCP architecture. On the other hand, PEO-*b*-PCL is the most common example of BCP coincident crystallization with a large collection of research literature.[15-16] The two studies presented here have expanded the scope to include the influence of solvent quality in film formation[52] and additives for ionic conductivity.[53] Brigham and coworkers[52] manipulated the crystallization sequence of symmetric PEO-*b*-PCL copolymer films ($M_n^{overall}$ = 20.3k, w_{PEO} = 0.49) using different casting solvents. Typically, PCL crystallizes first from the melt and chloroform, the most common solvent for preparation. Based on the relative solubility parameters, FTIR analysis showed that PEO crystallized first in the as-cast film from toluene and ethyl acetate solution. Subsequent melt-recrystallization showed that PCL was first once solvent effects were removed. Typically, PEO-*b*-PCL forms a homogeneous melt. Huang *et al*.[53] demonstrated that microphase separation could be induced through the incorporation of inorganic salt. Different chloride salts were added to PEO-*b*-PCL with a w_{PEO} = 0.23, and the salt preferentially interacted with PEO as determined by FTIR. At high salt loading, lamellar microphase separation was observed using SAXS with $T_{ODT} > T_c$. Subsequent cooling led to crystallization of each block. Crystallinity of PEO was greatly decreased due to the selective interaction with the salt. PCL crystallinity also decreased, and it was proposed that at high salt loading, the salt began associating with PCL. It was unclear whether the microphase separation itself had any impact on the crystallization of each block. Another BCP where the blocks have similar T_cs is poly(β-propriolactone) (PPL) and PE (PPL-*b*-PE), which is strongly segregated in the melt.[54-55] To obtain similar T_cs, the PE block had 18 mol% ethyl branches to reduce its T_c to one closer to T_c^{PPL}. However, coincident crystallization was achieved only when PPL crystallized in the δ-form. For β-form crystals, long induction times and even sequential crystallization was measured by FTIR and WAXD. The PPL structure was controlled by casting from chloroform (δ-form) or annealing the film at 130ºC (δ-form to β-form). Samples were melted and crystallized at an isothermal T_c = 62ºC. When coincident crystallization occurs, the lamellar microphase-separated morphology becomes distorted. For sequential crystallization, minimal changes in the lamellar morphology were detected. In addition, it was found that the PE crystallinity, controlled by ethyl branch content, played a role in the morphology for the β-form sequential crystallization.[55] At high crystallinity, PE breakout crystallization was observed due to the soft confinement of PPL. At moderate crystallinity, the lamellar phase was maintained. When PE did not crystallize (ethyl branching of 31%), breakout crystallization occurred when PPL crystallized during cooling. These variabilities in crystallization order, block sequence and coincident versus sequential, are important for future work in controlling the hierarchical structure of CC BCPs.

Confined crystallization is one of the more commonly studied crystallization phenomena due to the importance of domain size on crystallization properties. In this section, the term confined crystallization is specific to the research approach. When T_c and crystallinity decrease in BCPs, confined crystallization is typically presented as the reasoning, though the size of the confinement is not always known. As presented here, controlled confinement is applied to both the domain for the crystallizable block and the material as a whole. Nucleation and kinetics of PCL blocks (M_n = 11.6k) confined in the

lamellar domains of poly(4-vinylpyridine)-*b*-PCL (P4VP-*b*-PCL) were monitored using ultrafast DSC, which is advantageous for separating nucleation and growth events.[30] The analysis showed that in addition to inhibition of crystal growth, nucleation was inhibited in the BCP, where the critical nucleation size was similar to the PCL domain thickness. The Nojima group has done a thorough systematic study of various factors, such as microphase-separated morphology,[31-33] tethering considerations,[32,34,36] domain size,[31-33,35] and end-group size,[37] on the confined crystallization of PCL using PS-*b*-PCL diblock and triblock copolymers. Each parameter influenced the T_m^{PCL} (related to crystal thickness), crystallinity, and crystallization kinetics. Table 2 summarizes the influence of each parameter on the PCL confined crystallization. PDLLA-*b*-PE with a strongly-segregated lamellar microstructure was monitored using simultaneous SAXS/WAXD to understand the development of PE crystal orientation.[40] During initial crystallization, the PE *c*-axis was oriented perpendicular to the interface normal direction and remained over long isothermal crystallization times when the isothermal T_c was low (fast crystallization rate). At higher T_c (slower crystallization rate), the orientation was random at early times. The preferred orientation developed as crystallinity increased. The authors propose that this orientation is kinetically-driven and helps to maximize crystallinity. Similar results were found with PE-*b*-PLLA for PLLA crystallization with amorphous PE fraction; however, PLLA crystals were oriented with the *c*-axis parallel to the interface normal.[40] The developed orientation is related to the nucleation density as well, and therefore, it has a slight isothermal T_c dependence.[20-22]

TABLE 2 Summary of PS-*b*-PCL Confined Crystallization Studies[31-37]

Controlled Parameter	T_m^{PCL}	PCL Crystallinity	Crystallization Rate
Morphology[a]			
Lamellar	No effect	Decrease	*difficult to compare because of large decrease in T_c
Cylindrical	Decrease	Decrease	
BCP Micprophase Domain Size			
Lamellar	Large Decrease	Decrease	Decrease
Cylindrical	Decrease	No effect	Decrease
Tethering Number[b]			
One end	Decrease	Small decrease	Decrease
Two ends	Large decrease	Large decrease	Large Decrease
Free End-Group Size Increase	Small decrease	Small increase	Small increase

[a] compared to unconfined homopolymer PCL (PCL in cylindrical phase)

[b] relative to photocleaved junction points to create untethered homopolymer PCL

In the previous systems, the confining block was glassy. Soft confinement was studied for a poly(methyl butylene)-*b*-*h*PE (*h*PMB-*b*-*h*PE) made by hydrogenation of poly(high-3,4-isoprene)-*b*-poly(high-1,2-butadiene)[38] and hydrogenated poly(hexafluoroisopropanol norbornene)-*b*-poly(norbornene) (*h*PHFAN-*b*-*h*PN).[39] When the blocks are strongly-segregated, breakout crystallization did not occur at low crystallinity (Table 1) and provided an opportunity to compare rAC and gAC confinement within the microphase structure. Atomic force microscopy (AFM) was used to follow the development of *h*PE crystals in *h*PMB-*b*-*h*PE in as-cast (melt cast) and AFM-tip-aligned cylindrical phase films. At low T_c, crystals were confined in the *h*PE cylinders, while at high T_c, breakout crystallization was observed. Figure 3 shows an AFM image demonstrating the two crystallization directions (Figure 3h) and the crystal growth rate parallel (along the cylinder) or perpendicular (breakout) as a function of T_c (Figures 3a

and 3b). The crossover temperature range (templated crystallization) between these two mechanisms was much higher for the aligned films compared to the as-cast. *h*PN crystallized within the lamellar microphase-separated morphology under soft confinement of the *h*PHFAN. Interestingly, the long period increased during crystallization, even with an increase in *h*PN crystalline density, because of the energetic cost of creating the fold surface from the amorphous *h*PN near the interface. Additionally, the crystal stems tilt with respect to the interface normal direction resulting in lateral contraction when the long period increases.

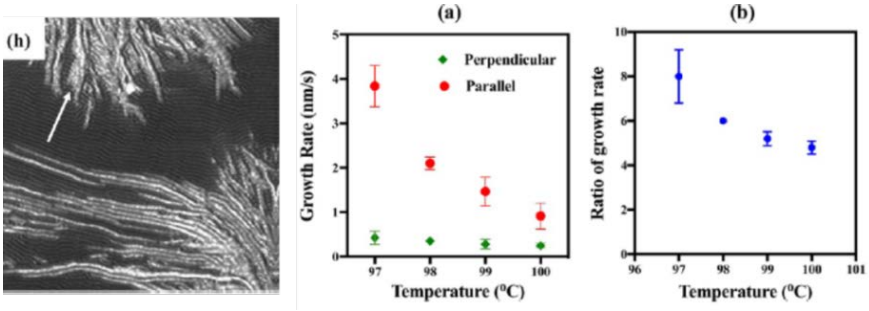

FIGURE 3 (h) *In-situ* AFM phase image of *h*PE crystallization in *h*PMB-*b*-*h*PE at T_c = 101°C, showing crystallization along (lower portion) and across (top portion) the *h*PE cylindrical domains. (a) Relationship between crystalline growth rate and isothermal T_c for different growth directions relative to the cylindrical axis. (b) The ratio of the two growth rates from (a). (Reproduced from [39] with permission from the American Chemical Society.)

In CC block copolymers, the interplay of the two crystallization processes presents a new set of confinement effects. For one unique sample, syndiotactic poly(*p*-methylstyrene)-*b*-PLLA (*s*PPMS-*b*-PLLA), each possible combination was accessible, as described in the schematic in Figure 4.[57] Such diverse control over interactive confinement was due to the low chain mobility for both blocks. Cooling rate was used to access each of the different highlighted regions. Two samples were studied, one with a PLLA cylinder morphology and one with a lamellar morphology. For the cylinder morphology, no PLLA crystallization (M_n^{PLLA} = 4.9k) was detected due to confinement in the cylinders. The microphase-separated structure became distorted after *s*PPMS crystallization due to the soft PLLA phase at $T_c^{sPPMS} > T_g^{PLLA}$. The lamellar *s*PPMS-*b*-PLLA sample (M_n^{PLLA} = 9.8k) contained double crystalline components. This was used to probe crystallization in each of the highlighted areas of Figure 4. Coincident crystallization was not achieved by direct cooling due to limited *s*PPMS chain mobility, but was possible using a self-seeding technique where *s*PPMS nuclei promoted crystallization to occur in a temperature window where PLLA crystallization occurred. Phase-separated morphologies varied depending on thermal treatment. Isothermal crystallization of sPPMS was performed first with subsequent quenching for PLLA crystallization using the following temperature profiles: (a) T_c^{sPPMS} = 160°C → T_c^{PLLA} = 100°C, (b) T_c^{sPPMS} = 150°C → T_c^{PLLA} = 100°C, and (c) T_c^{sPPMS} = 140°C → T_c^{PLLA} = 100°C. SAXS data showed that Profile (a) resulted in breakout crystallization; Profile (b) resulted in mono-sized lamellae for both blocks; and Profile (c) resulted in dual-sized lamellae. When the crystallization order was reversed, T_c^{PLLA} = 100°C → T_c^{sPPMS} = 140°C, mono-sized lamellae were found. It appeared that the structure was determined by the crystallization of the first block and its role in confinement for all cases. This unique BCP was shown to provide an opportunity to study the fundamental processes in interactive crystallization given a wide set of crystallization conditions.

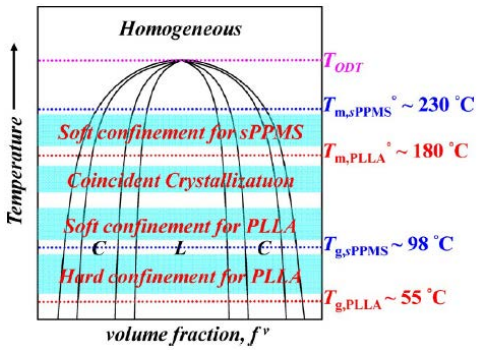

FIGURE 4 Interactive confinement in *s*PPMS-*b*-PLLA based on various thermal properties. (Reproduced from [57] with permission from the American Chemical Society.)

Confinement of the BCP material influences both the microphase separation behavior and the crystallization. Using a common confinement environment, anodic aluminum oxide (AAO) was used to template BCP confinement in both PS-*b*-PE[41] and PEO-*b*-PCL.[60] For gAC PS-*b*-PE, T_c^{PE} was depressed for all confined samples; however, an extraordinary decrease was measured for w_{PE} = 0.26. In this sample, the microphase-separated morphology was formed where PE was in contact with the AAO wall with embedded PS spheres similar to the core-shell morphology. In this case, PE was confined by both the AAO and glassy PS, resulting in much lower T_c^{PE}. For CC PEO-*b*-PCL, an asymmetric M_n^{PEO} = 5k and M_n^{PCL} =10k (w_{PEO} = 0.33) was infiltrated into AAO. WAXD and DSC showed only PCL crystallization within the pores at much lower T_c compared to the bulk. The nucleation process was shown to be primarily homogeneous. PEO displayed no crystallinity after infiltration because it was Block 2 in the crystallization sequence. PCL crystals developed first in the confined space resulting in additional confinement of PEO to the point of complete suppression of PEO nucleation.

Thin and ultrathin films are another form of confinement for the material, but differ in that there is a free surface to allow for changes in volume by dewetting and crystal thickening. For crystallizing polymers, this type of confinement typically influences the morphology and growth mechanism most.[63] AFM and transmission electron microscopy (TEM) images were used to monitor the morphology of BCP thin films (film thickness less than 100 nm) under different crystallization conditions. For systems that showed single crystal type crystallization in the thin film,[25,27,47,49] BCP crystal morphologies were distorted single-crystalline or dendritic in nature. This showed that for specific isothermal T_cs, the typical kinetically-controlled single crystal growth transitioned toward diffusion-limited fractal growth due the amorphous block "impurities." Selective interaction of one block with the substrate, i.e. PEO and mica in poly(isoprene)-*b*-PEO (PI-*b*-PEO),[27] or the free surface, PLLA in PEO-*b*-PLLA,[47] led to changes in the BCP assembly and crystallization. For a CC PEO-*b*-PLLA system,[49] two-step crystallization was achieved. Single crystals resembling the lozenge shape of PLLA were formed first. Following cooling to room temperature, the crystal thickness increased due to PEO crystallization on the basal surfaces of the formed PLLA crystal. De Rosa *et al*.[56] observed the influence of a nucleating agent, *p*-terphenyl, on thin films of *s*PP-*b*-PE. Two important observations were made *via* TEM and selected area electron diffraction (SAED). First, epitaxial growth on the surface of *p*-terphenyl (3Ph) was found for both blocks with preferred, but not exclusive, nucleation for *s*PP. Since coincident crystallization was possible, there was a small probability of finding sections where PE crystallized first. Crystallization of the second block in each case occurred between the lamellae of the first to crystallize on the 3Ph surface. Second, the

epitaxial nucleation resulted in a preferred orientation for the *s*PP and PE crystals, edge-on crystals with the *c*-axis perpendicular to the 3Ph surface normal. *s*PP crystals' *b*-axes were parallel to the 3Ph *b*-axis. A schematic of the orientation is shown in Figure 5. PE exhibited a cross-hatched-type morphology with the c-axis oriented parallel with the (110) and (1$\bar{1}$0) of 3Ph. The orientation preference was two-fold, one related to epitaxial growth on the nucleating agent and one due to epitaxial growth in the interlamellar region. Figure 5 also shows the preferred orientation and stem tilt based on the interactive crystallization.

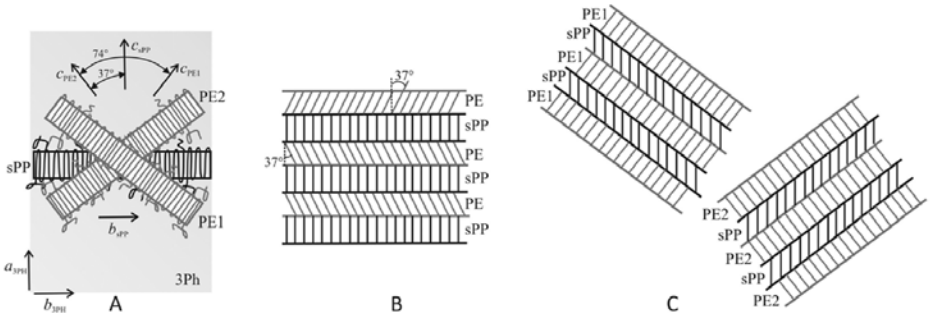

FIGURE 5 (A) Schematic orientation of *s*PP and PE crystals on the surface of *p*-terphenyl (3Ph). (B) Relative orientation of crystal lamellae and crystal stems when *s*PP crystallized first and (C) when PE crystallized first. (Reproduced from [56] with permission from the American Chemical Society.)

While most research regarding architectural differences is discussed in the following sections, crystallization in an rAC star BCP, a CC star BCP, and a cyclic CC BCP are briefly described here. 6-arm atactic poly(3-hydroxybutyrate)-*b*-PLLA (*a*P3HB-*b*-PLLA), where *a*P3HB was amorphous and the blocks were miscible, was compared to 6-arm PLLA.[42] The *a*P3HB's presence decreased T_m^{PLLA} and the crystallinity while also distorting the PLLA spherulites. 2-arm (triblock) and 4-arm star PEO-*b*-PLLA, where PEO was the interior block, showed two trends with increased number of arms.[60] First, T_m^{PLLA} and crystallinity decreased with an increase in the number of arms. This was also true for PEO crystallization. Secondly, no PEO crystallization was observed for $w_{PEO} = 0.15$, $w_{PEO}^{2\text{-arm}} = 0.20$, and $w_{PEO}^{4\text{-arm}} = 0.28$, indicating that architecture had a confining effect on PEO nucleation. Linear and cyclic PCL-*b*-PLLA and PCL-*b*-PDLA with $M_n^{overall} \approx 9$k and $w_{PCL} \approx 0.50$ were synthesized by Liénard and coworkers.[61] The cyclic counterparts exhibited different crystallization behavior. Interestingly, PCL did not crystallize in the cyclic compounds; whereas, PLLA did not crystallize in the linear ones using DSC cooling rates of 20°C/min. PLLA did crystallize in both systems at $T_c = 100$°C, where the PLLA spherulitic morphology was observed using POM. The cyclic compounds had a higher nucleation density than the linear due to the smaller chain coil size through connected end-groups thus making the PLLA chains closer in proximity. Both linear and cyclic copolymers possessed distorted spherulites due to the PCL block.

Bulk and film crystallization of these conventional crystalline copolymers exhibited many of the same behaviors as previous studies, as to be expected. However, the library of possible diblock copolymers is growing, and understanding of fundamental aspects of nucleation and growth for BCPs is improving thanks to continued work in this area.

Solution Crystallization Behavior

Solution self-assembly of BCPs allows for a wide range of particulate nanostructures to form.[16-18] These structures impact a variety of applications ranging from composite reinforcement to drug delivery.

Solution assembly and crystallization falls into three categories based on solvent interactions and temperature: kinetically-controlled crystallization to form single crystals, diffusion-controlled crystalline core micelle formation, and thermally-controlled micelle formation above T_m with subsequent crystallization upon drying/cooling.[17] Crystallization in this third category has been shown to lead to morphological changes in the micelles. Because of the inherent difference in solvent interactions with each block, all BCPs are amphiphilic to some degree. This amphiphilicity is critical to the crystallization mechanism as the more solvophilic block promotes dissolution, while the more solvophobic block promotes assembly/crystallization/precipitation. The same crystallizable polymers from the bulk crystallization discussion are prevalent in solution crystallization. One prominent crystallizable polymer in this field is poly(ferrocenyldimethylsilane) (PFS).[64] While it is not a traditional semi-crystalline block copolymer, its prevalence in this area warrants inclusion with other, more common crystalline polymers. Refs.18 and 64 are quite current and comprehensive; therefore, we will only include a few articles published since or most recently as representative examples of solution crystallization.

Solution crystallization, the method of crystallizing polymer samples out of a homogeneous dilute solution, is an efficient way to understand fundamental aspects of polymer crystals. Using this technique, polymer crystals are easily formed when the solvent quality for the crystalline block decreases. Self-seeding is the most common technique for achieving a high population of single crystals.[65] Polymer single crystals are nearly 100% crystalline and provide individual lamellae that make identifying structural, mechanistic, and thermodynamic aspects of crystallization more accessible.[66] Polymer single crystal research has continued to be a vibrant field studying fundamental aspects of polymer crystallization. With the development of BCPs, the field has diversified even more from fundamental polymer physics to applications of functional crystal particles. For BCPs, the non-crystallized block is covalently attached to the surface. Recent studies have focused on preparation techniques (thermal treatment versus co-solvent),[67-68] surface characteristics of the tethered chains,[69-71] and functional crystalline nanoparticles.[72-74] The review by Agbolaghi *et al*.[18] provides a nice, comprehensive summary of BCP single crystals for further reading.

TABLE 3 Morphologies of PEO-*b*-PLLA Measured by TEM[75]

	Morphology from Common Solvent		
Copolymer Composition	DMF	THF	Dioxane
PEO (5k)-*b*-PLLA (66.4k)	Lozenge[a]	Lozenge and Spheres	Spheres
PEO (5k)-*b*-PLLA (33.5k)	Lozenge	Lozenge	Spheres
PEO (5k)-*b*-PLLA (22.5k)	Lozenge	Lozenge	Lozenge and Spheres
PEO (5k)-*b*-PLLA (9.4k)	Lozenge-like[b] and Cylinders	Lozenge-like and Cylinders	Lozenge-like and Cylinders
PEO (5k)-*b*-PLLA (2.6k)	Lozenge-like and Cylinders	Lozenge-like and Cylinders	Lozenge-like and Cylinders

[a] single crystal morphology of PLLA [b] aggregation of cylinders

Micelle formation is a more active field than single crytsals; therefore, more details are provided for crystallization in these assemblies. The second method for BCP solution crystallization is the

formation of a micelle phase where the cores crystallize after changes in the environment, i.e. cooling or drying. Depending on the thermodynamic stability of the micelles, crystallization is confined to the core, particularly for sphere and cylinder micelles.[75-76] Likewise, breakout-like crystallization is possible and disrupts the micelle core leading to further aggregation of individual micelles transitioning to a new micelle morphology, usually cylindrical or branched-cylinders,[77-80] or to lamellar, single-crystal-like platelets.[81-83] Wang and coworkers[75] designed PEO-*b*-PLLA copolymers with different M_n^{PLLA} to study the role of hydrophobic block length and solvent quality (PEO corona solvation) on solution self-assembly. DMF, THF, and dioxane were used as common solvent due to their increasing compatibility with PEO, respectively, and water was added dropwise to form aggregates. Table 3 provides a summary of the morphological changes observed with different PEO-*b*-PLLA compositions and different common solvent. All aggregates were shown to have a melting peak in DSC after centrifugation indicating the presence of PLLA crystals. Spherical micelles had the lowest crystallinity, as would be expected. The lozenge morphology indicated growth of PLLA single crystals in solution. Spheres and cylinders (or rods) were representative micelles. Lozenge-like aggregation of cylindrical micelles indicated the morphological transition associated with aggregation due to break-out-like crystallization. In some instances, the morphologies appeared to be a mixture of separate single crystal lozenges and cylinders. Li *et al*.[76] observed a micelle morphology change from spheres to disc-like after the crystallization of PE in a PEO-*b*-PE system. Other studies of PEO-*b*-PE[78] and PEO-*b*-PCL[77] demonstrated examples of morphological transitions and phase ripening after crystallization in the core. Figure 6 shows TEM images of this process for the PEO-*b*-PCL copolymer as an example.

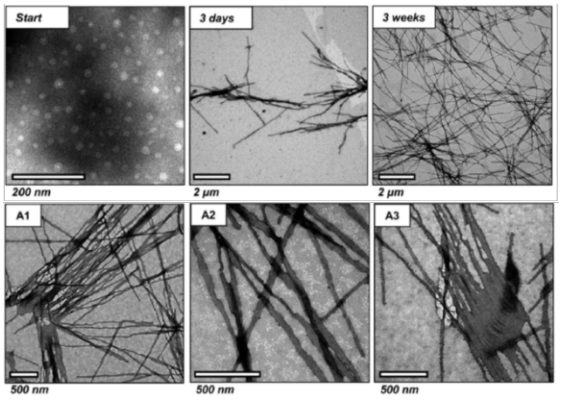

FIGURE 6 TEM bright field images of aged PEO-*b*-PCL micelle solutions. Top row shows the transition of spheres to cylinders over the time span indicated on the images for M_n^{PEO} = 2k and M_n^{PCL} = 3k. Series A1-A3 shows the transition of rods to ribbons over a 3-month period for M_n^{PEO} = 2k and M_n^{PCL} = 2.7k. (Reproduced from [77] with permission from the Royal Society of Chemistry.)

Changes in morphology have been shown to be sensitive to additives as well.[79-84] These additives manipulated either the corona block[79-81] or the core block.[82-84] He and coworkers[79-80] prepared micelles of poly(acrylic acid)-*b*-polymethylene (PAA-*b*-PM) with crystalline PM cores using the thermal treatment method. When adding polyethylene polyamine ($C_{2n}H_{5n}N_n$), the fractionally-deprotonated PAA block and protonated amines complexed to change the volume of the corona. This led to morphological transitions from spheres to ribbons to platelets. In addition, the size of the micelle changed resulting in stronger

confinement of PM and resulted in some micelles without crystalline cores. Similar results were seen with ionic salt additives.[80] Yang and coworkers[81] added hydrogen bond donors, phenol and L-threonine, to PEO-*b*-PCL rod micelles. Phenol caused the micelles to fracture by swelling the PEO; whereas, the L-threonine promoted rod growth by "cross-linking" PEO chains and decreasing the hydrodynamic radius of a single chain. This process was shown to be reversible. For PEO-*b*-PCL and PAA-*b*-PCL micelles, homopolymer PCL was added to dioxane or DMF with the copolymer.[82-83] The presence of homopolymer PCL shifted the morphology from 1D to 2D after micellization and storage in water. Since the homopolymer was hydrophobic, it selectively increased the volume of the crystalline cores. When a critical size was reached, the hydrophilic PEO corona was no longer an effective shield from the solvent. The result was aggregation of rod micelles to form platelet-like "rafts." These resembled the truncated lozenge single crystals of PCL; however, rod-like protrusions were observed at the (110) edges, for comparison of these two morphologies see Figure 7. Finally, this homopolymer additive method was extended to co-micelle assemblies – those that contain more than one type of copolymer in the micelle – to form engineered platelet surfaces.[84] This work also achieved co-micelles with different crystallizable blocks *via* heteroepitaxial growth since the two crystals have similar lattice spacing.

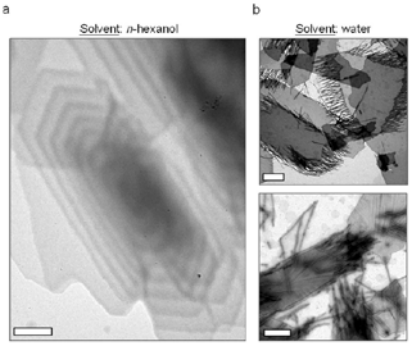

FIGURE 7 (a) TEM bright field images of PEO-*b*-PCL single crystals grown in *n*-hexanol. (b) PEO-*b*-PCL "raft"-like assemblies formed after the single crystals were placed in water. Note the rod-like protrusions and rod-shaped micelles, mirroring the aggregation process in reverse. Scale bars represents 1 μm. (Reproduced from [82] with permission from John Wiley and Sons.)

The last form of solution assembly is crystallization-driven self-assembly, or CDSA. Here, micelles are formed due to the crystallization of one block. Unlike single crystal formation, restriction of lateral crystal growth results in rod-like crystals, and a portion of the core remains amorphous. It has been shown that CDSA has the added advantage of being a "living" type of assembly, where the length of the cylindrical micelle grows with addition of more unimer chains.[85] For more details on the "living" nature of CDSA, see Refs. 17 and 64. PFS is the most common crystalline block for these micelles. Work has been done to understand the thermodynamics of assembly to control assembly to make uniform nanoobjects. Poly(*N*-isopropylacrylamide)-*b*-PFS (PNIPAM-*b*-PFS) was added to ethanol and propanol in an attempt to form "living" CDSA cylinders.[86] PNIPAM-*b*-PFS with M_n^{PNIPAM} = 24.5k and M_n^{PFS} = 13.3k formed spheres and rods similar to the step-wise micelle crystallization mechanism, while a sample with M_n^{PNIPAM} = 67k and M_n^{PFS} = 6.3k formed CDSA cylinders. Hence, the molecular characteristics of a single BCP type changed the crystallization mechanism. Guerin and coworkers[87] annealed PI-*b*-PFS micelles at elevated temperatures to increase the crystallinity. As the amorphous fraction decreased, the cylinders increased in width (the crystallographic direction was not mentioned). This supports the idea

that CDSA cylindrical morphology was driven by restricted 1D crystal growth – along the long axis of the cylinder. Pitto-Barry *et al.*[88] used different hydrophilic blocks, poly(4-acryloyl morpholine) (P4AM), poly(*N*,*N*-dimethylacrylamide) (PDMA), and PEO, with a PLLA hydrophobic block in THF/water to control the length of the cylindrical micelles. PEO-*b*-PLLA and PDMA-*b*-PLLA formed shorter cylinders than P4AM-*b*-PLLA. Since the w_{PEO} was equal for all samples, the relative hydrophilicity of the corona block controlled the cylinder length. In another study, the corona size was manipulated using methyl iodide additive to quaternize poly(2-vinyl pyridine) (P2VP) blocks of P2VP-*b*-PFS.[89] The lightly quaternized (< 6 mol%) P2VP forced the PFS to crystallize with slightly larger widths than unquaternized samples. Unquaternized, or less quaternized, cylinders were able to attach to the end of the higher quaternized ones. This indicated that the crystal cores were epitaxially crystallized similar to the formation mechanism from micelle seeds. As with previous work in micelle crystallization, the corona's thermal characteristics were prominent in determining the morphology.

CDSA-type micelles have been used to develop new hierarchical assemblies. Interactions between crystalline portions, analogous to the ripening of crystal formation during micelle morphology transitions described previously, or the amorphous corona provide directed assembly pathways for new structures. Mixed coronas of co-micelles were formed in a solution of PNIPAM-*b*-PFS and P2VP-*b*-PFS due to different growth kinetics of each block.[90] Figure 8 shows TEM images of CDSA cylinders with "patchy" coronas, where microphase separation created portions of the cylinder with one corona block, PNIPAM lighter portions, and sections with the other, darker P2VP (stained with Karstedt's catalyst). Structures were tailored based on order of assembly and seed formation. These "patchy" coronas were achieved with linear and brush copolymers, too.[91] In another example, Fan and coworkers[92] assembled single crystals of P*t*BA-*b*-PE with rod-like micelles on the growth surface. This assembly was driven by the epitaxial attachment of the micelle PE core with the growth surface of the single crystal, similar to the report by Rizis and coworkers for PCL.[81-82] and Gonzalez-Alvarez *et al.*'s work with PFS.[89] This hierarchical assembly was facilitated by the inclusion of homopolymer PE, which promoted the two different types of solution crystallization. All of these methods benefited from being one-pot solution assemblies. Cylinders were assembled using hydrogen bonding interactions between coronas as well.[93] The P2VP-*b*-PFS branched-cylinders also were used as templates to create 1D silver nanoparticle assemblies by adsorbing silver to the P2VP corona.[94] For all of CDSA cylinders, control over the cylinder size and hierarchical structure was very good even with diverse compositions.

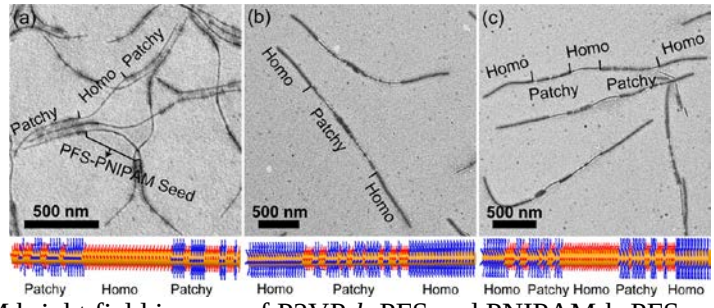

FIGURE 8 TEM bright field images of P2VP-*b*-PFS and PNIPAM-b-PFS co-micelles with "patchy" phase-separated coronas. A blocky architecture was formed by controlling the kinetics of CDSA growth and the composition of unimers in solution. P2VP portions are darker due to staining with Karstedt's catalyst. Below each image is a schematic representation of the assembly where yellow represents PFS, blue represents P2VP, and red represents PNIPAM. (Reproduced from [90] with permission from the American Chemical Society.)

Hierarchical assembly also was achieved on the surface of other materials through corona-surface interactions. Immobilizing uniform nanostructures on a mesoscale substrate is a favorable approach to prepare nanometer to micrometer-sized materials with new functionalities. Uniform hollow basket structures of controlled size, depending on their template, were formed dependent on both the nature of the substrate and the components deposited. Jia and coworkers[95] found a new approach to fabricate a colloidal nanofibrous hollow assembly based on templated CDSA of core-crystalline cylindrical BCP micelles, where colloidal silica-coated polystyrene microbeads serve as a mimic template to attach P2VP-*b*-PFS seeds to grow cylindrical micelles. The network was secured by crosslinked micelles via an *in-situ* generation of small Pt nanoparticles. When the mimic template was removed, this yielded an open vesicular structure. Atomic mass spectrometry revealed that 85% of the template's surface was covered with micelle seeds. These fiber-basket-like polymersomes were structurally different from the vesicles more commonly formed by amphiphilic small molecules or BCPs. The templated fabrication protocol, shown in Figure 9, should apply to any block copolymer that forms elongated core-crystalline micelles. By fabricating hierarchical coating structures, this expands the generality and scope of template-assisted synthesis to build advanced hierarchical materials with also having precise morphology. Using coordination chemistry, microfibers and macroscopic films were fabricated by assembling poly(methylvinylsiloxane)-*b*-PFS (PMVS-*b*-PFS) with 35 mol% diphenylphosphine functionalization of the pendant vinyl group on the PMVS.[96] Palladium was added to complex with the phosphine, and it showed the ability to complex with more than one micelle in a directed way where the ends were attached to form large microfibers. This complexation-driven hierarchical assembly was extensive enough to create macroscopic sheets.

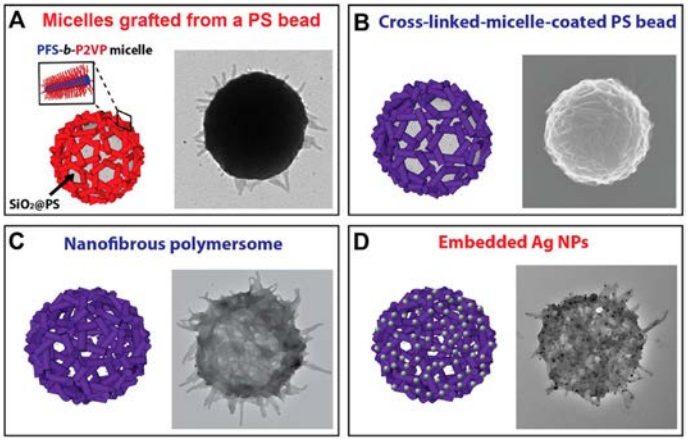

FIGURE 9 (A) Short micelles of PFS-*b*-P2VP attached to SiO2@PS template through the "seeded growth" strategy. (B) The P2VP corona of the short micelles was cross-linked by addition of Karstedt's catalyst and 1,1,3,3-tetramethyldisiloxane (TMDS) in 2-PrOH. (C) The removal of PS beads in DCM leads to hollow nanofibrous assemblies. (D) Ag NPs in the PFS-*b*-P2VP micelles of the nanofibrous assemblies via an *in situ* reduction of Ag^+ ions by the Fe(II) moieties of the swollen redox-active PFS core in DCM. (Reproduced from [95] with permission from the American Chemical Society.)

Analytical methods that enable visualization of nanomaterials derived from solution self-assembly processes in organic solvents are highly desirable, and are often a challenge, when it comes to characterization of BCP nanostructures. There are three main problems with current analysis techniques:

1) provides either ensemble (e.g. DSC or scattering techniques) or local measurements (e.g. microscopy techniques), 2) limited resolution (e.g. optical microscopy), or 3) require invasive removal of solvent prior to imaging (e.g. electron microscopy or X-ray analysis). Boott and coworkers[98] demonstrated the need for simpler analytic techniques that enable visualization of BCP assembly and nanostructure self-assembly using organic solvents. Super-resolution fluorescence microscopy techniques, such as stimulated emission depletion microscopy (STED) and single-molecule localization microscopy (SMLM) were used to visualize nanostructures of micelles formed by CDSA in organic solvents using fluorescently-tagged PFS BCPs. These techniques provided images comparable to TEM bright field. The fluorescent tag did not compromise the micelle morphology.

Solution crystallization has become a robust method to fabricate hierarchical crystalline BCPs. Using one of three different methods, single crystal formation, micellar crystallization, or CDSA, control of these structures provides a promising method of analyzing fundamental crystallization mechanisms and designing new technologies. These are only a few examples of recent work, though most work in this area is a variation of the types of work reviewed here.

CONVENTIONAL CRYSTALLIZABLE TRIBLOCK COPOLYMERS

Linear triblock and multiblock copolymers provide a methodology for changing the chain topology in crystalline-block containing copolymers. Here, the blocks that represent chain ends can be viewed in a way similar to diblock copolymers. However, blocks in the middle of the chain have reduced degrees of freedom because both ends are attached to additional blocks. The copolymers are constructed using a variety of chemical sequences. In triblock copolymers, ABA or ABC structures have different influences on the crystallization of either A, B or C in systems with one or more crystallizable blocks. In multiblock copolymers, especially whose composition is greater than pentablock, the chemical alternation of different blocks imparts new properties to the microphase-separated behavior due to the possibility for tie and loop conformations of individual chains. A separate review could be written on the progress in this field of block copolymer crystallization as it is quite extensive. Therefore, it will not be discussed in detail here. A review from 2011 is included for reference.[98]

Triblock copolymers have a larger set of microphase-separated structures.[99-101] When evaluating the crystallization mechanisms in these materials, Table 1 is applicable still; however, there is a larger set of relative temperatures. Additionally, the location of the crystallizable block(s) in the chain, whether the composition is ABA or ABC, and chain architecture lead to changes in crystallization behavior.[12,14,102] Solution assembly of these BCPs is also more complex depending on the miscibilities of the blocks and each block with solvent.[103-104]

Multiblock copolymers range from tetrablock to segmented block copolymers, where diblock or triblock subunits are connected through step-growth techniques using functional end-groups and often hexamethylene diisocyanate (HMDI) chain extenders to form multiple alternating blocks of the form $(AB)_n$.[98] These multifunctional materials are synonymous with typical thermoplastic elastomer chemistries due to the aggregation of like components which is different than the more structured microphase-separated block copolymer morphologies in di- and triblock copolymers.[98,105] If one of the components is crystallizable, the phase behavior and structure are driven by this aggregation behavior; however, because the blocks are covalently linked, the mobility and assembly of the single-component rich domains is between block copolymer meso-structures and the more macrophase separation of blends. Additionally, crystals operate like cross-linking points and help stabilize the network structure. These two factors make the crystallization mechanisms, kinetics, and morphologies unique to these systems.[98]

Tetrablock and pentablock structures are more similar to triblock copolymer behavior but are more complex due to the variety of compositional architectures available.[105-106] More details about crystallization in these systems can be found in the references cited above.

The two major architectures for triblock copolymers provide three different opportunities for single-crystallizable-block systems. ABA-type triblock copolymers have two: the A block is crystalline and behaves similar to diblock copolymers or the B block is crystalline with restricted mobility due to its double-tethered nature. For ABC-type triblock terpolymers, whether the crystalline block is A or C, typical BCP crystallization behavior is expected. Again, if it is the B block, similar mobility restraints exist compared to ABA-type. Crystallization within phase-separated domains or from the homogeneous melt depends on relative temperatures described in Table 1. With multiple crystalline blocks, the phase behavior becomes richer. Samples discussed here have crystalline blocks of PE,[107-109] PEO,[110-118] PCL,[29,115-121] or PLLA.[25,115-118,120,122-125] Some double crystalline samples include one of these blocks combined with other polyesters,[111,122] isotactic polypropylene oxide (*it*-PPO),[112-113] or poly(vinylidene fluoride) (PVDF).[124] Again, bulk and film samples will be discussed separately from solution assembly.

ABA Triblock Copolymers

First, we will look at recent studies of ABA-type triblock copolymers. Since these are two component systems but with new topology, their phase behavior tracks well with diblock copolymer phase behavior. Molecular weight and volume fraction (*f*) of A blocks differ from diblock copolymers since there are two A chains created by the inclusion of a middle B block. For example, Castillo and coworkers[29] showed that when PCL was the B-block for PTMC-PCL BCPs, its crystallization was retarded significantly compared to PTMC-*b*-PCL and PCL-*b*-PTMC-*b*-PCL, and the diblock and BAB architectures' kinetics were nearly identical. For these BCPs, Table 1 applies in a similar way as diblock copolymers. Each section below focuses on a particular crystalline polymer in rAC, gAC, or CC type combinations.

As in the diblock copolymer section, PEO is a prevalent component for ABA-type triblock copolymers. To better understand the nucleation process in confinement, Chen and Wang[110] used PS-*b*-PEO-*b*-PS to study PEO crystallization in a gAC triblock with no free chain end on the PEO. For CC-type triblock copolymers poly(butylene terephthalate) (PBT) was used as the A-block with PEO as the B-block.[111] This new synthetic approach allowed for a poly(ether-ester) with largely different T_ms ($T_m^{PEO} \approx 50^oC$ and $T_m^{PBT} \approx 210^oC$). Because $T_m^{PBT} > T_m^{PEO}$, the PBT portion consistently crystallized first. PEO crystallization was confirmed by DSC even for $w_{PEO} = 0.30$. At lower w_{PEO}, T_m^{PEO} and crystallinity decreased. However, PBT showed increases in T_m with larger w_{PBT} content. Chiral *it*-PPO-*b*-PEO-*b*-*it*-PPO copolymers were synthesized,[112] and the interplay of *it*-PPO and PEO crystallization and melting were probed by Shi and coworkers.[113] In this double-crystalline, strongly-segregated copolymer, *it*-PPO and PEO ($w_{PEO} = 0.33$) showed cooperative sequential crystallization behavior. During cooling, PEO crystallized at 50°C and *it*-PPO crystallized at 45°C. Since the PEO crystallized first, it provided a hard confinement for *it*-PPO and caused a slight depression of $T_c^{it\text{-PPO}}$. A unique feature of this low molecular weight *it*-PPO-*b*-PEO-*b*-*it*-PPO was that the metastability of the PEO crystal was smaller than the *it*-PPO crystal. During heating, the PEO melted first even though it crystallized first. Clearly, the crystalline *it*-PPO influenced the PEO metastability. After melting of PEO, the *it*-PPO crystals thickened to achieve a crystal thickness that provided integer folds. Homopolymer *it*-PPO also exhibited strong melt-recrystallization behavior during heating. These combined results indicate that in the triblock copolymer, *it*-PPO crystals were more stable during heating, which led to PEO crystals melting first. A schematic of

the crystal behavior for both blocks during heating as measured by SAXS/WAXD is shown in Figure 10. This unique BCP double-crystalline behavior, especially for low molecular weight samples, may occur for other block combinations where the transition temperatures are similar. Understanding the relative metastabilities of the blocks is crucial for evaluating structure-property relationships.

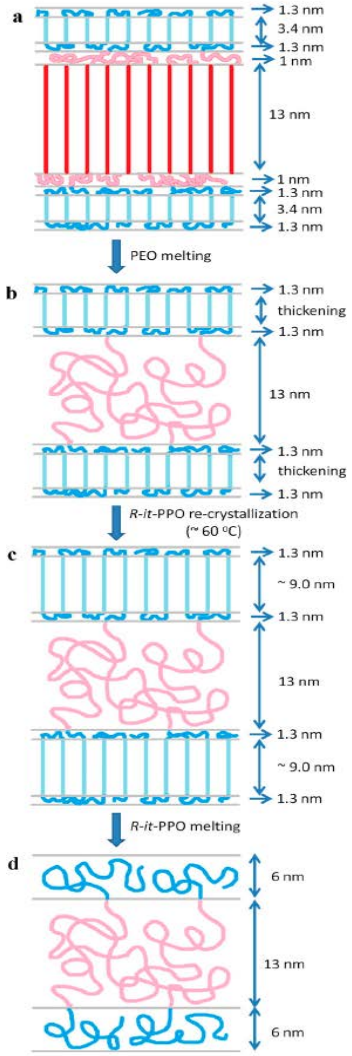

FIGURE 10 Schematic representation of the melting and crystal thickening behavior of *it*-PPO-*b*-PEO-*b*-*it*-PPO during heating. *it*-PPO blocks are blue, and PEO blocks are red. (Reproduced from [113] with permission from the American Chemical Society.)

Two sets of poly(dimethylsiloxane) (PDMS)/polyester triblock copolymers were synthesized where PDMS imparts soft confinement on the PCL or PLLA block. A series of PCL-*b*-PDMS-*b*-PCL copolymers with varying molecular weights and w_{PCL} were synthesized to study the phase behavior, PCL crystallization, and surface segregation of films.[119] For all samples, PCL exhibited expected breakout crystallization behavior as observed in POM. At sufficient cooling, PDMS also exhibited crystallization behavior (exothermic DSC peaks during heating from -130°C to 80°C) when $w_{PDMS} > 0.33$. PDMS crystallized between the PCL lamellae, but the crystallization behavior was not studied in detail. For most samples, the films' water contact angles were similar to PDMS, demonstrating that the PDMS

concentration was enhanced at the free surface. PDMS crystallization was evaluated more closely in a strongly-segregated PLLA-*b*-PDMS-*b*-PLLA (w_{PDMS} = 0.29, $M_n^{overall}$ = 19.3k) triblock copolymer.[123] Here, the difference in T_c was quite large (~100°C). Additionally, both blocks remained amorphous with a moderate cooling rate of 30°C/min and showed cold crystallization behavior upon heating. Through numerous experimental techniques, the phase behavior was monitored in detail during heating. Figure 11 shows a well-constructed plot that aggregates all data during thermal treatment. The phase behavior during heating is summarized as follows. At -120°C, the microphased-separated material was amorphous with a lamellar morphology. During heating, PDMS exhibited cold crystallization at -110°C (*via* WAXD analysis), while the SAXS data remained unchanged, indicating that PDMS crystallized in phase separated domains under hard confinement of the PLLA. This T_{cc} is lower than for PDMS homopolymer; therefore, the PLLA had a nucleating effect on PDMS crystallization. The PDMS crystals melted at -50°C, well above T_g^{PDMS}. At 50°C, the SAXS data indicated a large increase in the long period, suggesting that both PDMS and PLLA domains thickened (chain stretching) at T_g^{PLLA} because of the formation of a PLLA mesophase prior to crystallization at T_{cc}^{PLLA} = 70°C. WAXD data showed that the crystals formed were a mixture of the α′ and α polymorphs similar to PEO-*b*-PLLA.[45] Isothermal crystallization experiments showed that the α′ form was more prevalent at lower temperatures. This was an indication that the disordered chain-packing of the α′ form was facilitated near T_g^{PLLA}. In this temperature range, PDMS provides soft confinement; therefore, breakout crystallization would be expected. However, due to the high segregation strength, a distorted microdomain structure was observed in SAXS and not true breakout crystallization. At T > 150°C, the PLLA crystals were completely melted, and the original lamellar microphase-separated morphology was recovered. It should be noted that sample behavior at room temperature falls in the rAC category, but cooling below -50°C resulted in PDMS crystallization under hard confinement.

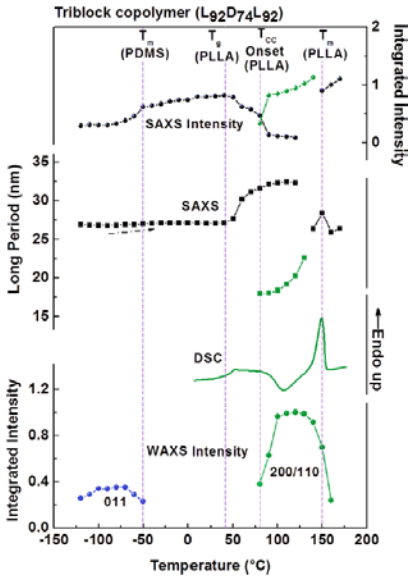

FIGURE 11 Comparison of SAXS, WAXD, and DSC data for the heating of amorphous PLLA-*b*-PDMS-*b*-PLLA from -120°C to 170°C. Green data represents PLLA phase behavior, and blue represents PDMS phase behavior. (Reproduced from [123] with permission from the American Chemical Society.)

Other PLLA-based triblock copolymers were studied to gain a better understanding of PLLA crystallization and its role in double-crystalline ABA triblocks. As is often the case, and is discussed in various sections of this review, block copolymers of PLLA help improve the thermoplastic behavior of PLLA-based materials. Rubbery amorphous blocks of PDMAEMA[25] and poly(butylene carbonate) (PBC)[122] were copolymerized with PLLA with this idea in mind. Additionally, both PDMAEMA and PBC show potential for medical applications. In PDMAEMA-*b*-PLLA-*b*-PDMAEMA,[25] the phase behavior was similar to the diblock copolymer described previously. Because of the inclusion of two PDMAEMA blocks with a central PLLA block, the retardation effect on the crystallization kinetics was enhanced, indicating that the w_{PLLA} and architecture influence the crystallization process. Morphologically, the triblock copolymer exhibited a distorted hexagonal shape for $w_{PLLA} = 0.48$. No thin film crystallization was observed for $w_{PLLA} = 0.33$. For PLLA-*b*-PBC-*b*-PLLA, since PLLA was the exterior A-block, crystallization of PBC was suppressed completely at $w_{PBC} < 0.53$ with $M_n^{PBC} = 30.1$k.[122] PLLA crystallization followed typical trends for T_c (T_m) and crystallinity as w_{PLLA} decreased. Double crystalline PLLA-*b*-PCL-*b*-PLLA[120] and PLLA-*b*-PVDF-*b*-PLLA[124] showed slightly different PLLA BCP crystallization behavior. Although PLLA was the A-block component, the crystallization sequence was different for the two triblock copolymers. For PCL, crystallization was hindered compared to PCL-*b*-PLLA due to the tethering of both PCL ends to the PLLA crystal surfaces.[120] For PVDF, its T_c is higher than T_c^{PLLA}. Crystallization-induced microphase separation occurred above T_g^{PLLA}.[124] The characteristics of PVDF crystallization ($0.43 < w_{PVDF} < 0.75$) were affected minimally by the varying w_{PLLA}. The PVDF crystals did impart a nucleation effect on the PLLA crystallization, however. It was observed that β-form PVDF crystals formed from DMF solution casting but reverted to the α-form after melt-recrystallization similar to other PS-*b*-PVDF-*b*-PS[125] and P*t*BMA-*b*-PVDF-*b*-P*t*BMA[126] BCP materials.

Solution crystallization mechanisms of ABA triblock copolymers are similar to diblock copolymers, however, the tethering density of the non-crystalline block is twice as large since it is covalently attached at both ends of the B-block. PS-*b*-PE-*b*-PS BCP samples with identical PE blocks and varied PS blocks were synthesized by Xu and coworkers.[107] They studied the micelle behavior of the triblock copolymer in 1,4-dioxane. Both spherical and cylindrical morphologies were observed. Cylindrical micelles were more prominent when the w_{PS} increased. Yu *et al.*[127] studied the assembly behavior of PDMA copolymers with PLLA as the crystalline block, PDMA-*b*-PLLA-*b*-PDMA. They systematically changed the molecular weights and weight fractions to observe methanol solution assembly as the hydrophobic block (PLLA) changed composition. This provided a more direct understanding of how hydrophobicity influences CDSA. Figure 12 shows TEM images of the common morphologies along with a phase diagram based on M_n^{PLLA} and w_{PLLA}. CDSA samples were prepared by dissolving 5 mg polymer in 1 mL of methanol by vortexing and allowing the solution to age for 24 hrs (no mixed solvent or thermal treatment was used). At low PLLA content (bottom right of phase diagram), single crystal type CDSA was observed. Lozenge-shaped crystals formed, indicating PLLA crystallization. At moderate PLLA content, a transitional phase between single crystals and cylindrical micelles was observed. At high PLLA content (right side of phase diagram), cylindrical micelles were formed. This indicated that smaller PLLA fractions were easier to crystallize in methanol solution than larger PLLA fractions. In other words, the kinetics of crystal formation dominated at low PLLA content; while, micellization dominated at higher PLLA content. Control of assembly within a single solvent system without thermal treatment is a promising new area for CDSA.

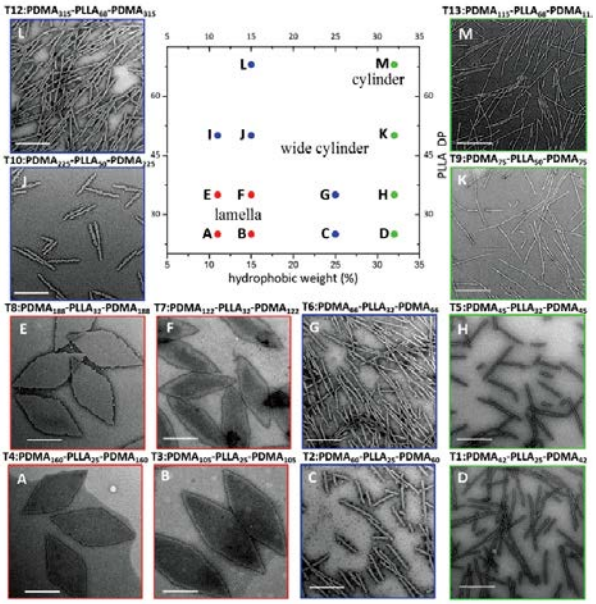

FIGURE 12 TEM images of a series of PDMA-*b*-PLLA-*b*-PDMA triblock copolymers. Samples were negatively stained using uranyl acetate. A phase diagram based on the size (DP = degree of polymerization) and weight fraction of PLLA is also included. (Reproduced from [127] with permission from The Royal Society of Chemistry.)

ABC Triblock Terpolymers

ABC-type BCPs have a richer set of microphase separated morphologies. This creates a broader range of templated morphologies for crystalline components.[12,103] Materials with single crystallizable blocks recently have been studied to elucidate the influence of microstructure on crystallization.[114,120] PI-*b*-PS-*b*-PEO terpolymer was synthesized to promote formation of a PEO gyroid phase when exposed to solvent vapor annealing with chloroform (f_{PI} = 0.30, f_{PS} = 0.53, f_{PEO} = 0.12, and $M_n^{overalll}$ = 80k).[114] Figure 13 shows optical microscopy and GIWAXS data for as-cast and solvent annealed samples. The microscopy images show that PEO spherulites form as-cast, but large domains with uniform birefringence appeared after solvent vapor annealing. The grazing-incidence wide-angle x-ray scattering (GIWAXS) data confirmed preferential alignment of PEO crystals in both instances. The authors determined that PEO crystallized along the gyroid phase after vapor annealing with the *c*-axis parallel to the phase normal direction, which maximizes crystallinity by growing along the phase direction. This feature resulted in uniform birefringence within a given domain and provided a unique opportunity to identify domain sizes after BCP microphase separation. Wang *et al.*[121] studied the influence of having a miscible central block on phase behavior for PCL-*b*-poly(*n*-butyl acrylate)-*b*-PS (PCL-*b*-P*n*BA-*b*-PS), where P*n*BA is miscible in both PCL and PS. Because of the mutual miscibility, the P*n*BA block created a large, low T_g interfacial area between the PCL and PS and created an apparent f_{PCL} and f_{PS} similar to a bi-phasic system. This led to breakout crystallization even with high T_g PS domains when apparent $f_{PS} < 0.63$.

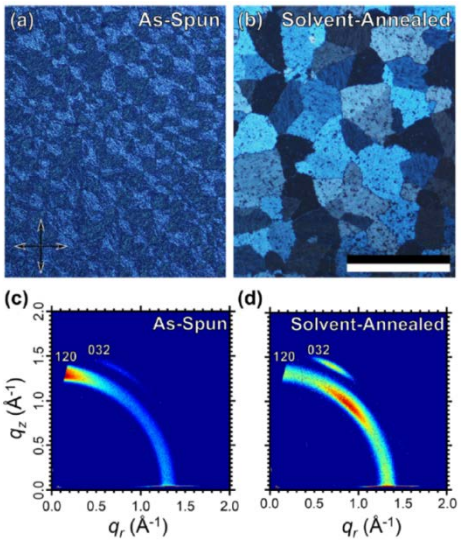

FIGURE 13 POM images of PI-*b*-PS-*b*-PEO films (a) as-cast and (b) solvent annealed in chloroform. GIWAXS data demonstrating the alignment of PEO crystals in (c) as-cast and (d) chloroform solvent annealed preparations. (Reproduced from [114] with permission from the American Chemical Society.)

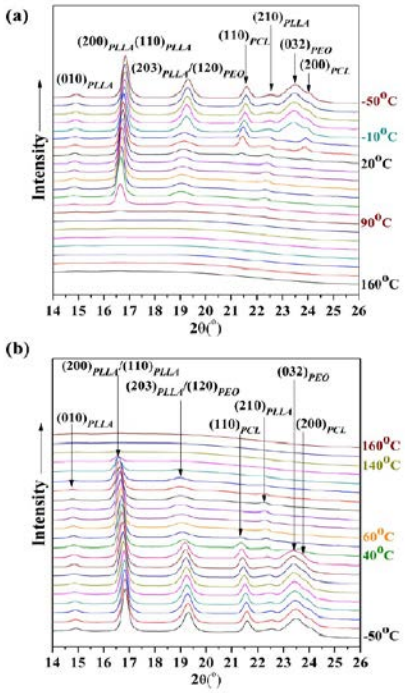

FIGURE 14 WAXD patterns for (a) cooling and (b) heating of PEO5-PCL3-PLLA6. Rates were 10°C/min for both with temperature steps of 10°C. (Reproduced from [115] with permission from the American Chemical Society.)

New advances in triple crystalline triblock copolymers were studied by Chiang *et al.*[115] and Palacios *et al.*[116-118] In all cases, PEO-*b*-PCL-*b*-PLLA was the BCP of interest. These components were miscible in the melt; therefore, phase separation was driven by crystallization of the PLLA block (highest

T_c). Chiang and coworkers were interested in single crystal growth in thin films,[115] while Palacios and others studied the relationships among transition temperatures,[116] morphology,[117] and growth kinetics[118] in the bulk. In thin films spun cast from chlorobenzene onto carbon-coated substrates, melt-recrystallization was studied using DSC, WAXD, and TEM for two samples, PEO5-PCL3-PLLA1 and PEO5-PCL3-PLLA6, where the number represents the M_n for each component in kg/mol.[115] Bulk analysis showed that the PEO5-PCL3-PLLA1 sample did not exhibit PLLA crystallization, only PEO and PCL, likely due to the small M_n^{PLLA} and w_{PLLA} and low chain mobility. However, T_c, T_m, and WAXD data confirmed crystallization of all three components of PEO5-PCL3-PLLA6, even with low PCL content (w_{PCL} = 0.20). Interestingly, the crystallization sequence according to WAXD was $T_c^{PLLA} > T_c^{PCL} > T_c^{PEO}$ even though $M_n^{PEO} > M_n^{PCL}$ ($w_{PEO} > w_{PCL}$) and PEO was the A-block, as shown in Figure 14. It may be that PCL's proximity to the PLLA crystal served as a nucleating agent to induce PCL crystallization second. In thin films, non-faceted, single layer crystals were observed using TEM. Different isothermal T_cs and some solvent vapor annealing were used to manipulate the crystallization of each block. SAED data was used to confirm the presence of PEO, PCL, and PLLA crystals.

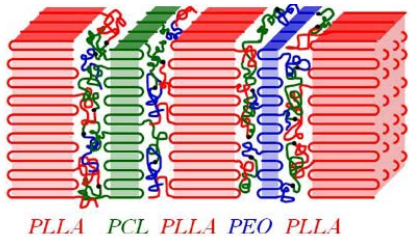

FIGURE 15 Schematic representation of trilayered lamellar morphology for PEO5-PCL7-PLLA5. (Reproduced from [117] with permission from the American Chemical Society.)

Further work was done on triple crystalline BCPs of PEO-*b*-PCL-*b*-PLLA with larger molecular weights. Using the same labelling convention, PEO5-PCL7-PLLA5 and PEO5-PCL7-PLLA9 were studied along with diblock copolymers with similar compositions for comparison. Initial studies showed that all components were crystalline as observed by three T_cs (T_ms) in DSC and representative diffraction peaks in WAXD.[116] For these samples, the crystallization sequence was again PLLA first, PCL second, and PEO third, though T_c^{PEO} was much higher compared to the previous study. Compared to PCL-*b*-PLLA and PEO-*b*-PLLA copolymers, crystallization of PLLA was hindered more in the ABC triblock. As evidenced by POM, PLLA axialites and spherulites formed during cooling with subsequent PCL and PEO crystallization within the polycrystalline morphology. Further evaluation of the PEO5-PCL7-PLLA5 copolymer identified a trilayered morphological structure with PEO and PCL crystallization segmented between different sets of PLLA lamellae.[117] This detailed work was performed using a combination of AFM, SAXS, WAXD, and intricate thermal processing to develop the lamellar morphology shown in Figure 15. This unique morphology showed that between individual PLLA lamellae, there existed either PCL lamella or PEO lamella, not both. In regions where PCL crystals formed, PEO remained amorphous and vice versa. In looking at crystallization kinetics, each block displayed different crystallization rates compared to homopolymer and diblock copolymer systems of similar molecular weight.[118] Figure 16 shows isothermal crystallization rate data for each block with different preparation techniques. PLLA was first to crystallize at high temperatures. For the triblock copolymer (closed symbols), PLLA crystallization (far-left graph of Figure 16) was faster than a comparative diblock system (open symbols) because of its increased mobility due to the plasticization of PCL and PEO components. PCL, as the

second crystallizable block, was studied in two scenarios (center graph of Figure 16): (1) PLLA crystals formed first during cooling to T_c and (2) quench to T_c to maintain amorphous PLLA. Compared to homopolymer PCL (stars), crystallization was accelerated when PLLA crystals were formed first (diamonds). When PLLA was amorphous (circles), PCL crystallization was slowed. This implied that the PLLA crystals act as a nucleating agent for PCL crystallization. Finally, PEO crystallization rate (far-right graph of Figure 16) was decreased significantly in the triblock (triangles) compared to homopolymer PEO (asterisks) due to confinement effects. The field of triple crystalline triblock terpolymers is rich for further analysis of the interplay of chain characteristics, processing parameters, and the manipulation of crystalline structure.

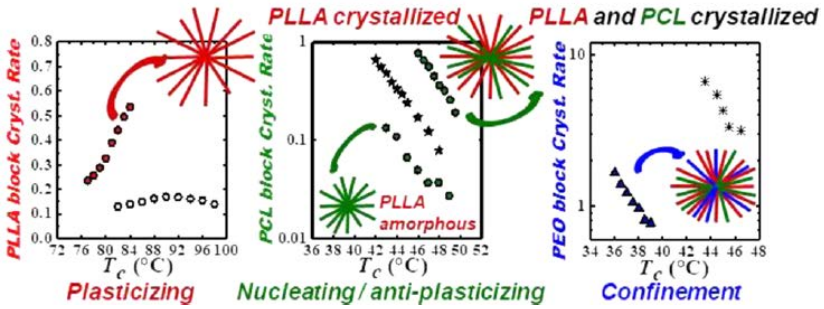

FIGURE 16 Crystallization rate data as a function of isothermal T_c for each block in PEO5-PCL7-PLLA5 along with data from comparable systems. See text for detailed discussion. (Reproduced from [118] with permission from the American Chemical Society)

Solution assembly of triblock terpolymers also has led to interesting advances in the field of BCP crystallization. In most cases, CDSA was used to form worm-like micellar structures with crystalline cores of either PE[108-109,128-130] or PFS.[131] While the current focus of CDSA research is related to controlled micelle growth and hierarchical assembly,[82-96] triblock terpolymers provide another opportunity to tailor the corona of the micelle to form "patchy" morphologies on the micelle surface.[108-109,128-130] For diblock copolymers, this was achieved by mixing two copolymers.[90] ABC terpolymers achieve this without using multiple components. In both PE and PFS triblock systems, corona morphology was driven by phase segregation of the two non-crystalline blocks without BCP mixing. Since the crystallizing central B-block does not have any orientation preference during assembly, changes in the corona's structure were determined solely by the attached A-block and C-block components.

PS-*b*-PE-*b*-PMMA[108-109,128-130] and PS-*b*-PFS-*b*-PMMA[131] BCPs were assembled in solution to monitor the CDSA process and to create micelles with tunable, multicomponent coronas. Similar to micelles grown from mixing diblock copolymers that co-crystallize,[90-91] the central PE forms the crystalline core with two different solvophilic blocks around the exterior. PS and PMMA are immiscible in the melt; therefore, the corona formed a phase separated secondary structure. If the blocks were miscible, it is more likely that the corona would behave as an average of the two components without any regular or modulated physical structure periodicity. Control of crystallization and micelle growth[17,90] allow for tailoring the periodicity, which would make these assemblies ideal for patterned surfaces. Schmelz *et al*.[109] used spherical micelle seeds of PS-*b*-PE-*b*-PS, instead of the typical cylindrical seeds, to control the morphology and length of assembled triblock copolymer cylinders with PE crystalline cores. Figure 17 (left) shows a TEM bright field image of the patchy PS-*b*-PE-*b*-PMMA micelles grown from a PS-*b*-PE-*b*-PS seed in THF. The PS block was selectively stained with RuO_4. Finally, the researchers

were able to selectively assemble gold nanoparticles into PMMA domains by functionalizing the methacrylate with *N*,*N*-dialkylethylenediamines.[108,130] PFS B-block copolymers with PS and PMMA terminal blocks also formed patchy coronas with PS or PMMA domains.[131] Using triblocks of different PS and PMMA lengths, the rigidity of the cylindrical micelle was tailored. Longer corona blocks used as seeds resulted in straight co-micelles with shorter corona terminal blocks due to crowding near the central seed. However, when the sequence was reversed, the co-micelle appeared curved due to crowding on the ends. Figure 17 (right) shows TEM images of two assemblies grown in acetone as described. It should be noted that mixed systems, such as those described here, were much more sensitive to preparation conditions due to competing PE or PFS assembly processes restricted by corona chain compatibility.

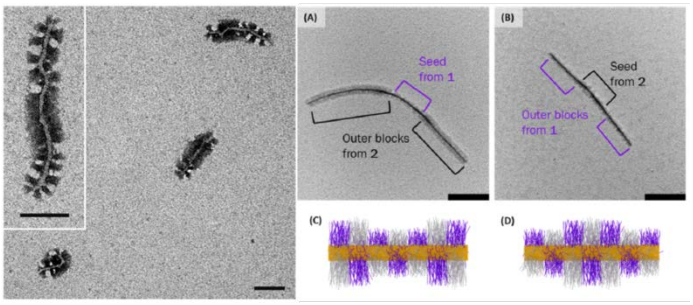

FIGURE 17 (left) TEM micrograph of PS-*b*-PE-*b*-PMMA co-micelle grown from PS-*b*-PE-*b*-PS seed. PS has been selectively stained with RuO_4. Scale bar represents 100 nm. (right) TEM micrographs and cartoon representations of representative patchy co-micelles of PS-*b*-PFS-*b*-PMMA with short corona block seeds (A and C) or long corona block seeds (B and D). Scale bars are 200 nm. (Reproduced from [109] and [131] with permission from the American Chemical Society.)

POLYLACTIDE STEREOCOMPLEX CRYSTALLIZATION

Because of the multitude of research findings in the area of stereocomplex crystallization in poly(lactides), PLLA and PDLA, a separate section was included here. The field has been studied intensely over several decades,[132] but with the recent development of stereoblock copolymers, where one block is the L(*S*)-enantiomer and one is the D(*R*)-enantiomer, a new library of crystallization behavior has been curated. Over the years, these block copolymers have been investigated in their pure form, in blends with single enantiomer homopolymers, and with varying stereoblock architectures. Each enantiomer, PDLA or PLLA, is capable of crystallizing in the homochiral form (hc). The most common crystal form of both enantiomers is the α-form with 10/3 helices in a pseudo-orthorhombic lattice for hc crystals.[133-134] PLLA crystals have left-handed helices packed upward and downward at the center and corner of the unit cell, respectively. The upward and downward orientation allow for the –OH substituent to pack closely to the main-chain of neighboring stems (the projection of neighboring –OHs shows that they are superimposed over each other depending on the number of helical turns). Crystals of PDLA have right-handed helices packed in a similar fashion. Because of the helical nature and handedness of the crystal stems, it is possible to pack left-handed PLLA chains anti-parallel (opposite directionality) to right-handed PDLA chains in a disordered packing model over the local crystal domains.[135-138] This leads to the formation of stereocomplex crystals (sc) because the difference in chirality, and therefore crystal packing and helical formation (3/1), results in a new crystal structure *via* the co-crystallization of the two enantiomers. These stereocomplex crystals have a melting temperature that is approximately 50°C higher

than the homochiral form. Also, the diffraction pattern for the stereocomplex differs because of the orientation of the chain stems. The most common methods for detecting sc crystals are using DSC and WAXD. The higher melting temperature means higher stability when sc crystallization occurs. The higher stability imparts more robust mechanical properties as well. These two benefits, compared to pure PLLA or PDLA with hc crystallization, ignited interest in this field because of the limitations of PLAs as engineering materials. SC crystallization has been shown to occur in a number of situations, but it was discovered using 50/50 blends of equal molecular weight PLLA/PDLA.[138] For a review of the literature regarding earlier work in stereocomplex crystallization, see, for example, Ref. 132.

More recently, block copolymers have been used to induce sc crystallization. These methods include blending BCPs with a PLLA (PDLA) block with PDLA (PLLA) homopolymer, respectively, blending BCPs, where one copolymer has a PLLA constituent and one has a PDLA constituent, or creating stereoblock copolymers where there is a PLLA block and a PDLA block (in this case, no blending is needed). Additionally, some groups have altered the architecture of these block copolymers to observe its role on forming sc crystals and the subsequent crystallization kinetics. It has been shown that the proximity and mobility of enantiomeric chains based on topology influenced the ability to form and grow sc crystals.

Since the first sc crystals were formed using blends of enantiomeric homopolymers, a logical extension was to use block copolymers containing one enantiomer of PLA to blend with the other enantiomer. The phase behavior and macroscopic properties of these materials are altered compared to the pure block copolymer, not only because of homopolymer blending with block copolymers, but also because the blend results in sc crystals instead of the hc crystals found in the pure block copolymer. One advantage of this area of study is that while sc crystals have been well-characterized, the synthesis of new PLA-containing block copolymers has the additional benefit to explore sc crystallization in systems with tertiary components from the block copolymer. Secondarily, block copolymers with enantiomeric blocks, i.e. PLLA-*b*-PDLA, provide new restrictions on the crystallization kinetics and crystal stability due to the inclusion of junction points at the surface of sc crystals, which were previously non-existent in blend systems.

Many variations of BCPs containing either PLLA or PDLA have been blended with homopolymer enantiomers to evaluate the ability of the PLAs to form sc crystals. One of the most popular combinations is the inclusion of PEO as the alternate block[139-143] because it has been shown to improve mechanical properties of PLLA in blends.[140] When the amount of PDLA-*b*-PEO-*b*-PDLA exceeds 30% in blends with PLLA, sc crystals were the dominant species as determined by DSC and WAXD. At 50%, hc crystals disappeared completely, similar to homopolymer blends. Two studies published at nearly the same time evaluated sc crystal formation in PDLA-*b*-PEO-*b*-PDLA/PLLA blends with high PLLA content. One focused on the role of M_n for each component;[141] while, the other elucidated the role of PEO in improving sc crystal formation.[142] Because of the high PLLA content, both hc and sc crystals formed. When the L/D molar ratio was greater than 4:1, hc crystals were able to form.[141] The M_n^{PDLA} influenced the T_m and crystallinity of the sc crystals as shown in Figure 17. It also demonstrated that solution casting provides better mixing to achieve sc crystals. Compared to PDLA/PLLA blends, the BCP/homopolymer blends formed sc crystals at lower T_{cc}^{sc}.[142] T_{cc}^{sc} decreased as M_n^{PEO} increased, meaning that the PEO component lowered the free energy of forming sc crystals. The T_m^{sc} also increased as shown in Figure 18. The improved mobility of PDLA chains (lower T_g) likely contributed to the ease of nucleating sc crystals instead of hc crystals of the PLLA matrix. It should be noted that the M_n for the block components was only a few thousand grams per mole, while M_n^{PLLA} was

45k. In a study by Nakajima *et al.*,[143] PDLA was immobilized on a silicon surface. Both PEO-*b*-PLLA and PLLA-*b*-PEO-*b*-PLLA was added to form tethered sc crystals. In nearly all cases here, PEO was a small fraction of the materials, and therefore, was not crystalline. Similar results were found for PCL-*b*-PLLA multiblock copolymers blended with PDLA.[144]

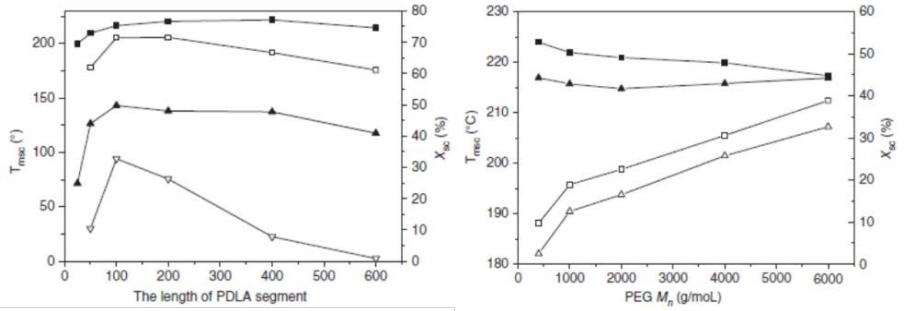

FIGURE 18 T_m (squares) and crystallinity, or X_{SC}, (triangles) of sc crystals in PLLA/PDLA-*b*-PEO-*b*-PDLA blends as a function of (left) PDLA length and (right) PEO length. Closed symbols represent solution cast samples, and open symbols represent melt-recrystallized bulk samples. (Reproduced from [141] with permission from John Wiley and Sons.)

Boissé *et al.* [25] included a morphological study of PDMAEMA-*b*-PLLA and PDMAEMA-*b*-PLLA-*b*-PDMAEMA sc crystal formation with homopolymer PDLA. Both BCPs displayed characteristic single crystal morphologies in thin films. At equimolar ratios of PLLA and PDLA for the diblock copolymer, hexagonal crystals were observed; at non-equimolar ratios, triangular crystals were formed due to frustrated crystal growth, which was analogous to PLLA/PDLA homopolymer blends.[145-146] For the triblock sample, non-equimolar ratio sc crystals were triangular, however this was true for the equimolar ratio as well. Triangular single crystals are formed when the chain characteristics of the PLLA and PDLA chains are different.[136] Because the PLLA was the central block in the triblock copolymer, its mobility was decreased, leading to non-equivalent chain characteristics with the PDLA homopolymer and to the observed triangular morphology.

Stereocomplex formation was studied in blends of BCPs where one BCP included the PLLA enantiomer and the second BCP included the PDLA enantiomer. In each case, the non-PLA block was the same for the blend and was crystallizable. For PA11-*b*-PLLA and PA11-*b*-PDLA blends,[49] sc crystallization was observed immediately, contrary to hc crystallization in the neat BCPs as discussed in the previous section. Additionally, the PA11 and sc PLLA/PDLA crystallization occurred coincidentally during cooling below T_c^{PA11}, which is lower than T_c^{sc}, even though the components were immiscible. This behavior is likely similar to the T_c depression for *s*PP-*b*-PE in Ref. 56. During heating, however, two distinct melting peaks were observed. PA11 adopted the piezoelectric δ′-form, as confirmed by WAXD, when crystallized as-prepared in the presence of sc crystals. The neat diblock afforded the typical α-form of PA11. Blends of PEO-*b*-PLLA/PEO-*b*-PDLA with w_{PEO} = 0.17 - 0.71 per block (M_n^{PEO} = 5k) and analogous 4-arm stars were synthesized by Zhou and coworkers.[147] For high w_{PEO}, PEO crystal melting was observed in DSC in addition to sc melting for both linear and 4-arm star BCPs. The T_m^{sc} and crystallinity were lower for the 4-arm star architecture compared to the linear, implying that the steric hindrance of the central junction point led to more imperfect crystals. PEO crystallization in the diblock was more favorable than in the triblock copolymers, discussed previously,[141-143] where PEO was the midblock. This was confirmed by lower T_m^{PEO} and crystallinity in the 4-arm blends where PEO is the

center block. High molecular weight blends of PDLA-*b*-PEO-*b*-PDLA and PLLA-*b*-PEO-*b*-PLLA made and analyzed by Han *et al*.[148] support the observation that PEO improves sc crystal formation. They also found that shorter PLLA and PDLA end-blocks results in faster crystallization and higher crystallinity. Interestingly, they demonstrated that fast cooling (100°C/min) to isothermal T_cs of 80°C and 160°C led to the formation of hc crystals that underwent melt-recrystallization to form sc crystals during heating. PEO crystallization did occur for large PEO midblock fractions, but the crystallinity was small.

A newer approach to stereocomplex crystallization is the synthesis of stereoblock copolymers.[149] Both linear[150-155] and star[154-160] BCPs including a PLLA and PDLA block in the molecule, sometimes with a third component to form ABC triblock copolymers,[150,160] were investigated. Here, the block length determines the concentration of each enantiomer. Linear diblock copolymers were found to form sc crystals, exclusively, when the enantiomeric content was w_{PDLA} = 0.28 - 0.50, a mixture of hc and sc at w_{PDLA} = 0.10 – 0.17, and only hc for PLLA at w_{PDLA} < 0.10.[151] Though it was not studied here, it is assumed that similar results would occur for w_{PDLA} > 0.50 due to the symmetry of the block copolymers. However, isothermal crystallization at lower temperatures promoted hc formation at moderate w_{PDLA}.[152] Figure 19 shows WAXD data for three separate weight ratios at varying T_c. At w_{PLLA} = 0.50, the sc crystals are most crystalline with the highest T_m, indicating that this composition forms the most stable sc crystals, similar to enantiomeric blends. Additionally, increases in $M_n^{overall}$ increased the T_m^{sc} and lamellar thickness. With lower PLLA content, the fraction of sc crystal (f_{sc}) decreased (Figure 19D, purple triangles and green diamonds data). Multiblock copolymers demonstrated similar trends with molecular weight at w_{PLLA} = 0.50.[151-154] These materials had smaller values compared to the diblock counterparts likely due to the inclusion of HMDI chain-extenders as impurities. These impurities altered the chain mobility as well, which resulted in higher T_gs and more pronounced cold crystallization for the multiblocks.

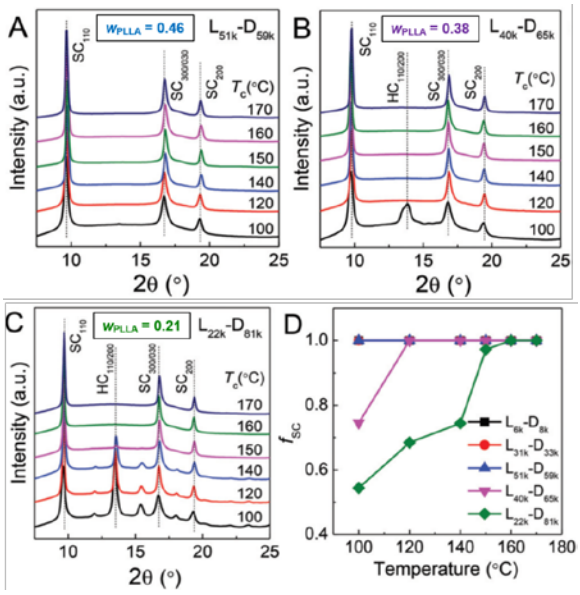

FIGURE 19 (A-C) WAXD patterns for isothermal crystallization of PLLA-*b*-PDLA with varying w_{PLLA} and overall molecular weight. (D) Relative fraction of sc (f_{sc}) compared to hc in crystal phase at different T_c and w_{PLLA}. Black, red, and blue data show no change and are overlapped. (Reproduced from [152] with permission from the Royal Society of Chemistry.)

Star-shaped stereoblock PLA samples introduce two new factors: (1) more limited mobility and (2) steric hindrance of interior blocks. Han *et al.*[155] evaluated the role of chain topology on the formation of sc crystals. With similar molecular weight, an increase in the number of arms, from linear to 3-arm stars to 6-arm stars, led to decreased T_m^{sc} and crystallinity as determined by DSC. The data is shown in Figure 20. The 6-arm star stereoblock copolymer also had the slowest crystallization kinetics. Steric factors in sc crystal nucleation were confirmed by blending 4-arm stars with different core-shell compositions (PDLA as the internal block of one and external of the other).[157] Here, blends of the stereoblock stars exhibited accelerated kinetics compared to the pure 4-arm stereoblock. The interaction of the PDLA shell of one component with the PLLA shell of the other improved sc crystal formation compared to PDLA-shell:PLLA-core interactions. Additionally, the nucleation density was much greater for the blend compared to the pure 4-arm stars as determined by POM, as shown in Figure 21. Similar results were found for 4-arm star stereoblends with an amorphous PLA shell or core block and PDLA or PLLA second blocks.[158] In one case, the stereoblock copolymer, linear and 4-arm star architectures, were blended with neat hompolymer to observe sc formation.[157] It was found that the blend was less crystalline than the pure stereoblock copolymers, especially when the homopolymer enantiomer was identical to the exterior block of the 4-arm star.

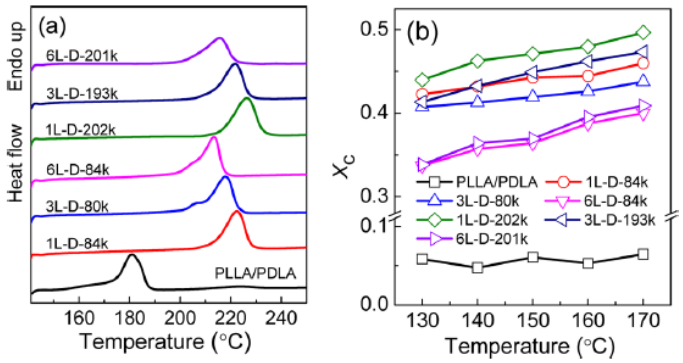

FIGURE 20 (a) DSC heating curve of linear stereo diblock (1L-D), 3-arm stereo diblock stars (3L-D), and 6-arm stereo diblock stars (6L-D) with two different molecular weights after crystallization at T_c = 140°C. (b) Crystallinity of samples held at different T_c. A racemic blend of PLLA and PDLA was included for comparison (black lines). (Reproduced from [155] with permission from the American Chemical Society.)

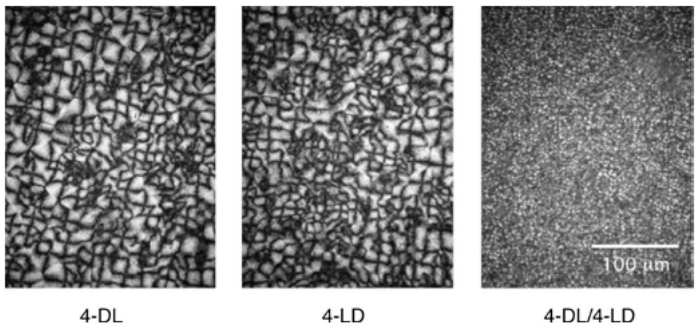

FIGURE 21 POM micrographs of neat 4-arm star stereo-diblock copolymers (4-DL and 4-LD) and of a racemic mixture of the two star architecture crystallized at T_c = 140°C. Scale bar of 100 µm for all images. (Reproduced from [157] with permission from Elsevier.)

Formation of sc crystals in solution also was analyzed for enantiomeric mixtures of PLA-*b*-PEO diblocks,[161] for PEO-*b*-PDLA-*b*-PLLA[161] and for PAA-*b*-PLLA/PAA-*b*-PDLA.[162] In solution, there is the possibility of enantiopure micelle cores that form hc crystals or a core mixture of PLLA and PDLA to form either hc or sc crystals, depending on factors such as molecular weight and polymer solute composition. For both sets of diblocks, racemic mixtures of the two enantiomers resulted in sc crystal core micelles with PEO or PAA coronas. The sc crystal formation resulted in a morphological change compared to the enantiopure, hc crystal micelles. In PAA-*b*-PLLA/PAA-*b*-PDLA mixtures, the morphology changed from cylindrical for the homochiral solution to spherical due to sc crystallization.[162] In the PEO-*b*-PLLA/PEO-*b*-PDLA solution, spherical micelles were obtained for both; however, the mixed solution's micelles were smaller in diameter due to sc crystallization-induced contraction.[161] The morphological transition from cylinders to spheres was likely due to a similar contraction upon sc crystallization. For the stereo triblock copolymer, sc crystallization was observed except when the middle PDLA block was small, in which case a mixture of hc and sc was found. Additionally, the sc-crystallized spherical micelles maintained their morphology after drying; whereas, the hc-crystallized samples did not. This morphological change was further evidence that sc crystals are more stable.

Overall, sc crystallization was promoted by using BCP PLA materials. The inclusion of another block improved the mobility of the PLA chains to enhance sc crystal formation. This behavior seemed to supersede formation of hc crystals in systems where hc crystallization would be more favorable. For stereoblock copolymers, the covalent attachment of the two enantiomers promoted sc crystal formation compared to enantiomeric BCP/homopolymer blends. Chain architecture also impacted the crystallization mechanism, kinetics, and crystallinity. The restricted mobility and core-shell architecture hindered sc crystallization and formed less stable crystals compared to their linear counterparts.

UNIQUE BLOCK COPOLYMERS AND THEIR ASSEMBLIES

In this section, we will review crystalline BCPs where the chemical structure is designed for unique applications or for unique crystallization possibilities. Primarily, rod-coil block copolymers where the rod-like block undergoes crystallization have gained popularity in recent years with the development of organic electronics. It is known that the conductivity of these polymers increases in the crystalline state due to proximity of charge carriers.[163] Different main chain as well as alkyl side-chain (to enhance mobility and solubility) structures have been synthesized to improve conductivity in these materials. The inclusion of additional blocks provides templating or dielectric constant contrast for specific applications.

Highly-branched polymers of different architectures[164] have gained interest due to their modified assembly structure, chain relaxation, and potential for using common polymer chemical composition in new architectures to impart different mechanical, optical, environmental, or other properties. Here, these structures include graft (block) copolymers, where block chemistry is changed between the main chain and grafts, with two different grafts, or a block copolymer with one block grafted and the other not. Few studies have looked at the crystallization of densely-branched architectures because of steric factors; though, a couple studies are highlighted here.

Other synthetic strategies include using biological or polypeptoid-based blocks with conventional semi-crystalline components to form diblock copolymers. The assembly of these copolymers can be used to help tailor materials for specific biological or environmental applications. Supramolecular block copolymers are formed through non-covalent interactions, such as hydrogen bonding or metal-ligand complexation, at the junction point. The supramolecular strategy has been employed for diblock, triblock,

and multiblock copolymers. This unique coupling technique changes the mobility and crystallization of polymers. These strategies provide polymeric materials with new chemical and physical properties in conjunction with the hierarchical structure of crystalline BCPs, opening new avenues for polymer applications.

Copolymers with Rod-Like Blocks

Copolymers with rod-like blocks have been the focus of recent work because the rod-like moiety often involves conjugated polymers, which can be used in photovoltaic, semiconductor, and other electronics technologies.[165-166] Much of the work has been focused on controlling the morphology of the conjugated block's domain, which can be accomplished by a variety of methods, including using varying solvent quality for solution assembly,[167-174] thermal history for bulk samples,[175-182] and varying compositions,[167-182] to improve the conductive qualities of the material. Most rod-like blocks studied here are thiophene-based and were combined with either a coil block that may or may not be semi-crystalline,[167-173,178-182] or a second rod-like block (all-conjugated).[174-177] Alternatively, copolymers with liquid crystalline blocks (LC) that behave as rod-like chains have advantageous optical and electronic properties. The rigidity of the mesogenic portion imparts the rod-like chain structure. Here, crystallization of the coil block is influenced by the phase behavior of the ordered microphase separation as well as the rigidity of the LC block.[183-190] LC properties of these materials will not be discussed.

Most conjugated polymer work has focused on poly(alkylthiophenes). There have been several studies concerning the morphological behavior of the most common BCP rod-like polymer, poly(3-hexylthiophene) (P3HT), because of its value as a conductor and light absorber. Because the alkyl chain on the 3-position of polythiophenes helps to organize the structure and provide increased solvent processability, work has focused on other polythiophene block copolymers such as poly(3-(2′-ethyl)hexylthiophene) (P3EHT)[174,178-180] and other poly(alkylthiophenes), such as poly(3-butylthiophene) (P3BT) and poly(3-dodecylthiophene) (P3DDT).[177,181-182] With longer substituent alkyl chains, poly(alkylthiophenes) exhibit depressed melting temperatures relative to P3HT which allows them to robustly form microphase-separated domains that confine the other block in block copolymer mixtures.[178,180]

Focusing on P3HT first, one method for controlling its morphology is solution crystallization with varying solvent quality. Many studies have been focused on PEO-*b*-P3HT[167-170] because PEO can help solubilize the polymer for controlled solution assembly. The assembly of these systems is driven by the precipitation of P3HT into cylindrical, or rod-like, crystals. Solvent selectivity for either the PEO or P3HT block, as well as the block length, affected the resulting cylindrical morphology. PEO provided colloidal stability for a variety of morphologies including cylinder rods,[167,169-170] nanowires,[168] and spherical and/or cylindrical micelles.[168] One study found that a "good solvent" for P3HT resulted in crystallization-driven assembly of P3HT into cylindrical micelles.[167,168] Poor solvents for P3HT led to larger aggregates to form more worm-like or densely-packed patterns. When starting with good solvent, like chloroform, solution crystallization of P3HT was induced by the addition of methanol, slowly making the solvent poorer for P3HT. Phase-separated PEO-*b*-P3HT films were formed from dilute chloroform solutions because of good solubility of both blocks. In solution, P3HT remains coil-like without aggregation as monitored by UV-Vis and PL spectroscopy. After film formation and drying, the BCP forms P3HT-rich and PEO-rich domains, where the P3HT likely stays amorphous. Unfortunately, crystallization of the coil-P3HT dried film was not evaluated for either P3HT or PEO.

The block length of PEO also affected the assembly, as one study by Reichstein *et. al.*[170] demonstrated. Using AFM, dynamic light scattering (DLS), and TEM, the morphology of assemblies with different PEO block lengths were observed. As shown in Figure 22, they found that when using methanol as a non-solvent for P3HT, the block copolymers of PEO-*b*-P3HT formed stable micellar aggregates that had spherical or cylindrical shapes if $w_{PEO} > 0.31$. Furthermore, use of shorter PEO blocks lead to bigger BCP micelles. The relationship between morphology and composition is shown in the schematic of Figure 21. Agbolaghi *et al.*[169] used a PEO-*b*-P3HT sample with $w_{PEO} = 0.42$ to crystallize in solution following different protocols to induce selective crystallization of one block and/or crystallization of both blocks. In amyl acetate, P3HT crystallized to form rod-like scrolled single crystals at temperatures below 30ºC with PEO chains attached to the *ab*-plane of the crystal. When the solution was cooled to 10ºC, both components were crystalline, as confirmed by TEM SAED. Interestingly, the PEO showed single-crystal-like diffraction with the (120) spot appearing with the (020) and (002) spots of the P3HT. Alternatively the order was switched, and PEO crystallized from homogeneous solution when homopolymer PEO crystal seeds were introduced. The PEO block crystallized on the homopolymer seed growth surface with P3HT tethers. In this case, P3HT crystallized at similar temperatures on the basal surface of the square PEO crystals as confirmed by the appearance of (100) and (020) diffraction spots in addition to the $(120)_{PEO}$, but no scrolling was observed. It has been shown that factors that influence crystallization of the secondary block include layer thickness and tethering density.[191] This may help explain the difference in tethered chain crystallization. Unlike the PEO seeded solution, when the solution was seeded with homopolymer P3HT crystals, fibrillar crystal stacks were formed with laminated P3HT backbones at one basal surface and coily PEO segregated to the other surface.

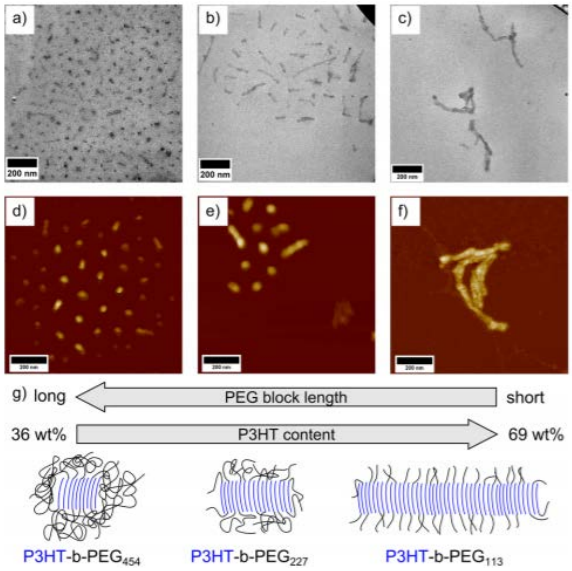

FIGURE 22 (a-c) Cryo-TEM and (d-f) AFM height images of PEO-*b*-P3HT micelles with decreasing PEO fraction (left to right). Schematic model of possible structures for the aggregates shown in images (g) (Reproduced from [170] with permission from the American Chemical Society.)

Assembly of all-conjugated systems demonstrated similar behavior. Researchers investigating poly(2,5-dihexyloxy-*p*-phenylene) (PPP)-*b*-P3HT[171-172,176] observed different assembly due to microphase separation driven by the selectivity of solvent or during drying of thin films. For PPP-*b*-P3HT copolymers,

both blocks are crystalline with $T_m^{PPP} < T_m^{P3HT}$. For the non-selective solvent chlorobenzene, both blocks maintained coil-like conformations in solution.[171-172] Films cast from chlorobenzene had microphase-separated morphology driven by aggregation/crystallization of the larger block. As the solvent quality decreased for the P3HT block (xylene and anisole), solution assembly occurred and was observed *via* a red-shift in UV-Vis, as shown in Figure 23, and fibrillar structures in AFM and TEM were observed when the P3HT block was sufficiently large. The crystallization of P3HT was the driving force for BCP assembly. To confirm that solution crystallization occurred, samples were cast from hot anisole, and microphase-separated morphologies similar to chlorobenzene films were seen. The crystallization of each block was influenced by the block lengths. Like most CC BCPs, when the weight fraction of the block was similar, both crystallized. Samples with a larger PPP or P3HT block had diminished crystallinity in the smaller block and the influence of solvent on the assembly pathway was less pronounced. Similar results were found for P3HT-*b*-poly(3-(6-hydroxy)hexylthiophene) (P3HT-*b*-P3HHT) materials,[173,175] where pyridine was the good solvent; methanol was the selective solvent to precipitate P3HT; and chloroform was selective for P3HHT. P3HHT has the added advantage of being cross-linkable through thermal condensation reactions.[175] A study by Lee *et. al.*[174] found that P3EHT-*b*-poly(thiophene) (PT) copolymers could form nanostar and nanonetwork aggregates during solution assembly in organic solvent due to the high solvophobicity of non-substituted PT. The PT block aggregated to form a crystalline core as evidenced by the (110) reflection in X-ray diffraction (XRD). Increasing the block length of the PT shifted the solution morphology from nanospheres to nanorods to nanostars to nanonetworks because of the increased exposure of the PT core to the surrounding solvent. DSC and XRD showed that the collection of aggregates and subsequent drying led to P3EHT crystallization in addition to PT. The proposed mechanism for nanonetwork formation is shown in Figure 24. The mechanism here may be similar to the one discussed in the diblock copolymer section; however, it may have been driven by assembly of the coronas while maintaining segmented crystalline cores instead of epitaxial crystal aggregation.

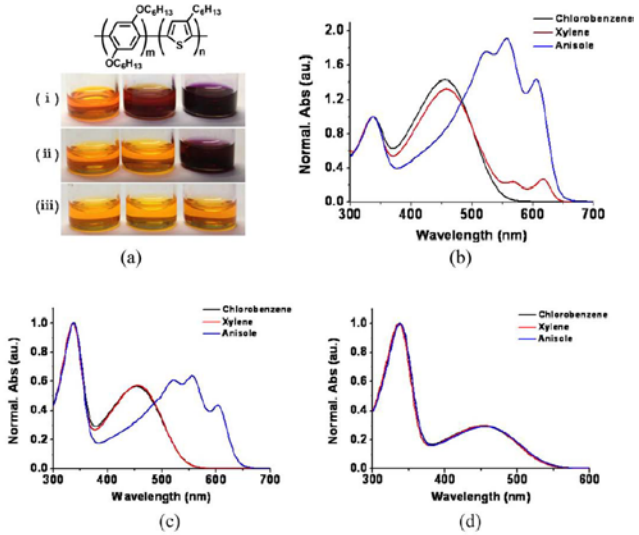

FIGURE 23 (a) Photographs of PPP-b-P3HT copolymers [(i) $w_{P3HT} \approx 0.62$; (ii) $w_{P3HT} \approx 0.41$; (iii) $w_{P3HT} \approx 0.07$] in various solvent (from left to right: chlorobenzene, xylene, and anisole). Normalized UV-Vis spectra for (b) $w_{P3HT} \approx 0.62$, (c) $w_{P3HT} \approx 0.41$, and (d) $w_{P3HT} \approx 0.07$ where solutions were left in a dark and vibration-free environment for 24 hrs at room temperature prior to analysis. (Reproduced from [171] with permission from Wiley.)

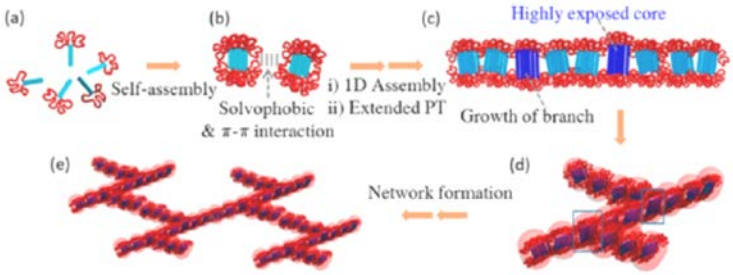

FIGURE 24 Proposed mechanism for solution assembly of P3EHT-*b*-PT into branched nanoparticles (Reproduced from [174] with permission from the American Chemical Society.)

In another attempt to control rod-like polymer assembly, Yang and coworkers[176] demonstrated that the crystal orientation of PPP-*b*-P3HT crystals in bulk materials could be manipulated using BCP self-epitaxy. Homopolymer PPP exhibited a face-on (ring-parallel) orientation in thin films,[192] while P3HT showed an edge-on (ring-perpendicular) structure.[193] In the pure BCP film, a sample with w_{P3HT} = 0.32 showed only PPP crystallization by 2D GIXD in the as-cast film with a face-on orientation in the as-cast film. The sample was heated to melt PPP crystals. During cooling, P3HT crystals formed at higher T with an edge-on orientation. Further cooling resulted in PPP crystals that also had an edge-on orientation, demonstrating that self-epitaxy influenced the PPP crystal orientation. If the sample was heated near the T_m^{PPP} (78° – 97°C range), partial melting of PPP resulted in favorable mobility and extension of P3HT blocks. The resultant P3HT crystals had face-on orientation due to self-epitaxy of the PPP face-on crystals and maintained this orientation even after melting of PPP crystals during a second heating. Edge-on orientation was regained after melting of P3HT crystals. This behavior was reproducible in other block copolymers where the size of each block favored double-crystalline materials. This demonstrates that interactive crystallization of coil-based crystalline polymers extends to rod-like polymers as well.

A study by Ge *et. al.*[177] found that in CC P3BT-*b*-P3DDT, P3BT blocks with shorter alkyl side-chains crystallized at high temperature ($T_m^{P3BT} \approx 230$°C). This crystallization led to the formation of microphase-separated lamellar structures as determined by SAXS and WAXD. Subsequent cooling resulted in the rapid crystallization of P3DDT blocks at relatively low temperatures ($T_m^{P3DDT} \approx$ 165-175°C). Surprisingly, the domain spacing for the crystallization-driven phase separation was unaffected by changes in the BCP composition with w_{P3BT} = 0.22 – 0.49. Additionally, within domains between the crystallites, there existed both amorphous P3BT and P3DDT in a miscible state since the crystallinity of both components is relatively low. Thus, controlling crystallization in these CC BCP materials may prove difficult as phase separation occurred only with crystallization sequence.

Microphase separation in BCPs with conjugated blocks provides another methodology for patterning and templating the conductive domains. Several studies by Davidson and coworkers[178-180] evaluated the crystallization of P3EHT in poly(methyl acrylate)-*b*-P3EHT (PMA-*b*-P3EHT) copolymers where the PMA block was above T_g. The rubbery PMA provided soft confinement and molecular mobility to promote crystallization in the P3HT domains (as compared to PS-*b*-P3EHT materials).[180] They designed and confirmed melt microphase separation for lamellae-forming ($f_{P3HT} \approx 0.46 – 0.66$)[179-180] and cylinder-forming ($f_{P3HT} \approx 0.10 – 0.21$)[178] samples using TEM and SAXS. P3EHT crystallization was possible in the phase-separated state for all samples, and break-out crystallization did not occur with soft confinement. Within the lamellar morphology, expansion and contraction of the P3EHT phase was

controlled by the T_c; however, the correlation was unexpected since larger T_c resulted in contraction of the domain. Similar results were found for the cylinder-forming BCP. In both morphologies, the P3EHT crystal chain axes aligned perpendicular to the domain interfaces due to the π–π stacking interactions. They found that the diblock copolymer domain size was significantly impacted by T_c as shown in Figure 25. The researchers determined that the unusual contraction at high T_c was due to more complete crystallization. It was assumed that high T_c would lead to thicker crystals and thus an expansion of the domain. However, the authors proposed that the low T_c crystals are smaller with lower crystallinity and higher RAF-like (rigid amorphous fraction) domains for the rod-like chain (extended chains excluded from the central crystal).[19] This led to a larger required volume (larger domain). When T_c is increased, the previously amorphous portions were included in the crystalline material, resulting in a decrease in the domain volume. They proposed that this was possible because the crystals are not typical chain-folded polymer crystallites. This feature was facilitated by the rubbery nature of PMA, allowing rearrangement of the P3EHT chains for inclusion in the crystal (Figure 25). Controlling crystallization in the cylindrical morphology was more difficult because of the orientation of the crystals' (100) direction along the long axis of the cylinder, therefore, melt-recrystallization mechanisms, like self-seeding, are better suited for improving crystallinity in this material.[178]

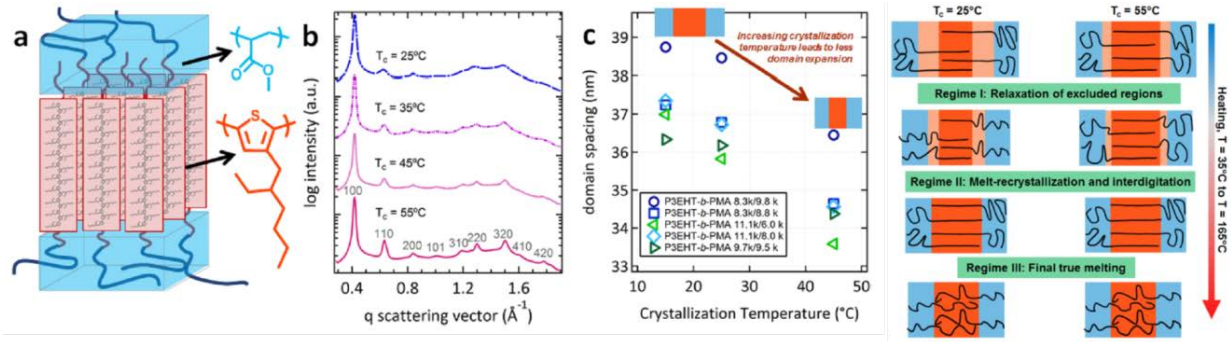

FIGURE 25 (a) Cartoon of crystalline PMA-*b*-P3EHT with P3EHT chains perpendicular to the domain interface. (b) WAXD data for isothermal crystallization of P3EHT phase where most compact structure occurs at highest T_c. (c) SAXS domain spacing as a function of T_c. Variability in molecular weight dependent domain size likely due to chain polydispersity. (far right) Cartoon of suggested relaxation and melting mechanism across the three regimes where the initial state depends on T_c. (Reproduced from [179] with permission from the American Chemical Society.)

Several groups also studied the influence of architecture on the crystallizability of one block. For conjugated polymer crystallization, P3DDT was studied in a PMMA-P3DDT$_2$ miktoarm star copolymer and compared to PMMA-*b*-P3DDT.[181-182] For the linear BCP, larger PMMA fractions led to typical BCP microphase-separated morphologies; however, with larger P3DDT, break-out crystallization occurred giving a crystalline fibril structure morphology.[182] In an attempt to control the morphology of majority-phase P3DDT, Park *et al.*[181] chose to make miktoarm star P3DDT$_2$-PMMA copolymers, where the PMMA block can be thought of as tethered to the central portion of the P3DDT component. In these materials, the w_{P3DDT} was varied between 0.33 and 0.76. For w_{P3DDT} = 0.33 and 0.48, a lamellar morphology was observed *via* TEM and SAXS. The linear counterpart showed P3DDT hexagonal cylinders for w_{P3DDT} = 0.33. When $0.59 \leq w_{P3DDT} \leq 0.76$, a PMMA hexagonal cylinder morphology was observed. Surprisingly, even at low temperature with crystalline P3DDT, the cylindrical morphology was maintained. This was due likely to the low crystallinity of P3DDT$_2$-PMMA compared to PMMA-*b*-

P3DDT with P3DDT fibrils. It is unclear how the large, central linker molecule influences the resulting behavior. For crystallization of a flexible polymer attached to a stiff, uncrystallized rod-like block, miktoarm star copolymers were evaluated using poly(*n*-hexyl isocyanate) (PHIC), a non-conjugated, helical, rod-like polymer.[183-184] In thin films of PCL$_m$-PHIC, PCL crystallization was observed with no apparent phase transitions in the PHIC block. With similar volume fractions of PHIC but different numbers of PCL arms (m = 1, 2, or 3), the PCL crystallization became more restricted.[183] Both the T_c^{PCL} and heat of fusion (ΔH_f^{PCL}) decreased significantly when going from a linear BCP (m = 1) to a miktoarm star of m = 2 or 3. Here, the rigidity of the rod-like block decreased mobility of the PCL and limited its ability to crystallize. With varying molecular characteristics (f_{PHIC} as low as 0.246), GIXS showed that the orientation of the lamellar microphase-separated state as well as PCL crystal orientation varied with preference for the PCL *c*-axis parallel to the layer normal direction.[184] These studies again demonstrated the influence of tethering placement on the formation of polymer crystals in systems with different chain physical structure.

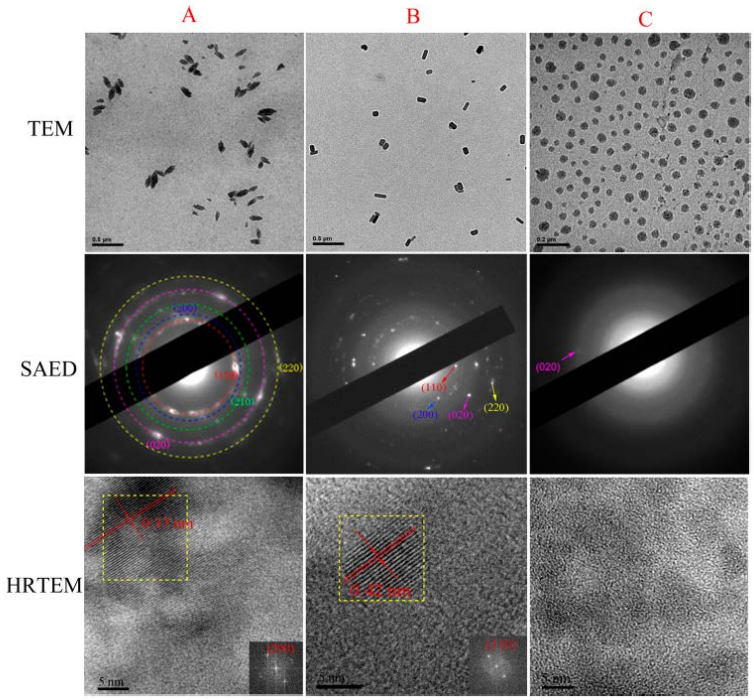

FIGURE 26 Self-assembled morphologies of *q*PDM/MO-*b*-PCL (A) w_{PCL} = 0.65, (B) w_{PCL} = 0.54, and (C) w_{PCL} = 0.36 (top) TEM images, (middle) SAED patterns, and (bottom) HRTEM images with fast Fourier transform image insets. (Reproduced from [186] with permission from the American Chemical Society.)

The influence of chain rigidity for the non-crystalline component was studied using another robust system, namely LC block copolymers. Steric interaction of LC block mesogens provides long persistence lengths that give the LC block rigid, rod-like properties similar to conjugated polymer backbones. Some studies have been performed looking at the influence of these LC blocks on the crystallization of PCL blocks,[185-186] PEO blocks,[187-189] and PLLA.[190]

LC interactions of the second block was shown to influence PCL crystallization both in the bulk[185] and in solution.[186] Poly(2,5-bis[4-methoxyphenyl]oxycarbonyl)styrene)-*b*-PCL (PMPCS-*b*-PCL)

was studied to evaluate the influence of lamellar "hard" confinement (T_g^{PMPCS} = 110°C) on PCL crystallization, crystal orientation, and melting temperature.[185] PMPCS is a mesogen-jacketed polymer, where the mesogen director is parallel to the polymer backbone, and has a columnar LC phase. Using 2D WAXD, it was found that at T_c^{PCL} > 10°C, the *c*-axis of PCL crystals was parallel to the layer normal direction. At T_c^{PCL} < 10°C, the *c*-axis was tilted, but the *b*-axis remained perpendicular to the layer normal. These results are similar to previous reports of confined crystallization in diblock copolymers.[30-41,56-58] Solution assembly was performed in another study by Tong *et al.*[186] where they investigated the effect of different weight fractions on the micellar morphologies of poly(quaternized 2-(dimethylamino)ethyl methacrylate/methyl orange)-*b*-PCL (*q*PDM/MO-*b*-PCL). Here, ionic interactions between the *q*PDM and MO created a LC-type polymer block in water. The hydrophobic PCL block formed the crystalline core; while, the *q*PDM/MO block formed the corona. The authors found that short *q*PDM/MO blocks (w_{PCL} = 0.65) formed spindle-like micelles; moderate blocks (w_{PCL} = 0.54) formed rod-like micelles; and large hydrophilic blocks (w_{PCL} = 0.36) formed spherical micelles. Additionally, PCL crystallization was confirmed by TEM SAED and High Resolution (HR) TEM for all non-spherical micelles, as shown in Figure 26. The researchers were able to control the morphology by the addition of hydrophobic surfactant, bis(2-ethylhexyl) sulfosuccinate sodium salt (AOT). AOT replaced the MO along the *q*PDM chain reducing the solubility of the corona-forming block. This change in corona free energy led to the formation of crystallization-driven PCL platelet, fibril, and dendrite-like morphologies. This study supports the idea that the free energy of the corona-forming block stabilizes the micelle morphology after crystallization of the core-forming block, preventing "breakout"-like single crystal morphologies.

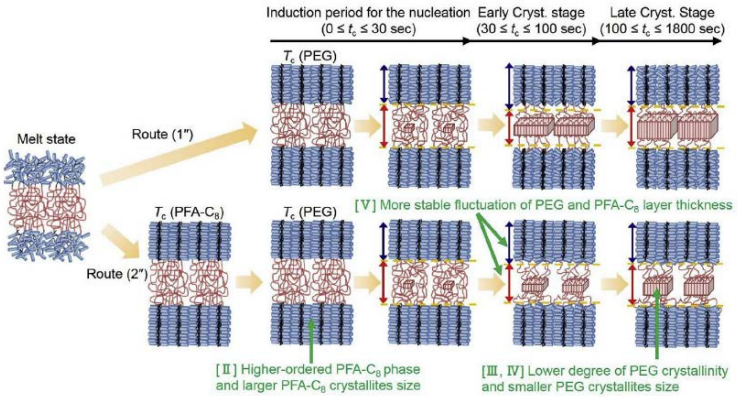

FIGURE 27 Schematic illustration of the structure formation process of PFA-C_8-*b*-PEO during isothermal crystallization via Routes (1″) and (2″). The green-colored descriptions indicate the structure parameter contrasts found between the two Routes. (Reproduced from [187] with permission from Elsevier.)

Bulk properties have been studied for PEO[187-189] and PLLA.[190] Poly(perfluorooctylethyl acrylate) (PFA-C_8) is an LC polymer that exhibits a highly-ordered smectic phase that resembles a disordered crystal phase due to low mobility.[194-195] Studies with strongly-segregated, lamellar PFA-C_8-*b*-PEO (f_{PEO} = 0.44) found that PEO crystallization (T_m^{PEO}, crystallinity, and kinetics) was influenced by the low mobility of the PFA-C_8 phase similar to other studies of rod-coil BCPs mentioned in this review. Nojima *et. al.*[188] found that in early stage isothermal crystallization of PFA-C_8-*b*-PEO after quenching to T_c^{PEO} (Figure 27, 1″), there was three dimensional growth of PEO lamellar crystals within a microphase-separated morphology. When the PFA-C_8 phase was less ordered (more mobile), the crystallization

process reduced the thickness of the PEO domain and increased the thickness of PFA-C_8 phase as determined by simultaneous SAXS/WAXD. On the other hand, in late stage isothermal crystallization, one dimensional growth of PEO lamellar crystals induced increases in PEO layer thickness, due to crystal thickening, and a reduction in thickness of the PFA-C_8 layer. If, however, the PFA-C_8 phase was pre-ordered by holding at the transition temperature for PFA-C_8 prior to isothermal crystallization at T_c^{PEO} (Figure 27, 2″), the PFA-C_8 layer thickness remained relatively constant in all stages of PEO crystallization, resulting in less perfect PEO crystallization.[187]

A study of PEO in a BCP with LC behavior, where LC structure was induced by complexation of 2-(3′,4′,5′-tris(octyloxy)benzamido)propanoic acid (TOBPA) ligand with P2VP, showed phase separation induced by the LC ordering of the amorphous P2VP phase during complex formation between the ligand and P2VP, a somewhat opposite effect compared to *q*PDM/MO-*b*-PCL with AOT.[186] The pure P2VP-*b*-PEO (w_{PEO} = 0.60) exhibited minimal PEO crystallization due to the miscibility and hydrogen bonding between the blocks.[196] When TOBPA was added, PEO crystallization was promoted and occurred at T_c^{PEO} = 20.5ºC during DSC cooling. With an increase in TOBPA content, PEO crystallization was hindered as evidenced by lower T_c^{PEO} and lower crystallinity. GISAXS and microscopy images showed that the higher TOBPA content created a microphase-separated state with P2VP-TOBPA as a smectic LC matrix phase and PEO hexagonally-packed cylinders as the minority phase. This phase separated state promoted PEO crystallization compared to the pure P2VP-*b*-PEO; however, due to "hard" confinement and mobility effects, PEO crystallization was less favorable in highly-ordered formulations.

PLLA provides more diverse crystallization behavior compared to other polymers, such as PEO and PCL. Recent work on poly(6-(4-(4-methoxyphenylazo)-phenoxy)hexyl methacrylate)-*b*-PLLA (PMMAzo-*b*-PLLA) found strong correlations among weak phase separation, LC ordering of the PMMAzo block, and crystallization of PLLA block.[190] PLLA crystallization intensified microphase separation as seen with sharper SAXS peaks and promoted LC ordering as seen in DSC. Alternately, when the LC structure was formed first, the crystallization of PLLA was hindered as seen by a lack of cold crystallization; however, when crystals were formed, break-out crystallization occurred destroying the weakly-segregated domains. There was some WAXD evidence of ε-phase PLLA crystal formation for specific samples, w_{PLLA} = 0.45 and 0.49 with $M_n^{overall} \approx$ 17k, when annealed at 115ºC, where the PMMAzo block was in the nematic phase. This implies that the free energy landscape of crystal formation was influenced by the moderate immobility of the PMMAzo. At other annealing and w_{PLLA} conditions, PLLA crystallization was diminished or the PMMAzo phase was destroyed during breakout crystallization.

Crystallization in BCPs with rod-like blocks is a growing field with three major foci: 1) self-assembly of rod-like blocks in solution, 2) crystallization behavior of conjugated, rod-like polymers for energy applications and 3) influence of rod-like blocks on the assembly and crystallization of semi-crystalline, coil blocks. Each of these areas are rich with new fundamental physics to be explored and unique opportunities for design of engineered materials. With fundamental understanding of rod-like block assembly and crystallization, it should be possible to tailor morphological features for smart design of materials and products with high, efficient transport of electrons and/or photons.

Copolymers with Highly-Branched Architectures

As discussed in previous sections, star copolymers are an important area that has been central to recent work.[42,60-61,147,154-160,181-184] Some work has compared these copolymer architectures to their linear counterparts and have found decreases in crystallinity and even different morphologies. If the common-tethered junction point restricts crystallization in materials with fewer than eight arms, the crystallization

properties of highly-branched materials with numerous tethering points and chain ends provides a more diverse approach to this phenomenon. Here, blocks are tethered/constrained in ways different than the single tether; however, the crystallization behavior is related. Recent work has been focused on the morphologies of highly-branched copolymers, such as graft copolymers,[197-203] brush copolymers,[204-207] and hyperbranched copolymers.[203,208-209] For this review, we have focused only on highly-branched BCP architectures (molecular schematics in Figure 28) where polymer chains are involved in the crystallization process. Specifically, systems that lower grafting density with homopolymer grafts, typically using random or precisely-controlled backbone copolymers with non-functional secondary monomers where the backbone chain remains highly flexible, diblock copolymer grafts, or brush architecture that includes two different graft chemistries are presented.

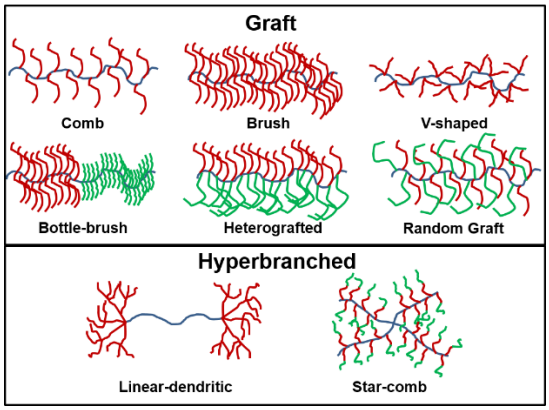

FIGURE 28 Schematic of the highly-branched BCP architectures discussed in this section.

Several studies have been conducted on PCL-based graft copolymers.[197-200] A P(HEMA-*g*-PCL)-*b*-PCL polymer was synthesized by Ninago and coworkers.[199] The architecture was a PHEMA-*b*-PCL backbone with PCL side chains either sparsely (comb-like) or densely (brush-like) tethered to the PHEMA only. These PCL-based graft copolymers demonstrated that the presence of branches reduced the PCL melting temperature by 5°C for brush-like architecture and 15°C for comb-like compared to linear PCL without affecting thermal stability. Additionally, more densely branched copolymers with higher molar masses led to a decrease in crystallization rate. It should be noted that the PCL chains were relatively short, especially compared to the linear standard. Another study of short chain PCL grafts was evaluated using poly(glycerol adipate) (PGA) backbones.[200] The PCL crystallization occurred at lower temperatures and nucleation density increased compared to homopolymer PCL of similar length. The same was true for PGA-*g*-PEO. Because of the short length of both PCL and PEO grafts, the lamellar thickness determined by SAXS confirmed the presence of extended chain crystals at small undercoolings.

Double crystalline graft copolymers with comb-like structures were evaluated with different compositions and architectures. PCL-*b*-PLLA chains were grafted onto PB backbones by Leng *et al*.[203] Here, $T_c^{PCL} < T_c^{PLLA}$ is an additional factor in development of polymer crystals. The PCL block was on the interior, and the PLLA was at the graft chain end. As the weight fraction of each block increased, its corresponding crystallinity increased. However, at $w_{PCL} = 0.20$, no PLLA crystallization was observed in DSC even though at $w_{PCL} = 0.35$ and 0.48, both components crystallized more effectively than the linear counterparts. The M_n^{PLLA} for the $w_{PCL} = 0.20$ was the largest of all samples. This, along with the grafted nature, implies that the mobility of PLLA was largely hindered. BCP grafts of PEO-*b*-PCL were studied with PEO[198] or PGA[200] backbones. The PGA-*g*-(PCL-*b*-PEO) had PCL as the interior grafted block, while

the PEO-*g*-(PEO-*b*-PCL) had PEO interior blocks in close proximity to the homologous backbone chain. Again, grafting of the PEO-*b*-PCL changed the crystallization behavior compared to ungrafted BCPs (similar to homopolymer graft results).[200] The crystallization of the PCL interior block was dependent on the PCL molecular weight. The small molecular weight of the grafted copolymer resulted in extended chain crystals with some amorphous cilia protruding from the surface for PCL and PEO crystals. For PEO-*g*-(PEO-*b*-PCL), the molecular weight of both components was larger than other studies. DSC data showed crystallization occurred for all samples; however, detailed information about the individual blocks was difficult to deconvolute. XRD data showed that when PCL blocks were large, only PCL crystallized, even with the PEO backbone. With smaller PCL blocks, diffraction peaks for both components was observed, as shown in Figure 29. An additional study of V-shaped PCL grafts in PEO-*g*-PCL_2 by Ma *et. al.*[197] found that both PCL and PEO were crystalline due to the large molecular weights of both blocks. Similar to linear PEO-*b*-PCL,[15,16] when PCL side chain content was small (w_{PCL} = 0.09), PEO crystallization dominated. When w_{PCL} = 0.59, the crystalline structure was dominated by PCL, and PEO crystallization, while still observed, was greatly diminished as determined by lower T_c and ΔH_f. At intermediate w_{PCL}, crystallization of the two blocks was comparable and somewhat indistinguishable.

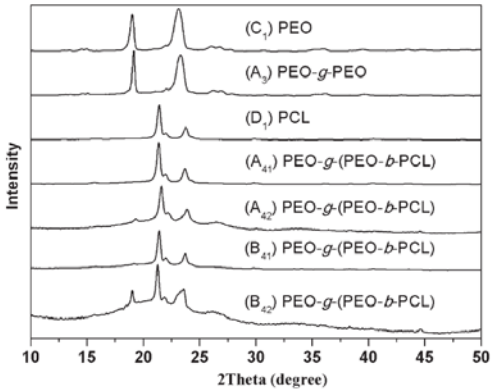

FIGURE 29 XRD data of linear PEO, linear PCL, PEO-*g*-PEO, and PEO-*g*-(PEO-*b*-PCL). A_{41} and B_{41}: large PCL blocks; A_{42} and B_{42}: small PCL blocks. In all PEO-*g*-(PEO-*b*-PCL) shown here, M_n^{PEO} is relatively similar. (Reproduced from [198] with permission from the Royal Society of Chemistry.)

Heterografted chains with a non-block configuration were studied by Gao *et al.*[201] to study the crystallization of PEO in PB-*g*-(PB;PEO). The heterograft was formed by epoxidizing the 2,3-alkene; using a "grafting to" approach to add PB to the 2 position in the presence of methanol to convert the epoxide into an alcohol on the 3 position; and using anionic polymerization to convert the alcohol into a PEO side chain. Here, the moderate molecular weight PB and PEO grafts occurred on the same monomer. Due to 1,2-diene content from anionic polymerization of butadiene (~10%) and fractional epoxide functionalization (~20%), the resulting architecture resembled comb-like polymers but with two grafts on the same monomer. The rAC nature of the copolymer provided flexible, mobile side chains in studying their effect on PEO crystallization. The w_{PEO} ranged from 0.06 to 0.35. At low w_{PEO}, small exothermic peaks were observed in DSC, demonstrating that PEO crystallization was difficult. At higher w_{PEO}, two peaks below 0°C were observed, indicating a fractionated crystallization process. The architecture of the graft copolymer had a clear confining effect on the PEO as homogeneous nucleation of PEO often occurs at T < -5°C depending on PEO volume.[210] This also was supported by Avrami exponents of n < 1.

Brush copolymers of varying architectures were used to study the crystallization of PEO,[204-205] PCL,[206] and stereo PLLA/PDLA side chains.[207] In one PEO study, a poly(norbornene) backbone was grafted with PS and PEO chains in a BCP type architecture where PS chains were grafted on one half while PEO chains were grafted on the other to form bottlebrush block copolymers (BBCP).[204] Each graft M_n was varied over a range of f_{PEO} = 0.22 – 0.81. Gai *et. al.*[204] found that lamellar and cylindrical phase-separated morphologies were observed dependent on f_{PEO} though somewhat independent of M_n^{PEO}. Crystallization of PEO occurred in the microphase-separated under hard confinement of the PS, as shown in Figure 30. The SAXS morphological features were maintained above T_m as measure by WAXD. In another brush copolymer PEO study, core-shell type grafts of PEO-*b*-PPO were attached to a poly(hydroxystyrene) backbone.[205] The placement of the PEO chain was switched between the core (inside) block and the shell (outside) block, and the M_n^{PEO} shell block was varied (w_{PEO} = 0.23 – 0.85). Based on DSC analysis, the PEO core block (M_n^{PEO} = 13.8k, w_{PEO} = 0.85) crystallized comparably to homopolymer PEO. Surprisingly, the PEO shell blocks (M_n^{PEO} = 1.7k – 11.8k, w_{PEO} = 0.23 – 0.68) crystallized at temperatures below 0°C with decreasing T_c and crystallinity for the smaller PEO fractions. It is expected that the shell blocks would crystallize more easily than the core blocks based on previous mid-block triblock and star-block copolymer crystallization trends. SAXS/WAXD analysis showed that the blocks are microphase-separated above T_m^{PEO}.

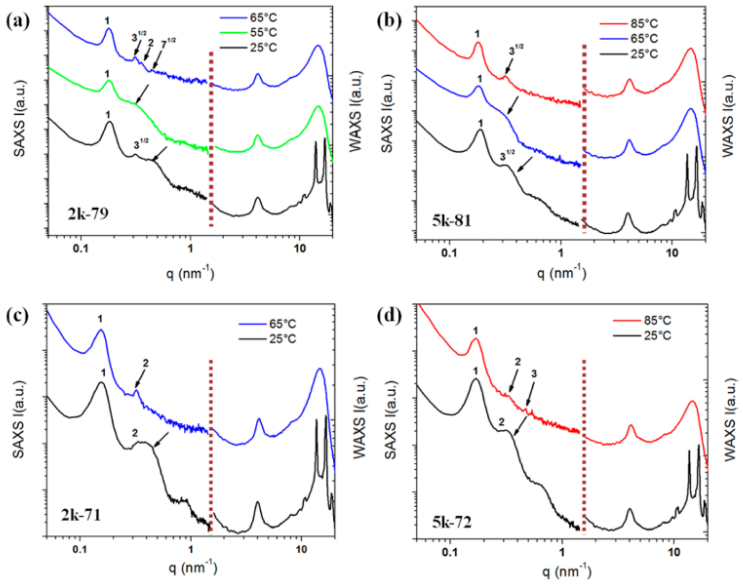

FIGURE 30 Temperature-controlled SAXS and WAXS 1D profiles of PS-PEO BBCPs containing high volume fractions of PEO: f_{PEO} = (a) 0.79 (M_n^{PS} = 2k) (b) 0.81 (M_n^{PS} = 5k) (c) 0.71 (M_n^{PS} = 2k) and (d) 0.72 (M_n^{PS} = 5k). (Reproduced from [204] with permission from the American Chemical Society.)

Crystallization of PCL also was influenced by high-density brush grafting.[206] From a polymethacrylate backbone, PS and PCL were grafted in a random pattern along the backbone due to copolymerization of different methacrylates. P(PS-*r*-PCL) copolymers with short molecular weights per graft and w_{PCL} = 0.22 – 0.58. Crystallization of PCL with lowered T_c was observed *via* DSC in all samples except w_{PCL} = 0.22. It was observed by AFM and SAXS that the material was phase separated, indicating hard confinement behavior of the PS (T_g = 90°C). Similarly, PLLA and PDLA were grafted onto a poly(norbornene) backbone in a random fashion to study stereocomplex crystal formation.[207] Both

components had M_n ~ 5.0k. A diverse set of architectures were developed, as shown in the cartoon of Figure 31, to evaluate the role of distribution and relative chain direction on the ability of PLLA and PDLA to co-crystallize. For all synthetic designs shown in Figure 31, solution-cast films formed sc crystals exclusively as observed by XRD and DSC. Blends of the starting material PLLA and PDLA resulted in mixtures of hc and sc crystals. It was found that samples with parallel orientation (left side of Figure 31) had higher T_ms, higher crystallinity, and better crystal uniformity compared to the anti-parallel arrangement (right side of Figure 31). Unfortunately, the more macroscopic crystal structure was not evaluated for this system.

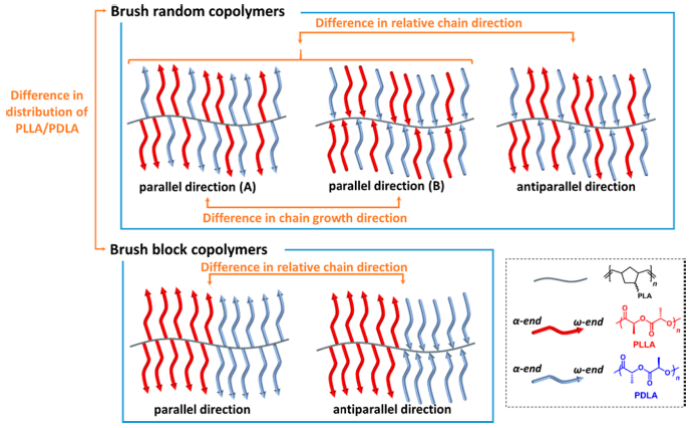

FIGURE 31 Schematic representation of parallel/antiparallel direction and brush architecture in PLLA-PDLA brush copolymers (Reproduced from [207] with permission from the American Chemical Society.)

Hyperbranched block copolymers have attracted some attention in recent years as well. The examples provided here have a star comb-like BCP graft architecture[202-203] or a linear Block A chain with dendritic Block B ends similar to an ABA triblock.[208-209] Leng *et. al.*[203] also studied star comb-branched scPCL-*b*-PLLA architectures. This topology was found to have only PCL crystallization (small exothermic DSC peak in highest PLLA fraction only). PLLA crystallization was facilitated by isothermal annealing at 110°C. Compared to the linear-comb topology, the star-comb shape presents some steric hindrance of the graft points which decreases the crystallinity of star-comb PCL-*b*-PLLA as shown by POM. Gao and coworkers[202] also studied 4-arm stars of their PB-*g*-(PB;PEO) copolymer. The DSC analysis showed similar results to those for the linear comb graft copolymer most likely because the backbone was short relative to the side chains, which provides a star-like architecture even in the linear form. Klein *et. al.*[208] conducted a study on a linear mid-block poly(oxymethylene) with hyperbranched polyglycerol (*hb*PG-*b*-POxM-*b*-*hb*PG) and found that thermal behavior, thermal stability, degree of crystallization, and surface properties of POxM were dependent on *hb*PG content. Compared to the linear POxM structures, the hyperbranched copolymers showed lower T_m by DSC, though not in a direct relationship with decreasing w_{POM}. As the molecular weight of the *hb*PG increased, the POM crystallinity decreased, as would be expected, and the introduction of the *hb*PG blocks does increase the thermal stability of the POxM, as observed in TGA experiments. A dendritic-linear-dendritic PCL-*b*-PEO-*b*-PCL copolymer was synthesized by Ju and coworkers[209] using anhydride end-functionalized PEO to undergo esterification with propionic acid to form dendritic branches capable of initiating PCL polymerization. This dumbbell-shaped copolymer crystallized in different ways depending on the dendron generation and

M_n^{PCL}. According to XRD, with one or two generations of dendron branching, both PEO and PCL were crystalline. As the copolymer was further branched with third and fourth generations, the PEO diffraction peaks disappeared, and only PCL diffraction peaks were observed.

The influence of chain architecture on crystallization is intriguing, and many studies have provided creative synthetic strategies to evaluate crystallization under these conditions. However, there is a large space in which to work to develop a stronger understanding of the observed behaviors mentioned here. Improvements in chain characterization, such as molecular weight and chain length of branches, should improve our understanding. Additionally, design of materials and experiments that minimize variables are crucial to highlighting the role of branching and branch architecture only.

Copolymers with Other Unique Chemistries

Other unique chemistries of interest include biopolymer conjugates[72,211-216] and supramolecular pseudoblock copolymers (SPBCPs).[217-220] Biopolymer conjugates include traditional synthetic polymers with a biopolymer block[72,211-213] or polypeptoids, which are comb-like, glycine-backbone polymers with substituents on the nitrogen of the glycine monomer.[214-216] SPBCPs do not have a covalent bond between the two blocks. They consist of two end-functionalized homopolymers. The end-functionalities then interact through strong secondary interactions, such as multiple hydrogen bonds, metal-ligand coordination, or ionic interactions to form the block copolymer.[221-224] These pseudoblock copolymers have junction points that are dynamic and exist in equilibrium between the associated and disassociated states; therefore, crystallization of one block should differ from traditional homopolymers and block copolymers. Scheme 1 is one example of this type of assembly from Ref. 218. This strategy also was used to form supramolecular multiblock copolymers with triblock copolymer building blocks.[217,219]

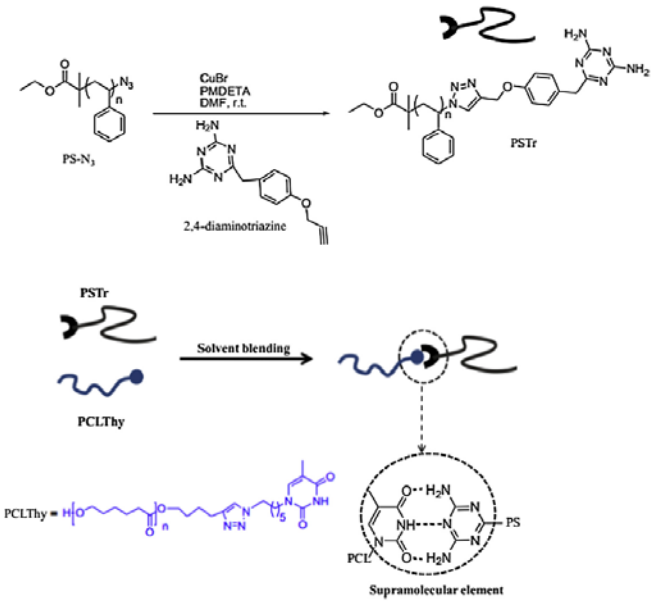

Scheme 1 Synthetic approach toward SPBCP of PS and PCL using 2,4-diaminotriazine (Tr) and thymine (Thy) to form three hydrogen bonds at the junction point. (Reproduced from [218] with permission from Elsevier.)

As with most studies in this section, the crystalline block may be the non-unique block or the chemically-unique, in this case biopolymer, block. A study by Song *et. al.*[211] concerning PLLA-*b*-poly(α-D-glucose carbonate) (PDGC) copolymers where the PDGC block was subsequently functionalized with cysteine side groups (PLLA-*b*-PDGC-cys). Interest in this copolymer stems from its fully degradable, amphiphilic nature along with the ability to synthesize it from natural products. These copolymers assembled in aqueous solutions with different morphologies depending on the PLLA weight percentage. The morphologies were investigated *via* TEM and AFM and found that when w_{PLLA} = 0.05 - 0.07, spheres formed, at w_{PLLA} = 0.13 – 0.19, cylinders formed, and at w_{PLLA} = 0.34, 2D platelet-like cylinder bundles formed. The CDSA was confirmed using WAXD. The spheres had the lowest crystallinity (if any), as would be expected. Solution crystallization of poly(1-*O*-acryloyl-D-fructopyranose)-*b*-PCL (PF-*b*-PCL) and poly(1-*O*-acryloyl-D-fructopyranose-*co*-(5,6-benzo-2-methylene-1,3-dioxepane)-*b*-PCL (P(F-*co*-BMDO)-*b*-PCL) was performed to make PCL platelets with carbohydrate-functionalized surfaces.[72] The PF-*b*-PCL and P(F-*co*-BMDO)-*b*-PCL formed elongated lozenge crystals, similar to other PCL solution crystallization. With longer PF or P(F-*co*-BMDO) blocks, the PCL crystals became thinner.

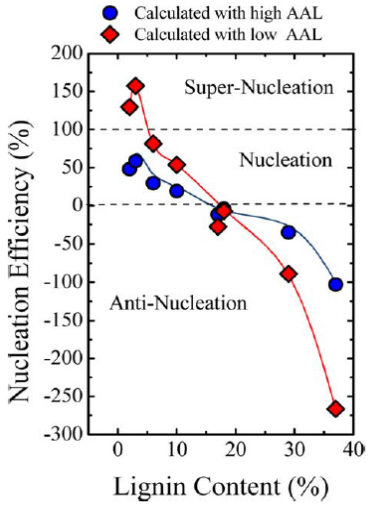

Figure 32 Nucleation efficiency of lignin on PCL crystallization in PCL-*g*-lignin. (Reproduced from [212] with permission from Wiley.)

One interesting copolymer under investigation is PCL-*g*-lignin. Alcaline soda lignin (wheat) was functionalized with PCL using ring-opening polymerization from the lignin's -OH groups.[212-213] The number of –OH groups/lignin molecule varied. To perform the study, bulk samples of lignin molecules with varying functionality and PCL chains of varying length (denoted as AAL, or average arm length) were analyzed using DSC to determine the crystallization behavior of the PCL. It should be noted that due to the complex nature of the molecules, only approximated molecular characteristics were used to describe the samples. For small PCL chains, no crystallization was detected even with a large number of PCL grafts.[213] For crystallizable samples, the lignin content influenced the nucleation and crystallinity of PCL.[212] At lower lignin contents, below 10 wt %, there were nucleating effects observed (higher T_c and higher ΔH_f) that increased crystallization of the PCL. At lignin contents greater than 18 wt %, anti-nucleation effects appear that decrease crystallization and reduce crystallinity due to a competition between nucleating effects and intermolecular interactions caused by hydrogen bonding interactions between the PCL and lignin blocks, as confirmed by FTIR.[213] Figure 32 shows the nucleation efficiency, a

measure of the T_c for polymer-nucleation agent mixtures relative to neat polymer T_c,[61-62] as a function of lignin content. At the higher lignin content, the morphology begins to limit the lamellar size and SSA experiments indicate that the hydrogen bonding interactions are so strong that they act as crosslinks that limit the lamellar domain and thus decrease the nucleation efficiency. The PCL-*g*-lignin copolymers have new thermal, mechanical, and rheological properties compared to blends.[213]

Polypeptoids are a newer set of crystallizable polymers that are nearly monodisperse but have better thermal processability than polypeptides due to reduced hydrogen bonding between backbone chains.[225] Bulk crystallization was performed on a polypeptiod copolymer of poly(*N*-decylglycine)-*b*-poly(*N*-2-(2-(2-methoxyethoxy)ethoxy)ethylglycine) (pNdc-*b*-pNte) to identify the role of monomer structure on the crystallization of polymers.[214] For pNdc-b-pNte, the pNdc glycine unit had a 10-carbon alkyl chain; while the pNte had a 3-repeat unit alkoxyl side chain. Previous work showed that the pNdc homopolypeptoid was crystalline[226] and that pNte was amorphous.[227] The BCPs exhibited a lamellar morphology for $0.29 < f_{pNte} < 0.71$, which indicated that $T_c > T_{ODT}$. Surprisingly, the crystallization of pNdc induced crystallization in pNte as evidenced by two distinct sets of diffractions in WAXS (*a*, *b*, and *c* subscripts denote unit cell direction) and two exothermic crystallization peaks in DSC as shown in Figure 33. The T_m^{pNte} was between 50° - 80°C below T_c^{pNdc} depending on f_{pNte}. The crystal structures for each are similar because of the nearly isosteric side chains. In fact, the authors believe that this feature seems to be crucial for crystallization of the pNte block as it is absent using another crystalline polypeptoid in a BCP with pNte. Aqueous solution assembly of shorter side chain block copolypeptoid of poly(*N*-(*n*-propyl)glycine)-*b*-poly(*N*-methylglycine) (pNp-*b*-pNm) was studied by Secker and coworkers.[215] Here, pNp was crystalline, and pNm was water-soluble. The copolypeptiod assembled in aqueous solution between 27°C and 43°C depending on pNm length to form aggregates with subsequent crystallization upon heating to ~48°C (similar to cold crystallization in polyesters). With crystallization annealing time, the pNp-*b*-pNm aggregate morphology went from spherical to fibrous intermediates to 2D platelets that also aggregate. In contrast, linear and cyclic pNm-*b*-pNdc underwent a gelation process in 5-10 wt% methanol solution due to the crystallization of pNdc.[213] Upon crystallization, a network of fibrillar crystalline micelle was formed. The free-standing gel formed by cyclic pNm-*b*-pNdc was stiffer than its linear counterpart because the density of assembled fibrillar bundles was higher.

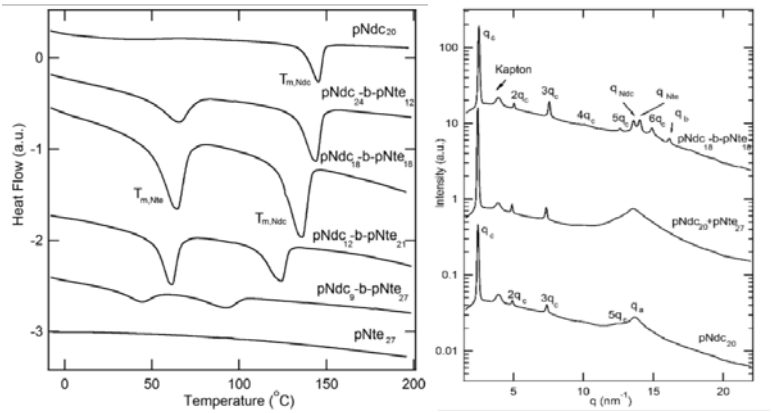

Figure 33 (left) DSC endotherms of pNdc and pNte homopolypeptoids and block copolypeptoids. (right) WAXS profiles at room temperature for pNdc-*b*-pNte, a blend of pNdc + pNte, and pure pNdc. Subscripts *a*, *b*, and *c* represent unit cell directions. All are vertically offset for clarity. (Reproduced from [214] with permission from the American Chemical Society.)

With polypeptoids, controlled synthesis and monomer functionality can be manipulated to study crystallization of macromolecules. Another chemical feature that may provide insight is the junction point between the blocks. For SPBCPs, it is possible to change the nature of the junction point. Often, the supramolecular interaction is through hydrogen bonding. They were thymine-2,4-diaminotriazine (Thy-Tr) or 2-ureido-4[1*H*]-pyrimidinone-2-ureido-4[1*H*]-pyrimidinone (UPy-UPy) interactions for the reports discussed here. These hydrogen bonding interactions were confirmed by FTIR.[218,220] Studies have shown that these hydrogen bonding interactions are dominant at low molecular weights of at least one of the blocks and that the hydrogen bonding has a confining effect. In Appiah *et al.*'s[218] study on (PCL-Thy)-*s*-(PS-Tr) (Scheme 1), the authors found that for low molecular weight PCL ($M_n^{PCL} \approx$ 3k or 6k), the glassy PS had a confining effect on PCL crystallization either through microphase separation, when w_{PCL} in the diblock was approximately 0.50, or fractionated crystallization, possibly indicating segregation between hydrogen-bonded and non-hydrogen-bonded PCLs, for other w_{PCL}. Cold crystallization was observed in the equal molecular weight samples, indicating that the Thy-Tr junction influenced the mobility of the PCL chains during crystallization. Ostas *et. al.*[220] found that in their study of SPBCPs of PCL and rubbery poly(isobutylene) (PIB) ($w_{PCL} \approx 0.50$), even the mobile PIB acted as a barrier to PCL crystallization as determined by DSC and SAXS. This barrier caused a strong decrease in the crystallization temperature and created fractionated crystallization of the SPBCP, neither of which was present for non-SPBCP samples. Figure 34 shows DSC cooling thermograms for pure PCL, associated PIB-*b*-PCL, and physical blends of PCL and PIB. Only the SPBCP showed a change in T_c^{PCL}. The gAC and rAC SPBCP both demonstrate that the crystallization of PCL was influenced by the strong hydrogen bonding interaction irrespective of the amorphous polymer attached.

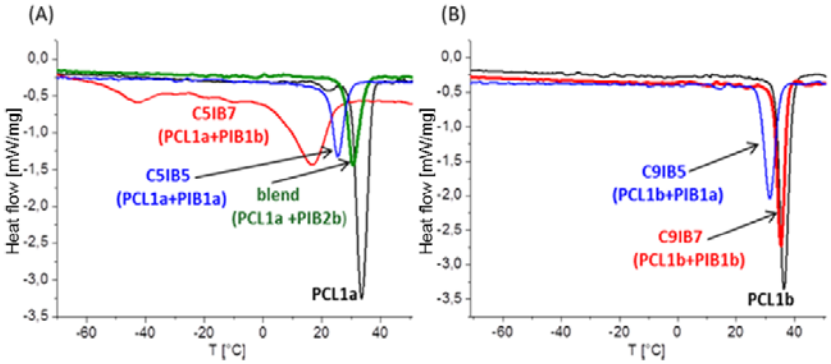

Figure 34 DSC cooling scans showing crystallization of PCL homopolymer, PIB-*b*-PCL and PCL + PIB blend. Coded designations are C for PCL block, IB for PIB block, and numerical values representing M_n/1000 g/mol for the respective block. (Reproduced from [220] with permission from the American Chemical Society.)

Pseudoblock copolymer techniques also were used to form multiblock copolymers from UPy-functionalized triblocks. Jing *et. al.*[219] worked with PLA-*b*-poly(δ-valerolactone)-*b*-PLA (PLA-*b*-PVL-*b*-PLA) triblock SPBCPs with either amorphous PDLLA or crystalline PLLA. They found typical changes in thermal properties, crystallization behavior, and crystalline structure for PVL by changing the length and stereostructure of the PLA blocks for the non-associated triblock copolymer. UPy-PLA-*b*-PVL-*b*-PLLA-UPy SPBCPs showed a decrease in crystallinity and crystallization temperature compared to the non-associated triblocks. This led to better optical clarity and mechanical properties for the SPBCP. A study by Chang *et. al.*[217] found that oligomeric UPy-PLLA-*b*-poly(ethylene-*co*-butene)(PEB)-*b*-PLLA-

UPy (or UPy-PDLA-*b*-PEB-*b*-PDLA-UPy) with various stereo mixtures of PLLA and PDLA blocks led to less ordered microphase-separated morphologies and different domain spacing than their enantiopure counterparts. In fact, crystallization of PLLA or PDLA did not occur for these SPBCPs. Only in the stereocomplex mixtures, where sc crystals formed, was crystallization observed. It is assumed that the UPy-UPy interaction diminished the ability for oligomeric PLLA (PDLA) to crystallize; however, the higher stability of sc crystals promoted crystallization in the mixture. These materials exhibited thermally induced shape-memory behavior, which can be modified by varying the crystallinity of the stereocomplex content. For both of these multiblock SPBCPs, the materials exhibited good shape-memory properties due to crystallization and end-group association.

Each of these unique chemical features discussed provides new fields of polymer crystallization, while still keeping the still unanswered fundamental questions in view. As new synthetic techniques develop, new rod-like, highly-branched, biopolymer conjugate, peptidic, supramolecular, enantiomeric, macromolecules or combinations therein certainly will be developed to harness the chemical structures necessary for advanced materials. As the field moves forward, it will be important to maintain the important work of understanding physical structure as well to ensure successful products.

APPLICATIONS OF CRYSTALLIZABLE BLOCK COPOLYMERS

The driving force for understanding crystallization behavior in polymeric materials, especially hierarchical assembly in block copolymers, is to develop the ability to engineer systems with controlled crystallization for specific applications. Crystallization of BCPs is, therefore, an important factor for how to design polymeric materials for a specific function. To conclude this review, a few applications of crystallizable BCPs and the influence of crystallization on macroscopic properties are discussed. These cover three broad classes of applications: 1) commodity and general mechanical properties, 2) biomedical, and 3) environmental.

Commodity Plastics

The development of new materials for commodity uses is still a vibrant research field even with the prevalence of polymeric products. New ways to tailor mechanical properties in thermoplastics is still a rich area of research. BCPs provide unique opportunities and challenges to this field. Mixing block copolymers with homopolymers or blends opens the door to tailor these properties in new ways. When the chemistry of a block is identical to a matrix component (homopolymer or constituents of the blend), the ability to crystallize the relevant block(s) with the matrix material enhances its ability to act as filler, compatibilizer, plasticizer, etc. In addition to being miscible with the matrix,[228-229] the opportunity to incorporate the appropriate block into the lamellar structure of the matrix's crystals ensures that the crystallizable block copolymer is fully assimilated into the material.

Recent studies of a CC PCL-*b*-PE block copolymer were used to demonstrate the inclusion of PCL homopolymer and the PCL block into a single lamella. Gondo *et al.*[230-231] used the crystallization of the PE block to confine the homopolymer PCL and block PCL into the same domain. Here, PCL crystallization with respect to the miscibility of the two types of PCL chains in the crystalline PE lamellar morphology was evaluated to expand upon their work with PB-*b*-PCL copolymers.[232] The isothermal crystallization behavior of PCL chains in binary blends consisting of PCL-*b*-PE copolymers and PCL homopolymers were evaluated using simultaneous synchrotron SAXS/WAXD, DSC, and FTIR. Because the crystallization temperature of PE blocks was much higher than that of the PCL chains, the PE block

crystallized first to form a crystalline lamellar morphology. Two blends were made to evaluate the miscibility of PCL homopolymers in microphase-separated melts. At high volume fraction of PCL, the PCL homopolymer was between the PCL blocks in the lamellar microdomain (effectively immiscible), and the isothermal crystallization of the PCL chains showed a composition-dependent asymptotic increase at the late stage of crystallization. Additionally, there were two lamellar thicknesses associated with the PCL crystallization. Ultimately, this suggested that the individual crystallization of PCL homopolymers and PCL blocks yield separate PCL lamellar crystals between the PE lamellar morphology (dry brush analogy). At low PCL volume fraction, the PCL homopolymer was homogeneously blended with PCL blocks (wet brush analogy), and the time evolution of crystallinity was identical to that of PCL blocks regardless of their composition. This indicated that the crystallization of PCL chains was controlled by the PCL blocks to form a mixed crystal structure which contain PCL blocks and PCL homopolymers. Although the results were similar to the PB-*b*-PCL study, the pre-formed PE crystals were able to effectively keep the PCL homopolymer localized to the PCL block domains even when microphase-separated at high volume fraction.

Polymer mixtures, either block copolymers or blends, allow for the tailoring of properties based on the interspecies interactions and self-assembly structure. Often, materials are incompatible as blends, but block copolymers are used as compatibilizers to broaden the scope of possible blend compositions. Pepels *et al*.[233] studied BCPs consisting of a PE-like block [poly(pentadecalactone), PPDL] and polar block for the compatibilization of PE/polar polymer blends or PE based composites. Introducing polar components to polyolefins add extra functionality to the printability and barrier properties or to compatibilize polyolefin/polar polymer blends and enhance interactions for fillers. Thermal properties and morphology of PPDL-*b*-PLLA and the compatibilization of HDPE/PLLA and LLDPE/PLLA blends were studied. DSC thermograms of PPDL-*b*-PLLA indicate that both blocks are crystalline at room temperature. During cooling, a coincidental crystallization driven process for both PPDL and PLLA (up to a certain block length) was observed as only one endothermic crystallization peak at T_c = 75°C. Two distinct exothermic peaks at T_m^{PPDL} = 89°C and T_m^{PLLA} = 165°C suggested that the thermal stability of the two block is quite different even with a similar T_c. The amorphous phase of both polymers is relatively miscible. This showed that the behavior of PPDL-*b*-PLLA is between the blend systems of HDPE−PLLA and LLDPE−PLLA. Applications for the PPDL-*b*-PLLA copolymer as compatibilizers were studied in both HDPE/PLLA and LLDPE/PLLA blends with varying mass fractions. Figure 35 shows scanning electron microscopy (SEM) images of the different morphologies for compatibilized HDPE-PLLA blends (D-F) compared to the non-compatibilized blends (A-C). For the HDPE-containing blends, a significant reduction of particle size was seen, while for the LLDPE-containing blends, there was a strong increase in the interfacial adhesion leading to improved tensile behavior even though the morphology was not affected. The PPDL-*b*-PLLA additive increased the stiffness, strength, and yield stress of LLDPE blends while decreasing the elongation at break. It was found that there needed to be a minimum length for the PPDL block to be considered for effective compatibilization because for both the LLDPE/PLLA and HDPE/PLLA blends, the compatibilization efficiency of the PPDL-*b*-PLLA increased when the length of the PPDL block increased. Based on DSC analysis, no co-crystallization of the HDPE and PPDL was observed (PLLA block should crystallize with PLLA component); however, the PE-like structure of PPDL provided a new method for compatibilizing PE with polar PLLA.

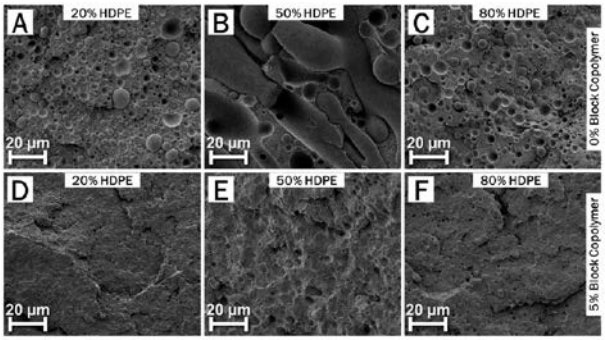

FIGURE 35 SEM images of the morphology of cryogenically fractured PLLA/HDPE blends with PPDL-*b*-PLLA compatibilizer added at (A-C) 0% and (D-F) 5%. (Reproduced from [233] with permission from the American Chemical Society.)

PLLA has high tensile strength and a high modulus. On its own, PLLA cannot be used in many applications due to its poor thermal resistance, thus improving crystallization in PLLA can increase the polymer's thermal resistance. It has poor chain mobility, which is a limiting factor for crystallization. Increasing the crystallization kinetics of PLLA has been a challenge, but introducing plasticizers has been a sufficient way to improve this. For example, improvement in mechanical properties was found for pure PLLA-*b*-PBC-*b*-PLLA copolymers due to the amorphous nature of PBC.[122] As mentioned previously in discussing sc crytallization, PEO has been used as an extremely efficient plasticizer for PLLA crystallization in pure BCPs, i.e. the plasticization effect was increased by increasing the content of PEO for PLLA-PEO copolymers.[140-143] Li and coworkers[234] examined PLLA-*b*-PEO-*b*-PLLA triblock copolymers as a plasticizer blended with PLLA homopolymer to study the miscibility and crystallization behavior of PLLA, specifically to enhance its crystallization. The non-isothermal and isothermal crystallization behavior and corresponding morphological changes were studied for PLLA with various amounts of added PLLA-*b*-PEO-*b*-PLLA copolymers (10%, 20%, 25% and 30% by weight) with short PEO segments used as an additive (10-30% by weight). PLLA-*b*-PEO-*b*-PLLA promoted nucleation, which is different from many traditional PLLA plasticizers that increase chain mobility and, therefore, crystal growth. Nucleation of PLLA-*b*-PEO-*b*-PLLA was favored when there are relatively longer PLLA segments. This weakens the spherulite growth rate and the degree of crystallinity is low. The steady reduction of the T_g^{PLLA}, T_{cc}^{PLLA} and crystallization half-time, $t_{1/2}^{PLLA}$, for blends with shorter PLLA segment suggests that the plasticization effect for chain mobility is favored. Figure 36 illustrates that even a small amount of triblock copolymer, 10 wt%, enhances PLLA crystallization. Ultimately, this led to a higher degree of crystallinity and the formation of more spherulites. The study found that as the molecular weight of PEO segment in triblock copolymers increases, the content of PEO increases concurrently, which also leads to higher chain mobility of PLLA. It can be concluded that triblock copolymers with relatively shorter PLLA segment and longer PEO segment are more likely to promote the crystallization of PLLA. Additionally, triblock copolymers play an important role in the inhibition of PEO crystallization-induced phase separation. This improves the compatibility and durability of the copolymer. When PLLA-*b*-PEO-*b*-PLLA has a relatively long PLLA segment, it can act as a nucleation site for the PLLA matrix. Since the longer PLLA segments have more nuclei centers, there is an increase in T_c^{PLLA} and T_m^{PLLA}, which weaken the plasticizing effect of the PEO segment. Liu *et al.*[140] showed that elongation-at-break increased from 6% to 100% while maintaining the tensile strength compared to neat

PLLA for PDLA-*b*-PEO-*b*-PDLA/PLLA blends. Further improvement in both elongation-at-break and tensile strength was made using a blend of enantiomeric PLA-*b*-PEO-*b*-PLA triblock copolymers.[148]

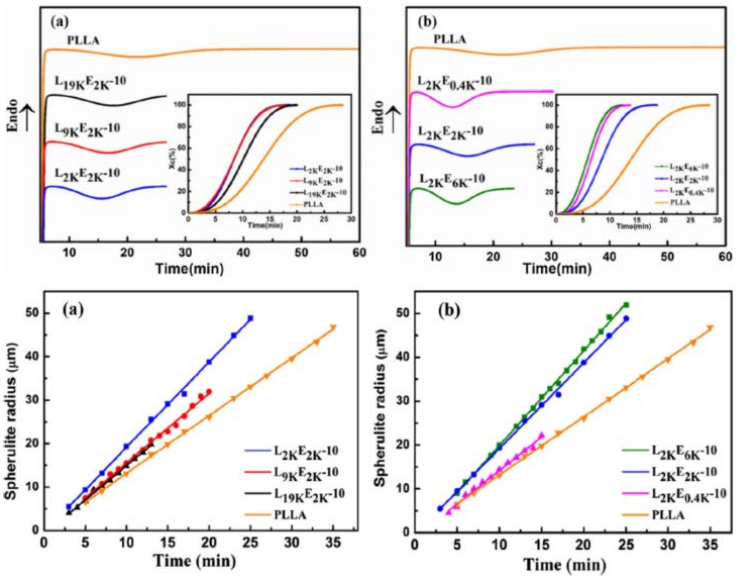

FIGURE 36 Data regarding crystallization of blends containing 10 wt% PLLA-*b*- PEO-*b*-PLLA copolymers with different M_n^{PLLA} (left side) or different M_n^{PEO} (right side) for the BCP. (top) Isothermal DSC curves for crystallization at 120°C. Insets show relative crystallinity as a function of time. (bottom) Spherulitic growth during isothermal crystallization at 130°C. (Reproduced from [234] with permission from Elsevier.)

Similar results were found when a star-shaped PLLA-*b*-PDLA stereoblock copolymer was introduced into a PLLA matrix.[235] The effects of PLLA-*b*-PDLA on PLLA melt crystallization, mechanical properties, and rheological properties were investigated in this study. It was concluded that PDLA-*b*-PLLA BCPs could significantly accelerate the crystallization rate of PLLA. It should be noted that the study focused on PLLA hc crystal formation. As such, the experimental temperature profile was designed to allow for sc crystal formation first at high T = 160°C. The study was performed on crystallization that occurred after sc crystal formation at lower T. Non-isothermal and isothermal experiments indicated that PDLA-*b*-PLLA has a concentration dependence for the accelerating effect on PLLA melt crystallization. The non-isothermal crystallization results showed the crystallization temperature shifting to a higher temperature with the addition of PDLA-*b*-PLLA. Isothermal analysis showed the half-time of crystallization to decrease as the weight fraction of copolymer increased from 0 wt% to 10 wt%. The crystallization rate remained constant above 5 wt% content of the PDLA-*b*-PLLA. The highest nucleation efficiency was reported to be 64.8% for PLLA samples with a PDLA-*b*-PLLA content of 10 wt%. POM revealed that the accelerating effect resulted from its good nucleation ability. The inclusion of sc crystals helped enhance the nucleation efficiency by lowering the free energy of activation for the hc crystals. In addition, dynamic mechanical analysis (DMA) tests indicated that the addition of the star-shaped PDLA-*b*-PLLA improved the storage modulus, enhanced the stiffness, and improved heat resistance compared to neat PLLA. Rheological properties of nucleated PLLA show evidence of a network structure of a stereocomplex crystallite, i.e. a reinforcement effect, when it is above 5 wt%.

Improving the mechanical properties of multiblock copolymers plays a major role in the development of future applications with sustainable polymeric materials. One method is to use supramolecular interactions, as discussed in the previous section.[217,219] These PLLA-based triblock copolymer assemblies have better tensile strength, moduli, and shape-memory behavior because of decreased crystallinity. Panthani and Bates[236] discussed the crystallization and mechanical properties of triblock and multiblock copolymers containing 70% (vol.) PLLA (matrix) and 30% poly(ethylene-*co*-ethylethylene) (PE/E_E) (cylinders morphology) when blended together to systematically tune $\langle n \rangle$, where $\langle n \rangle$ is the average number of connected triblock copolymers in each sample. DMA indicated that all samples had a $T_{ODT} > T_m^{PLLA}$. SAXS measurements of the BCPs at $T_m^{PLLA} < T < T_{ODT}$ shows that the samples had the same hexagonally packed cylinder morphology and identical domain spacing. Isothermal crystallization experiments indicated that samples with higher $\langle n \rangle$ had a lower percentage crystallinity after 1 h due to the differences in the average chain architecture. The reduced rate of crystallization of the multiblock copolymer is due to pinning of the interior PLLA matrix blocks to two PLLA-PE/E_E interfaces which reduces the mobility of the blocks.

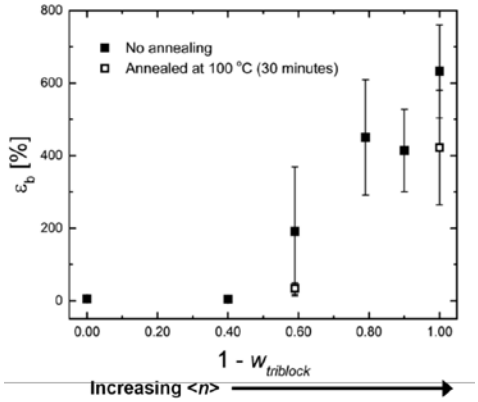

FIGURE 37 Strain at break as a function of multiblock component composition for PLLA-PE/E_E copolymers. Closed symbols represent quenched samples, and open symbols represent annealed samples. (Reproduced from [236] with permission from the American Chemical Society.)

The effect of crystallinity on the mechanical properties was investigated by annealing.[236] Blend samples exhibited mechanical properties that were affected by $\langle n \rangle$, where $\langle n \rangle$ increases with decreasing triblock composition. At $\langle n \rangle < 1.4$, samples were brittle; whereas, samples with $\langle n \rangle \geq 1.4$ were ductile with a sharp yield stress. These as-prepared samples had low crystallinity. Annealed samples had a significantly higher amount of crystallized PLLA compared to those that were not. A lower strain at break and the absence of a sharp yield stress may indicate that there were changes in the chain configuration induced by crystallization. Figure 37 shows the relationship between strain at break (ε_b) and triblock weight fraction for all samples. Again, the inclusion of triblock copolymer increases the ductility by increasing the number of bridging chains; however, increased crystallinity through annealing drastically decreased the number of bridging blocks. The interior PLLA blocks of the multiblock component were likely to crystallize at nucleation sites that were in close proximity to the chain, which could force a looping configuration since PLLA blocks have a high chance of returning to adjacent domains. With further crystallization, the motion of the PLLA blocks was further delayed. This resulted in an additional increase in the looping fraction. Moreover, the mechanical properties probably were dominated by interlamellar slip and/or interlamellar separation occurring within the PLLA crystals. This demonstrates

that the mechanical response and failure occurred by different mechanisms in the annealed samples. Additionally, the presence of the spherulites did not seem to influence greatly the mechanical behavior. The PLLA blocks in the PLLA-*b*-(PE/E_E)-*b*-PLLA were all dangling chains with only one end of the blocks pinned to the interface. These dangling chain ends have high mobility compared to the interior PLLA blocks of the multiblock copolymer. The restricted chain mobility of the loops and bridges restrict nucleation. Thus, the dangling ends have a higher probability of forming nuclei of critical size, which can then grow into lamellar crystals.

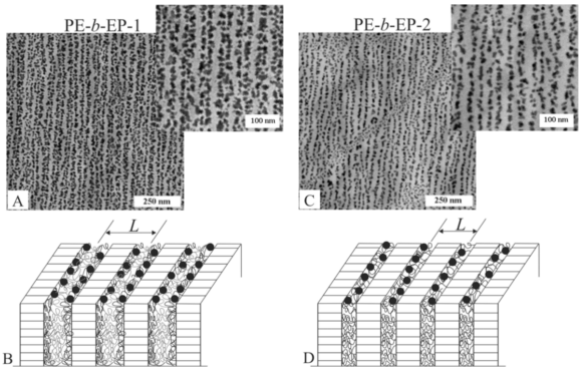

FIGURE 38 TEM images of gold decorated samples of (A) PE-*b*-EP-1 and (C) PE-*b*-EP-2. Samples were epitaxially crystallized onto *p*-chlorobenzoic acid for alignment. (B) Schematic of double row of gold nanoparticles (dark circles) embedded in the amorphous portion of the lamellar morphology of PE-*b*-EP-1. (D) Schematic of single row of gold nanoparticles embedded in the amorphous portion of the lamellar morphology of PE-*b*-EP-2. *L* represents the periodicity of the block copolymers. (Reproduced from [244] with permission from the American Chemical Society.)

BCP templating is another area of intense research. Amorphous polymer organization is done by utilizing external fields, surface wetting interaction, and block periodicity to orient or align domains preferentially on a surface.[237-241] These oriented domains are used to template nanoparticle alignment,[241] for lithography masks,[242] and in transport (ions, electrons, light, etc.) applications.[237] Bulk crystallization or epitaxial crystallization presents another method for organizing BCPs for to be used as templates.[243] For example, highly-ordered lamellar nanostructures with high orientation of lamellar microdomains have been obtained by epitaxial crystallization of crystalline PE-*b*-poly(ethylene-*alt*-propylene) (PE-*b*-PEP) BCPs constituted by a crystalline block of polyethylene and an amorphous block of a propene-ethene random copolymer with different molecular masses. De Rosa *et al.*[244] crystallized their samples by cooling from the melt to achieve the orthorhombic form of PE *via* epitaxial crystallization onto crystals of *p*-chlorobenzoic acid. This approach induced formation of crystalline PE lamellae oriented edge-on that were highly-aligned along one direction. This resulted in ordered lamellar nanostructures with perfectly aligned layers of crystalline PE which was shown to alternate between the amorphous layers of PEP block. The thickness of the lamellar structures is influenced by varying the molecular weight of the amorphous PEP block, which is shown in Figure 38. The two samples are shown: PE-*b*-PEP-1 and PE-*b*-PEP-2, where 1 has as lower volume fraction of PE (f_{PE} = 0.34) and M_n^{PE} of 120k and 2 has a higher weight fraction and molecular weight (f_{PE} = 0.48 and M_n^{PE} = 130k). Epitaxy has been coupled with the technique of gold decoration so that the ordered BCP nanostructures act as a template for the fabrication of long, straight, and parallel rows of gold nanoclusters, which could be used in many applications. For PE-*b*-

PEP-1, a double row of nanoparticles formed, as seen in Figure 38; however, for PE-*b*-PEP-2, a single row formed, likely because of the smaller fraction of amorphous PEP.

Medical

BCPs have been studied for biomedical applications, including nanomaterials, drug delivery, and tissue scaffolding, over the past several decades. Most often, solution assembly is used to develop materials with tailored structures for these applications. Here, the role of crystallization in a few of these materials is discussed. When the core of these assembled structures is crystallized, it will change the properties compared to particles with amorphous cores.

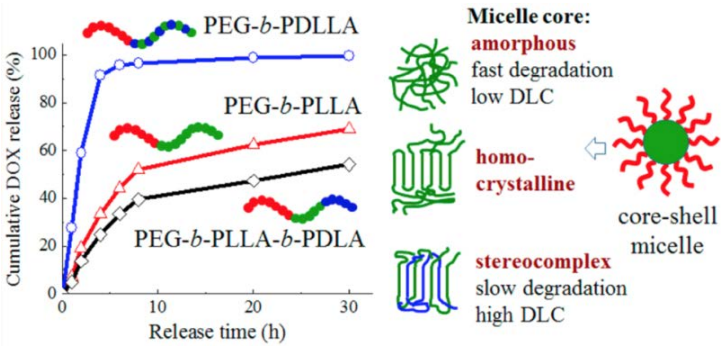

FIGURE 39 Release profiles of DOX from micelles made using different block copolymers. PEO-*b*-PDLLA (blue) had an amorphous core. PEO-*b*-PLLA (red) had an hc crystalline core. PEO-*b*-PLLA-*b*-PDLA had an sc crystalline core (PEO and PEG are equivalent). Schematics of the micelle morphology are shown on the right. (Reproduced from [245] with permission from the American Chemical Society.)

Amphiphilic BCPs are driven by self-assembly into the core-shell micelles comprised of hydrophobic cores. These cores are stabilized by the hydrophilic shell in aqueous solution due to the phase separation of the immiscible blocks. The micelle structure ideally is perfect for biomedical applications, specifically controlled drug delivery because the hydrophobic environment in micelle core is favorable for encapsulation of hydrophobic drugs. For the past several decades, polymeric micelles have been studied for having anti-tumor drug delivery capabilities. The release mechanisms of encapsulated drugs from micelle cores are diffusion and core degradation. Ma and coworkers[245] suggested that because the chemical structure and chain-packing mode of the hydrophobic block significantly influences the degradation of the micelle's core and diffusion of drugs, this would affect the drug's entrapment ability and its release kinetics profile. Their study focused on the effects of stereostructure on precise micelle structure, biodegradation, and *in vitro* drug release behavior of PEO-*b*-PLLA-*b*-PDLA BCPs. The triblock BCP was compared with PEO-*b*-PLA diblock copolymers with uncontrolled PLA stereostructure and PEO-*b*-PLLA/PEO-*b*-PDLA enantiomeric mixtures. It is important to note that the stereostructure, architecture, and crystallization of hydrophobic PLA blocks played an important role in the core structure, stability, thermal and physical properties of copolymer micelles. Stereoblock copolymers having similar PLLA and PDLA block lengths and enantiomerically-mixed copolymers assembled with sc crystalline core micelles, and the isotactic and atactic PEO-*b*-PLA copolymers formed hc and amorphous micelles. PLA segments in stereoblock copolymer micelles showed lower amounts of crystallinity compared to the isotactic and enantiomerically-mixed BCP micelles. This was due to the short block length and presence

of covalent junction between PLLA and PDLA blocks. Synchrotron radiation SAXS provided evidence that the stereoblock copolymer micelles have an overall larger size, micellar aggregation number, core radius, smaller core density, and looser packing of core-forming segments than the isotactic and enantiomerically-mixed copolymer micelles. Each system was used to study the release of doxorubicin (DOX) to compare the core structure to release profiles. Figure 39 (where PEO is replaced with PEG and PLA is represented by PDLLA) depicts the micellar DOX release overtime and the core structure and how it relates to the drug loading capacity (DLC). These results serve as the basis for designing micellar materials with tunable structures and optimizable functions.

High drug loading content, another crucial factor in developing polymeric micelles for efficient chemotherapy, was studied for a PEO-*b*-PCL micelle system. The hydrophilic shell of polymeric micelles, in this case PEO-*b*-PCL, reduce the uptake of reticuloendothelial system, which results in longer circulation and targeting tumors due to its enhanced permeability and retention effect. Liang *et al.*[246] provided a simple technique to achieve polymeric micelles with high drug loading content and efficient anticancer activity in both an *in vitro* and *in vivo* setting. Small molecules of cinnamic acid, 7-carboxymethoxy coumarin and chrysin with different π-conjugations were immobilized on the PCL core *via* terminal hydroxyl groups. These moieties provide opportunity to π-π stack with anticancer drugs, such as DOX, to improve drug loading content. DSC and XRD techniques revealed that the crystallization of PEO-*b*-PCL increased with the sequence of cinnamic acid, coumarin and chrysin modification. Additionally, the critical micelle concentration and mean diameters of modified block copolymer micelles decreased. The drug loading content increased dramatically from 12.9% to 25.5% after being modified. Specifically, chrysin (CHR) modifications of the micelles exhibited the highest drug loading content of 25.5% and an encapsulation efficiency of 93%. Micelles modified with chrysin are the most effective for anticancer drugs. The π-π stacking interactions between π-conjugated moieties and DOX was demonstrated to contribute the higher drug loading contents of the modified micelles even with higher crystalline content. The drug release from modified micelles was slower than that from non-functionalized PEO-*b*-PCL micelles. The IC_{50} profile showed that a lower release was detected when functionalized PCL was utilized. The PEO-*b*-PCL-CHR micelles were 4-fold lower than that of PEO-*b*-PCL micelles. It is important to note that the three modified PEO-*b*-PCL micelles were non-toxic to cells, and the drug loaded micelles were efficiently internalized in cancer cells. The *in vivo* study revealed that high DOX dosages of micelle formulations with less injection times could enhance the anticancer activity. The body weight shift of tumor-bearing mice, their survival rate and tissue histology conclude that the systemic toxicity of DOX was greatly reduced after being encapsulated in polymeric micelles.

In order to effectively and efficiently deliver drugs to their specific targets, methods for block copolymer functionalization, or shape alteration of nano-assemblies have been developed to construct multifunctional high drug-loading drug delivery systems. Gou and coworkers[247] looked at the self-assembly of polymeric micelles and demonstrated the feasibility of improving drug loading by physical blending of medium chain triglyceride (MCT) into PEO-*b*-PCL micelle cores instead of chemical modification of polymer structures. These were called oil-containing micelles, or OCMs. MCT inhibited PCL core crystallization as confirmed by DSC and AFM. When MCT was incorporated into polymeric micelles, the maximum drug loading capability was shown to increase, likely due to the decrease in crystallinity. At high MCT content, a phase-separated core was observed. The different micellar structures are shown in the scheme in Figure 38. The amount of loaded drug, including disulfiram, cabazitaxel or TM-2 (a taxane derivative), was cargo-polymer affinity dependent. Most importantly, the prepared OCMs showed a well-controlled particle size, great stability, and decreased drug release rate. Results of drug

loading and release of disulfamine are shown in Figure 40. By varying MCT content, it was possible to control the size of the OCMs. The addition of MCT was shown to have minimal effect on the performance of micelles in different cell studies and pharmacokinetic profiles. Preparation of oil-containing micelles shows a promising method to improve drug loading with only affecting the hydrophobic micelle cores.

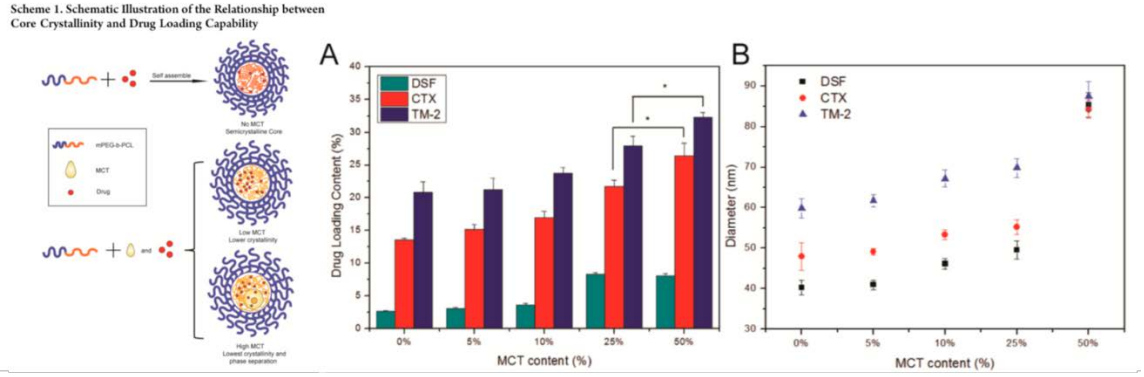

FIGURE 40 (left) Schematic of multicomponent micelles with incorporated MCT in the core. (A) Maximum drug loading of disulfiram (DSF, green), cabazitaxel (CTX, red), and TM-2 (purple) in PEO-*b*-PCL OCMs with varying MCT content. (B) *In vitro* drug release profile of DSF from MCT-free micelles and OCMs. (Reproduced from [247] with permission from the American Chemical Society.)

Shape, size, and surface properties of polymer microparticles and nanoparticles determine their overall function and properties.[248] Recently, non-spherical polymers have become of great interest due to their unique properties. These properties include: 1) long *in vivo* circulation time, 2) low cell uptake, 3) little perturbations on cell functions, and 4) shape influenced interaction with cells. However, it is difficult to investigate the biological properties these non-spherical polymers because of the limited preparation techniques available. Zhu *et al.*[248] examined "bamboo leaf-like" PEO-*b*-PCL single crystals (truncated lozenges with curved surfaces) that were prepared in THF/methanol mixed solution via crystallization-driven self-assembly. The polymer sheets, containing a PCL single-crystal layer in between two PEO layers, remained intact after transferring to water. The length and width were 10 μm and 2 μm, respectively, and the thickness was 13.5 nm. The morphology and structure of the sheets were confirmed by different microscopy techniques (TEM, SAED, and AFM) and X-ray diffraction. Interestingly, the polymer sheets displayed a selective internalization when co-culturing with different cells. Macrophages RAW264.7 (92%) endocytosed a considerable number of sheets in 24 h; 53% of U937 cells and 29% of HUVECs internalized polymer sheets in 24 h; only a few 293 T (5%) and HeLa (3%) cells internalized the sheets during the same period. These results indicate that BCP single crystals may be effective delivery vehicles as well.

Environmental

Environmental concerns for polymeric materials center around renewable resources for polymer synthesis, degradation of materials, and materials for alternative energy.[249-250] BCPs can be used in a wide range of applications to address concerns in the packaging, membrane, and alternative energy fields. Assembly of hierarchical BCP nanostructures can be designed that will enable unique properties in common materials. In this section, we will discuss how BCP crystallization influences materials with

environmental applications. In doing so, we will highlight the parameters that are of importance when designing materials that take advantage of BCP crystallization.

Fully biobased PLLA-*b*-polymyrcene-*b*-PLLA (PLLA-*b*-PMy-*b*-PLLA) triblock copolymers were synthesized to evaluate the impact of PMy, a bioavailable monomer, on thermoplastic behavior of the material. Zhou *et al.*[251] studied this triblock copolymer to better understand the structure-property relationships of thermoplastic elastomers, where PLLA acted as the hard component and PMy was the soft component. Fully biobased thermoplastic elastomers will be of great significance in expanding the applications of PLLA and in mitigating the use of petroleum-based polymers. Two separate T_g's were detected by DMA and DSC techniques, which indicated microphase separation. Moreover, tensile testing showed that with the increasing content of PMy, the tensile strength and tensile modulus decreased due to the low modulus and tensile strength of PMy elastomer. Additionally, the yielding behavior became diminished with the increased content of PLLA segment, which corresponded to the rigidity of PLLA. POM results indicated that the spherulites show the same characteristic Maltese cross patterns. With the content of PM becoming larger, the perfection of spherulites decreased, which was partially responsible for the change in mechanical properties.

A simple and scalable synthetic procedure was used to make hydroxypropyl methylcellulose (HPMC) lightly grafted with poly(β-methyl-δ-valerolactone)-*b*-PLLA diblock copolymer.[252] HPMC-*g*-(PMVL-*b*-PLLA) polymers, described in this letter, used inexpensive and renewable precursors, and provides exceptional rheological and mechanical properties attractive for a broad range of applications, which include packaging, medical equipment, and textiles. These materials are an important subclass of thermoplastic polymers that can achieve desirable mechanical properties in both the elastomeric and plastic limit based on polymer molar mass and composition. Because the T_{ODT} of conventional linear triblocks scale with the overall molecular weight, high molar mass triblocks often are not amenable to high shear melt processing. Contrarily, linear $(AB)_n$ multiblock polymers have shown considerable promise for their ability to decouple the T_{ODT} from total molar mass. Zhang *et al.*[252] studied fully sustainable HPMC-*g*-(PMVL-*b*-PLLA) using a facile two-step sequential addition approach. These thermoplastics contained rubbery PMVL, which functions as a bridge between the semi-rigid HPMC backbone and the hard PLLA end blocks. This specific arrangement facilitated PLLA crystallization. This induced microphase separation and physical cross-linking. By changing the backbone molar mass or side chain composition, these thermoplastic materials were altered to either have plastic or elastomer character. Increasing the PLLA volume fraction further transformed the material from an elastomer to a ductile plastic. Moreover, having graft block architecture helped to overcome processing limitations that are often seen when using linear block polymers systems. These new materials were characterized by relatively low shear viscosities in the melt state, which is an indication of easy processability. This is in addition to their excellent platform for tuning the elasticity, toughness, and tensile strength of the thermoplastics by varying backbone molecular weights and segment compositions of the dangling blocks. The crystallizability of the dangling blocks was critical for designing a material that meets all of the desired characteristics. Overall, these tough graft block HPMC thermoplastics have potential to be used in future industry applications due to their ability to deform plastically without necking and remain transparent, even when they are strained as much as 600% prior to failure.

Degradation behavior often is studied in concert with other biological characteristics; however, this quality is desired in environmental and sustainability applications as well. Polyesters are known to degrade through hydrolytic cleavage at the ester bond. For hydrolysis to occur, the material must have high water uptake to induce degradation. There are two important factors to control the degradation of

BPCs: wettability and crystallizability. Specifically, wettability is governed by chemical composition and surface structure. For BCPs, amphiphilic materials are desirable because the hydrophilic moiety will enable water uptake, while the hydrophobic component imparts structural stability. In many instances, PEO is used as the hydrophilic block.[253-254] Since the PEO segment is hydrophilic, increasing the amount of PEO incorporated in the polymer increases the water uptake. This leads to faster degradation rates. Ponjavic *et al.*[253] used melt-miscible PCL-*b*-PEO-*b*-PCL and PEO-*b*-PCL BCPs where the PEO block length was fixed (M_n^{PEO} = 1k) and the PCL block lengths varied (M_n^{PCL} = 10k – 40k) (w_{PEO} < 5%) to compare with homopolymer PCL (M_n = 62,970). The thermal properties and the degree of crystallinity of the copolymers were studied using DSC and WAXS. Both types of copolymers were semi-crystalline in PCL. The increase in M_n^{PCL} within the series of BCPs caused an increase in the degree of crystallinity. Diblock copolymers exhibited a higher degree of crystallinity in regard to triblock copolymers due to a longer PCL segment. The authors presented that a low content of PEO segments and its position as central or lateral segment in copolymer chains could be used in altering the thermal, morphological and surface properties of BPCs. Surface morphology of the copolymer films was investigated by OM and AFM analysis, which confirms the spherulitic structure with spherulites of different diameters depending on PEO content. This was due to surface roughness, which was affected by the content of PEO and correlated with the diameter of the spherulites. Thus, the presence of the PEO block affected the surface morphology. Water and moisture absorption of these BCPs slightly increased with increasing PEO content, as seen in Figure 41. With increasing PEO content, the hydrophilicity of the film surface increased minimally based on water contact angle testing; however, the crystallinity and spherulitic morphology of PCL were influenced, leading to increased water uptake. Cometa and coworkers[254] used PEO-PCL-based poly(ether ester urethanes) to show that water uptake increased 5-fold when the PEO fraction increased from 25% to 50% and that the crystallinity of PCL decreased from 42% to 32% with higher PEO content (PEO crystallinity also increased).

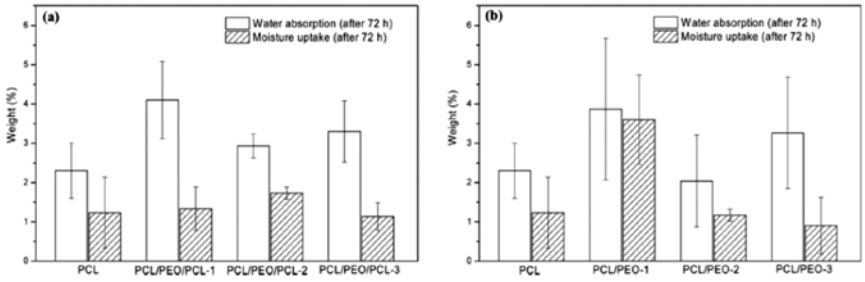

FIGURE 41 Changes in water absorption in phosphate buffer (pH = 7.4) and moisture uptake of copolymer films conditioned above saturated K_2SO_4 solution, 97% RH. (a) PCL and PCL-*b*-PEO-*b*-PCL copolymers where 1 = 10.6k each PCL block, 2 = 14.1k PCL, and 3 = 17.3k PCL. (b) PCL and PEO-*b*-PCL copolymers where 1 = 19.9k g/mol PCL block, 2 = 29.7k PCL, and 3 = 39.5k PCL. (Reproduced from [253] with permission from Springer.)

PEO's hydrophilicity is also important for water transport. Oparaji *et al.*[255-256] explored the role of crystallinity and BCP morphology on water transport. The effect of BCP morphology and polymer crystallization on water sorption was investigated using two amphiphilic PS-*b*-PEO BCPs with minority hydrophilic phase. Phase-separated morphology (lamellar or cylindrical) of PS-*b*-PEO membranes had a significant impact on the stability and extent of crystals in the PEO phase. Crystallinity was higher in the lamellar sample compared to the sample with cylindrical morphology. Water sorption is influenced by

crystallization of the PEO block as it changes the tortuosity of water diffusion. Crystallite dissolution was observed at moderate relative humidity.[256] The PEO crystallite dissolution promoted water sorption as measured by attenuated total reflectance-FTIR. The rate of dissolution relative to the rate of diffusion controlled the water uptake process. For microphase-separated BCPs, the PS block influences the crystallinity of the PEO block.[255] When PS was the majority phase (PEO cylinders), As shown in Figure 42, water diffusion was similar to homopolymer PS since the availability of hydrophilic PEO was limited. At lower temperatures, PEO crystallites slowed the water diffusion. Moreover, the water diffusion coefficient decreased with increasing water activity due to clustering of water molecules. Water desorption was much faster when the PEO was completely amorphous. These results indicate that a large PEO volume fraction is needed to obtain beneficial membrane transport properties. This is also true when the non-transport block was crystalline.[257]

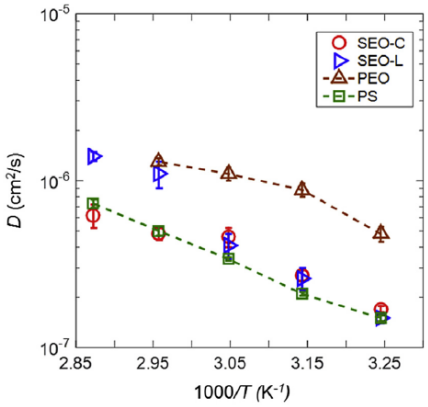

FIGURE 42 Arrhenius plot of water dilute solution diffusion coefficient in different homopolymer and block copolymer films. SEO-C represents PS-*b*-PEO with cylindrical morphology, and SEO-L represents PS-*b*-PEO with lamellar morphology. (Reproduced from [255] with permission from Elsevier.)

The degradation behavior of PLLA was studied using hydrophobic fluoropolymer (poly(2-perfluorooctyl ethyl methacrylate, PFMA) to reduce water absorption.[258] In PFMA-*b*-PLLA, the two blocks were miscible in the melt with phase separation induced by crystallization. Blends of PLLA/PFMA-*b*-PLLA (5 wt% PFMA) were used to monitor how PFMA content and PLLA crystallization influenced the hydrolytic degradation of films held in 88% RH. Samples were quenched to maintain amorphous PLLA content or isothermally crystallized at 90°C or 120°C. Because the PFMA content was small, the crystallinity of the films was similar between samples with higher crystallinity when held at 120°C compared to 90°C. The film surface was characterized by water contact angle to identify the presence of PFMA at the surface. The contact angle increased by 20° for PFMA containing films, indicating increased hydrophobicity. Even with increased crystallinity and surface hydrophobicity, the water absorption, as measured by FTIR, was comparable for all films. Degradation was monitored by molecular weight decrease in homopolymer PLLA and the blend samples. Degradation was fastest for films with longer chain PFMA components or higher crystallinity. These results are contrary to the expected behavior. The authors state that this increase in degradation was due to the higher water content in amorphous PLLA regions and a small amount of immiscibility between the PLLA homopolymer and the PFMA-*b*-PLLA block copolymer. The trend in relation to both PFMA content and crystallinity was less definitive. In 6-arm *a*P3HB-b-PLLA, the degradation rate of PLLA was tunable based on the length

of the *a*P3HB block due to competing influence of PLLA chain mobility and *a*P3HB water transport restrictions.[42]

Another area of environmental concern is alternative energy. BCPs have promise in the area of solid electrolyte membranes for ion transport, in particular lithium ion batteries.[259-260] PEO-containing BCPs are the prototypical choice as its low T_g allows for higher ionic mobility. Unfortunately, PEO is highly crystalline, and research shows that crystallinity inhibits the flow of Li^+ ions.[261] BCPs are advantageous because the second block adds strength to the membrane, the BCP morphology can help direct ion flow and the second block can inhibit PEO crystallization.[262-264] In BCPs, the salt concentration influences the morphology by changing the apparent volume fraction for the conductive block. Specifically, in PS-*b*-PEO systems, Chintapalli *et al*.[262] determined that small molecular weight systems showed a microphase-separated morphology transition to cylindrical from the lamellar with increased salt content. However, PEO crystallinity remained the same. In another study, the PEO end-group chemistry in PS-*b*-PEO copolymer was altered between single or double carboxylic acid or hydroxyl groups.[263] It was shown that the weaker primary alcohol association with Li^+ and a designed diol end-group were both more favorable to improve conductivity in the PEO phase. In addition, the inclusion of multiple end-groups for the PEO chain resulted in a decrease in crystallinity, which also favored higher conductivity compared to single end-group BCPs. Recent advances show that including a styrenic ionic second block with PEO results in improved conductivity with careful control of the block copolymer morphology.[265-268] In these systems, miscibility is important because conductivity occurs in both blocks. Phase separation was driven by crystallization of the PEO block; therefore, studies were done in the melt.

Hybrid systems are composed of functional organic and inorganic compounds that are useful in a variety of applications which include the following: coatings, energy harvesting and storage, sensing and catalysis, optoelectronic devices, and many others. In this case, Moshonov and Frey[269] were interested in hybrid photovoltaics. As described earlier, BCP self-assembly as templates for nanostructured and mesostructured materials, where the polymer itself should be templated, for instance, a conductive polymer domain, are technologically relevant. A rod−coil BCP, PEO-*b*-P3HT, was assembled using CDSA. Then, ZnO was added to the PEO domain using atomic layer deposition (ALD) to generate functional hybrid films. This procedure simplifies the process with no etching or burning steps. Self-assembly of PEO-*b*-P3HT and phase separation leads to the formation of fibrils ∼20 nm in diameter and microns long with crystalline P3HT cores and PEO amorphous corona. The affinity of PEO toward the ALD precursor directed the growth of ZnO selectively within the amorphous PEO domains confirmed by UV-Vis spectroscopy. Most importantly, size, distribution and orientation of the inorganic phase were directed by the BCP through its chemical structure and self-assembly. The combination of BCP and ALD offers a new approach to direct functional hybrid material due to the diversity of BCP synthesis and self-assembly. The obtained hybrid structure possesses the properties desired for bulk heterojunction materials in photovoltaic films because of their donor−acceptor continuous nanoscale interpenetrated networks as shown in Figure 43. Additionally, the P3HT phase remained crystalline, as determined by GIXRD, to promote electron transfer and light harvesting within these domains. Overall, the authors were able to turn the films into hybrid photovoltaics devices (glass / ITO / PEDOT:PSS / BCP:ZnO / Al) with some photovoltaic activity. This proved that combining self-assembly of functional BCPs and ALD was a simple, viable method to direct highly favored and complex hybrid morphologies. The performance of these devices was poor likely due to the incomplete network of ZnO, according to the authors.

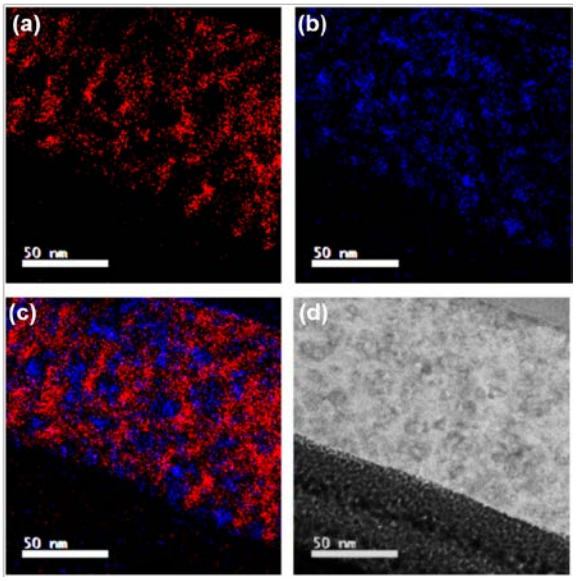

FIGURE 43 High-resolution TEM images of PEO-*b*-P3HT BCP film after 80 ALD cycles: (a) using the S $L_{2,3}$ edge transition (165 eV) and marking the sulfur rich areas in red; (b) using the Zn $L_{2,3}$ edge transition (87 eV) and marking the zinc rich areas in blue; (c) an overlay of images (a) and (b), and (d) a bright-field TEM micrograph of the same region. (Reproduced from [269] with permission from the American Chemical Society.)

Another hybrid material was made using a P3HT-based block copolymer with a second block of poly{3-[10-(4'-cyanobiphenyloxy)decyl]thiophene} (P3HT-*b*-PTcbp), where cbp is a mesogenic side group, and ZnO and CdS quantum dots with a 4'-hydroxy-[1,1'-biphenyl]-4-carbonitrile (cbp) ligand.[270] The PTcbp block was made with 5 or 7 repeating units, and the P3HT had 44 repeating units (M_n^{P3HT} = 7.4k). The matching of liquid crystalline-forming mesogens promoted the association of the quantum dots with the PTcbp domains. The crystallization of P3HT also promoted ordering of the BCP phases. The hybrid films were characterized using microscopy, thermal analysis, UV-Vis, and SAXS. Device performance was evaluated using CV and PL of the hybrid and J-V analysis on glass / ITO / PEDOT:PSS / P3HT-*b*-PTcbp hybrid / LiF / Al. The crystallization-driven assembly of P3HT as well as association of cbp moieties in the copolymer and ZnO or CdS ligands improved all J-V characteristics including V_{OC}, J_{SC}, FF, and PCE when compared to non-assembly-driven mixtures of similar components as shown in Table 4. Using CDSA of regiosymmetric P3HT-*b*-regioregular P3HT, Li and coworkers[271] demonstrated good conductivity in the fibers and analyzed them as active layers in field-effect transistor applications.

Understanding the crystallization behavior in BCPs is critical to designing new functional materials. While many studies focus on the fundamental crystallization behavior, it is important to recognize the applicability of these materials and how crystallization improves or hinders their development into new technologies. The marriage of fundamental physics and materials engineering is critical to the design of tailored nanomaterials. This section highlighted only a few of the recent studies in this area. Continued development in both areas is necessary to advance the field of BCP material applications.

TABLE 4 Characteristic J-V Parameters of Solar Cells[270]

Device Composition	V_{OC} (V)	J_{SC} (mA/cm^2)	FF	PCE
P3HT / ZnO	0.49	1.9	0.40	0.31 ± 0.1
P3HT / cbp@ZnO	0.53	2.51	0.35	0.46 ± 0.1
P3HT-*b*-PTcbp$_5$ / ZnO	0.48	2.4	0.50	0.58 ± 0.1
P3HT-*b*-PTcbp$_5$ / cbp@ZnO	0.51	3.8	0.50	0.97 ± 0.2
P3HT-*b*-PTcbp$_7$ / ZnO	0.46	2.0	0.40	0.37 ± 0.1
P3HT-*b*-PTcbp$_7$ / cbp@ZnO	0.50	2.9	0.49	0.71 ± 0.2
P3HT / CdS	0.71	2.9	0.39	0.80 ± 0.1
P3HT / cbp@CdS	0.70	4.5	0.44	1.40 ± 0.1
P3HT-*b*-PTcbp$_5$ / CdS	0.73	4.32	0.43	1.36 ± 0.1
P3HT-*b*-PTcbp$_5$ / cbp@CdS	0.77	5.5	0.55	2.33 ± 0.2
P3HT-*b*-PTcbp$_7$ / CdS	0.72	3.8	0.46	1.26 ± 0.1
P3HT-*b*-PTcbp$_7$ / cbp@CdS	0.75	5.1	0.53	2.03 ± 0.1

CONCLUSIONS

Crystallization in block copolymers is a rich field of study that has generated thousands of publications over the last few decades. It is clear that there are many unanswered questions in regards to fundamental understanding of the phase behavior and the tuning of macroscopic properties for engineered applications. As has been demonstrated in this review, BCP assembly, whether pre-crystallization or crystallization-driven, alters the crystallization behavior of semi-crystalline polymers. The inclusion of additional components influences many aspects of crystallization, including T_m or T_c, crystallinity, chain mobility, nucleation, and growth. Chain architecture also has been shown to manipulate crystallization in a similar way. In most instances, diluent, confinement, and chain tethering (immobility) result in inhibited BCP crystallization behavior; however, there are a few systems where the BCP secondary chains improve mobility for nucleation, in PLLA or PDLA, for example, or tethering induces chain stretching for well-segregated systems, where the stretching also facilitates nucleation. Highly-branched architectures have been shown to both improve and inhibit nucleation. The semi-crystalline chain's structure, flexible or rigid, leads to different self-assembly behavior, both in the crystals and the microphase separation. Crystallization-driven assembly has led to unique morphological observations and allows better control over the assembly process. In all, crystallizable BCPs present a wide range of possibilities for future work in engineering functional materials and for developing universal understanding of crystallization and assembly behavior.

As synthetic techniques for designing new architectures and better polymerization control continue to help innovate new materials, there will be new crystallization properties to study. One can imagine systems similar to biomacromolecules or biological systems with precise monomer control and chain structure with a variety of secondary and tertiary phase behavior. This could allow for predictive systematic studies of polymers that mimic biological materials. Additional assembly structures, such as liquid crystalline polymers and polypeptides, combined with crystallization in block copolymer systems

will diversify the range of applications. Whether in the bulk or in solution, our ability to control the assembly behavior to formulate structured materials continues to improve. Because the properties of these materials are intimately connected to the phase behavior and transition temperatures, it is critical that the mechanisms for phase development are well-understood. Although this review is not comprehensive regarding crystallization in BCPs, it highlights many of the important works and research areas that will help move forward the science and engineering of these materials.

ACKNOWLEDGEMENTS

The authors would like to thank the guest editors, M.L. Di Lorenzo, R. Androsch, and C. Schick, for the invitation to contribute this review to the *Advances in Polymer Crystallization* special issue. The authors would like to thank Alexandra Metzger for her help in gathering literature for the writing of this review. Financial support during the preparation of this manuscript was provided by NSF DMR-1606532.

REFERENCES AND NOTES

1. A. S. Dunn and H. W. Melville, *Nature* **1952**, *169*, 699
2. H. Mark, *Textile Res. J.* **1953**, *23*, 294.
3. M. Szwarc, M. Levy, and R. Milkovich, *J. Am. Chem. Soc.* **1956**, *78*, 2656.
4. A.-V. Ruzette and L. Leibler, *Nat. Mater*. **2005**, *4*, 19
5. L. Leibler *Macromolecules* **1980**, *13*, 1602.
6. F. S. Bates, H. E. Bair, and M. A. Hartney, *Macromolecules* **1984**, *17*, 1987.
7. F. S. Bates, *Macromolecules* **1984**, *17*, 2607.
8. F. S. Bates and M. A. Hartney, *Macromolecules* **1985**, *18*, 2478.
9. X. Quan, G. E. Johnson, E. W. Anderson, and F. S. Bates, *Macromolecules* **1989**, *22*, 2451.
10. I. W. Hamley, *Adv. Polym. Sci.* **1999**, *148*, 113.
11. Y. L. Loo and R. A. Register, In Developments in Block Copolymer Science and Technology; I. W. Hamley, Ed.; Wiley & Sons, Inc.: New York, **2004**; Chapter 6, pp 213-243.
12. A. J. Müller, V. Balsamo, and M. L. Arnal, *Adv. Polym. Sci.* **2005**, *190*, 1.
13. B. Nadan, J. Y. Hsy, and H. L. Chen, *Polym. Rev.* **2006**, *46*, 143.
14. A. J. Müller, V. Balsamo, and M. L. Arnal, In Lecture Notes in Physics: Progress in Understanding of Polymer Crystallization; G. Reiter; G. Strobl, Eds.; Springer: Berlin, **2007**; Vol. 714, Chapter 3, pp 229-259.
15. R. V. Castillo and A. J. Müller, *Prog. Polym. Sci.* **2009**, *34*, 519.
16. W.-N. He and J.-T. Xu, *Prog. Polym. Sci.* **2012**, *37*, 1350.
17. J. J. Crassous, P. Schurtenberger, M. Ballauff, and A. M. Mihut, *Polymer* **2015**, *62*, A-1.
18. S. Agbolaghi, S. Abbaspoor, and F. Abbasi, *Prog. Polym. Sci.* **2018**, *81*, 22.
19. H. Takeshita, T. Shiomi, K. Takenaka, and F. Arai, *Polymer*, **2013**, *54*, 4776.
20. S. Nakagawa, H. Marubayashi, and S. Nojima, *Eur. Polym. J.* **2015**, *70*, 262.
21. R. M. Michell and A. J. Müller, *Prog. Polym. Sci.* **2016**, *54-55*, 183.
22. L. Zha and W. Hu, *Prog. Polym. Sci.* **2016**, *54-55*, 232.
23. B. Lotz, T. Miyoshi, and S. Z. D. Cheng, *Macromolecules* **2017**, *50*, 5995.
24. M. A. Kryuchkov, C. Detrembleur, R. Jérôme, R. E. Prud'homme, and C. G. Bazuin, *Macromolecules* **2011**, *44*, 5209
25. S. Boissé, M. A. Kryuchkov, N.-D. Tien, C. G. Bazuin, and R. E. Prud'homme, *Macromolecules* **2016**, *49*, 6973.
26. S. Hölzer, T. N. Büttner, R. Shulze, M. M. L. Arras, F. H. Schacher, K. D. Jandt, and U. S. Schubert, *Eur. Polym. J.* **2015**, *68*, 10.
27. M. Kalloudis, E. Glynos, S. Pispas, J. Walker, and V. Koutsos, *Langmuir* **2013**, *29*, 2339.

28. W.-W. Wang, L. Jiang, W.-Y. Ren, C.-M. Zhang, C.-Z. Man, T.-P. Nguyen, and Y. Dan, *RSC Adv.* **2016**, *6*, 31934.
29. R. V. Castillo, G. Fleury, C. Navarro, A. Couffin, D. Bourissou, and B. Martin-Vaca, *Eur. Polym. J.* **2017**, *95*, 711.
30. L. Chen, J. Jiang, L. Wei, X. Wang, G. Xue, and D. Zhou, *Macromolecules* **2015**, *48*, 1804.
31. S. Nakagawa, K. Kadena, T. Ishizone, S. Mojima, T. Shimizu, K. Yamaguchi, and S. Nakahama, *Macromolecules* **2012**, *45*, 1892.
32. S. Nakagawa, T. Tanaka, T. Ishizone, S. Nojima, Y. Kakiuchi, K. Yamaguchi, and S. Nakahama, *Macromolecules* **2013**, *46*, 2199.
33. S. Nakagawa, T. Tanaka, T. Ishizone, S. Nojima, K. Kamimura, K. Yamaguchi, and S. Nakahama, *Polymer* **2014**, *55*, 4349.
34. S. Nakagawa, T. Ishizone, S. Nojima, K. Kamimura, K. Yamaguchi, and S. Nakahama, *Macromolecules* **2015**, *48*, 7138.
35. R. Kato, S. Nakagawa, H. Marubayashi, and S. Nojima, *Macromolecules* **2016**, *49*, 5955.
36. S. Nakagawa, Y. Yoneguchi, T. Ishizone, S. Nojima, K. Yamaguchi, and S. Nakahama, *Polymer* **2017**, *112*, 116.
37. K. Kawazu, S. Nakagawa, T. Ishizone, and S. Nojima, *Macromolecules* **2017**, *50*, 7202.
38. L. G. Alharbe, R. A. Register, and J. K. Hobbs, *Macromolecules* **2017**, *50*, 987.
39. A. B. Burns and R. A. Register, *Macromolecules* **2017**, *50*, 8106.
40. C.-L. Liu, M.-C. Lin, H.-L. Chen, and A. J. Müller, *Macromolecules* **2015**, *48*, 4451.
41. M. T. Casas, R. M. Michell, I. Blaszczyk-Lezak, J. Puiggali, C. Mijangos, A. T. Lorenzo, and A. J. Müller, *Polymer* **2015**, *70*, 282.
42. N. Jiang and H. Abe, *Polym. Degrad. Stab.* **2015**, *114*, 8.
43. C. Kundu and A. K. Dasmahapatra, *Polymer* **2014**, *55*, 958.
44. C. Kundu and A. K. Dasmahapatra, *Macromol. Symp.* **2015**, *354*, 314.
45. J. Yang, Y. Liang, and C. C. Han, *Polymer* **2015**, *79*, 56.
46. J. Yang, Y. Liang, W. Shi, H. S. Lee, and C. C. Han, *Polymer* **2013**, *54*, 3974.
47. D. Zhou, J. Sun, J. Shao, X. Bian, S. Huang, G. Li, and X. Chen, *Polymer* **2015**, *80*, 123.
48. M. L. Arnal, S. Boissé, A. J. Müller, F. Meyer, J.-M. Raquez, P. Dubois, R. E. Prud'homme, *CrystEngComm* **2016**, *18*, 3635.
49. L. Gardella, D. Cavallo, S. Colonna, A. Fina, and O. Monticelli, *J. Polym. Sci. Part A: Polym. Chem.* **2014**, *52*, 3269.
50. I. Navarro-Baena, A. Marcos-Fernández, J. M. Kenny, and L. Peponi, *J. Appl. Cryst.* **2014**, *47*, 1948.
51. W. Han, X. Liao, Q. Yang, G. Li, B. He, W. Zhu, and Z. Hao, *RSC Adv.* **2017**, *7*, 22515.
52. N. Brigham, C. Nardi, A. Carandang, K. Allen, and R. M. Van Horn, *Macromolecules* **2017**, *50*, 8996.
53. J. Huang, R.-Y. Wang, Z.-Z. Tong, J.-T. Xu, and Z.-Q. Fan, *Macromolecules* **2014**, *47*, 8359.
54. S. Osawa, R. Hijikawa, H. Marubayashi, and S. Nojima, *Polymer* **2017**, *122*, 249.
55. R. Hijikawa, L. Huang, G. Kiyofuji, H. Marubayashi, and S. Nojima, *Polymer* **2014**, *55*, 6960.
56. C. De Rosa, R. D. Girolamo, F. Auriemma, M. D'Avino, G. Talarico, C. Cioce, M. Scoti, G. W. Coates, and B. Lotz, *Macromolecules* **2016**, *49*, 5576.
57. S.-H. Huang, Y.-W. Huang, Y.-W. Chiang, T.-J. Hsiao, Y.-C. Mao, C.-H. Chiang, and J.-C. Tsai, *Macromolecules* **2016**, *49*, 9048.
58. Y. Suzuki, H. Duran, M. Steinhart, H.-J. Butt, and G. Houdas, *Macromolecules* **2014**, *47*, 1793.
59. D. Zhou, J. Shao, G. Li, J. Sun, X. Bian, and X. Chen, *Polymer* **2015**, *62*, 70.
60. R. Liénard, N. Zaldua, T. Josse, J. De Winter, M. Zubitur, A. Mugica, A. Iturrospe, A. Arbe, O. Coulembier, A. J. Müller, *Macromol. Rapid Commun.* **2016**, *37*, 1676.
61. B. Fillon, B. Lotz, A. Thierry, and J. C. Wittmann, *J. Polym. Sci. Part B: Polym. Phys.* **1993**, *31*, 1395.

62. B. Fillon, J. C. Wittmann, B. Lotz, and A. Thierry, *J. Polym. Sci. Part B: Polym. Phys.* **1993**, *31*, 1383.
63. R. M. Van Horn and S. Z. D Cheng, In Polymer Thin Films; O.K. C. Tsui and T. P. Russel, Eds.; World Scientific: Rivers Edge, New Jersey, **2008**; Chapter 7, pp 163-191.
64. R. L. N. Hailes, A. M. Oliver, J. Gwyther, G. R. Whittell, and I. Manners, *Chem. Soc. Rev.* **2016**, *45*, 5358.
65. B. Lotz and A. J. Kovacs, *Colloid Polym. Sci.* **1966**, *209*, 97
66. P. H. Geil, Polymer Single Crystals. Krieger Publishing Co.: Huntington, NY, **1963**
67. J. Wang, W. Zhu, B. Peng, and Y. Chen, *Polymer* **2013**, *54*, 6760.
68. W. Zhuo, Y. Li, R. Zhang, R. Huang, J. Zhou, Z. Tong, and G. Jiang, *J. Appl. Polym. Sci.* **2017**, *134*, 45089.
69. S. Agbolaghi, F. Abbasi, S. Abbaspoor, and M. Alizadeh-Osgouei, *Eur. Polym. J.* **2015**, *66*, 108.
70. S. Agbolaghi, M. Nazari, S. Abbaspoor, H. Gheybi, and F. Abbasi, *Eur. Polym. J.* **2016**, *82*, 196.
71. J. X. Zheng, R. M. Van Horn, and S. Z. D. Cheng, *Polymer* **2017**, *116*, 334.
72. S. Ganda, M. Dulle, M. Drechsler, B. Förster, S. Förster, and M. H. Stenzel, *Macromolecules* **2017**, *50*, 8544.
73. M. Inam, J. R. Jones, M. M Pérez-Madrigal, M. C. Arno, A. P. Dove, and R. K. O'Reilly, *ACS Cent. Sci.* **2018**, *4*, 63.
74. S. Mei, H. Qi, T. Zhou, and C. Y. Li, *Angew. Chem. Int. Ed.* **2017**, *56*, 13645.
75. Z. Wang, Y. Cao, J. Song, Z. Xie, and Y. Wang, *Langmuir* **2016**, *32*, 9633.
76. Z.-Y. Li, R. Liu, B.-Y. Mai, W.-J. Wang, Q. Wu, G.-D. Liang, H.-Y. Gao, and F.-M. Zhu, *Polymer* **2013**, *54*, 1663.
77. G. Rizis, T. G. M. van de Ven, and A. Eisenberg, *Soft Matter* **2014**, *10*, 2825.
78. J. Puig, I. A. Zucchi, M. Ceolin, W. F. Schroeder, and R. J. J. Williams, *RSC Adv.* **2016**, *6*, 34903.
79. Q. He, Y. Yuan, F. Chen, Z. Ma, X. Zhu, and R. Song, *Polymer* **2017**, *108*, 322.
80. Q. He, J. Ren, J. Ren, K. Pang, Z. Ma, X. Zhu, and R. Song, *Eur. Polym. J.* **2017**, *95*, 174.
81. J.-X. Yang, B. Fan, J.-H. Li, J.-T. Xu, B.-Y. Du, and Z.-Q. Fan, *Macromolecules* **2016**, *49*, 367.
82. G. Rizis, T. G. M. van de Ven, and A. Eisenberg, *Angew. Chem. Int. Ed.* **2014**, *53*, 9000.
83. G. Rizis, T. G. M. van de Ven, and A. Eisenberg, *ACS Nano* **2015**, *9*, 3627.
84. A. Nazemi, X. He, L. R. MacFarlane, R. L. Harniman, M.-S. Hsiao, M. A. Winnik, C. F. J. Faul, and I. Manners, *J. Am. Chem. Soc.* **2017**, *139*, 4409.
85. X. Wang, G. Guerin, H. Wang, Y. Wang, I. Manners, and M. A. Winnik, *Science*, **2007**, *317*, 644.
86. H. Zhou, Y. Lu, M. Zhang, G. Guerin, I. Manners, and M. A. Winnik, *Macromolecules* **2016**, *49*, 4265.
87. G. Guerin, P. Rupar, G. Molev, I. Manners, H. Jinnai, and M. A. Winnik, *Macromolecules* **2016**, *49*, 7004.
88. A. Pitto-Barry, N. Kirby, A. P. Dove, and R. K. O'Reilly, *Polym. Chem.* **2014**, *5*, 1427.
89. M. J. Gonzalez-Alvarez, L. Jia, G. Guerin, K. S. Kim, V. An Du, G. Walker, I. Manners, and M. A. Winnik, *Macromolecules* **2016**, *49*, 7975.
90. J. Xu, H. Zhou, Q. Yu, I. Manners, and M. A. Winnik, *J. Am. Chem. Soc.* **2018**, *140*, 2619.
91. J. R. Finnegan, D. J. Lunn, O. E. C. Gould, Z. M. Hudson, G. R. Whittell, M. A. Winnik, and I. Manners, *J. Am. Chem. Soc.* **2014**, *136*, 13835.
92. B. Fan, R.-Y. Wang, X.-Y. Wang, J.-T. Xu, B.-Y. Du, Z.-Q. Fan, *Macromolecules* **2017**, *50*, 2006.
93. X. Li, Y. Gao, R. Harniman, M. A. Winnik, and I. Manners, *J. Am. Chem. Soc.* **2016**, *138*, 12902.
94. H. Qiu, V. An Du, M. A. Winnik, and I. Manners, *J. Am. Chem. Soc.* **2013**, *135*, 17739.
95. L. Jia, L. Tong, Y. Liang, A. Petretic, G. Guerin, I. Manners, and M. A. Winnik, *J. Am. Chem. Soc.* **2014**, *136*, 16676.
96. D. J. Lunn, O. E. C. Gould, G. R. Whittell, D. P. Armstrong, K. P. Mineart, M. A. Winnik, R. J. Spontak, P. G. Pringle, and I. Manners, *Nat. Commun.* **2016**, *7*, 12371.
97. C. Boott, R. Laine, P. Mahou, J. Finnegan, E. Leitao, S. Webb, C. Kaminski, and I. Manners, *Chem. Eur. J.* **2015**, *21*, 18539.

98. R. J. Gaymans, *Prog. Polym. Sci.* **2011**, *36*, 713.
99. U. Nagpal, F. A. Detcheverry, and J. J. de Pablo, *Macromolecules* **2011**, *44*, 5490.
100. J. Qin, F. S. Bates, and D. C. Morse, *Macromolecueles* **2010**, *43*, 5128.
101. M. Liu, W. Li, F. Qiu, and A.-C. Shi *Macromolecules* **2012**, *45*, 9522.
102. M. J. Barthel, F. H. Schacher, and U. S. Schubert, *Polym. Chem.* **2014**, *5*, 2647.
103. N. Hadjichristidis, H. Iatrou, M. Pitsikalis, S. Pispas, and A. Avgeropoulos, *Prog. Polym. Sci.* **2005**, *30*, 725.
104. I. W. Wyman and G. Liu, *Polymer* **2013**, *54*, 1950.
105. C. M. Koo, M. A. Hillmyer, and F. S. Bates, *Macromolecules* **2006**, *39*, 667.
106. H.-H. Liu, C.-I. Huang, and A.-C. Shi, *Macromolecules* **2015**, *48*, 6214.
107. S. Xu, C. Zhang, L. Li, and S. Zheng, *Polymer* **2017**, *128*, 1.
108. J. Schöbel, M. Karg, D. Rosenbach, G. Krauss, A. Greiner, and H. Schmalz, *Macromolecules* **2016**, *49*, 2761.
109. J. Schmelz, A. E. Schedl, C. Steinlein, I. Manners, and H. Schmalz, *J. Am. Chem. Soc.* **2012**, *134*, 14217.
110. S. Chen and L. Wang, *J. Therm. Anal. Calorim.* **2017**, *127*, 2341.
111. J. Chen, W. Huang, Q. Xu, Y. Tu, X. Zhu, and E.-Q. Chen, *Polymer* **2013**, *54*, 6725.
112. A. J. McGrath, W. Shi, C. G. Rodriquez, E. J. Kramer, C. J. Hawker, and A. N. Lynd, *Polym. Chem.* **2015**, *6*, 1465.
113. W. Shi, A. J. McGrath, Y. Li, N. A. Lynd, C. J. Hawker, G. H. Fredrickson, and E. J. Kramer, *Macromolecules* **2015**, *48*, 3069.
114. R. Dehmel, J. A. Dolan, Y. Gu, U. Wiesner, T. D. Wilkinson, J. J. Baumberg, U. Steiner, B. D. Wilts, and I. Gunkel, *Macromolecules* **2017**, *50*, 6255.
115. Y.-W. Chiang, Y.-Y. Hu, J.-N. Li, S.-H. Huang, and S.-W. Kuo, *Macromolecules* **2015**, *48*, 8526.
116. J. K. Palacios, A. Mugica, M. Zubitur, A. Iturrospe, A. Arbe, G. Liu, D. Wang, J. Zhao, N. Hadjichristidis, and A. J. Müller, *RSC Adv.* **2016**, *6*, 4739.
117. J. K. Palacios, A. Tercjak, G. Liu, D. Wang, J. Zhao, N. Hadjichristidis, A. J. Müller, *Macromolecules* **2017**, *50*, 7268.
118. J. K. Palacios, J. Zhao, N. Hadjichristidis, A. J. Müller, *Macromolecules* **2017**, *50*, 9683.
119. E. Yilgör, M. Isik, C. Kosak Söz, and I. Yilgör, *Polymer* **2016**, *83*, 138.
120. I. Navarro-Baena, A. Marcos-Fernández, A. Fernández-Torres, J. M. Kenny, and L. Peponi, *RSC Adv.* **2014**, *4*, 8510.
121. R.-Y. Wang, X.-Y. Wang, B. Fan, J.-T. Xu, and Z.-Q. Fan, *Polymer* **2017**, *117*, 140.
122. D. B. Konwar, S. Sethy, B. K. Satapathy, and J. Jacob, *Polymer* **2017**, *123*, 87.
123. S. Nagarajan and E. B. Gowd, *Macromolecules* **2015**, *48*, 5367.
124. V. S. D. Voet, G. O. R. Alberda van Ekenstein, N. L. Meereboer, A. H. Hofman, G. ten Brinke, and K. Loos, *Polym. Chem.* **2014**, *5*, 2219.
125. V. S. D. Voet, M. Tichelaar, S. Tanase, M. C. Mittelmeijer-Hazeleger, G. ten Brinke, and K. Loos, *Nanoscale* **2013**, *5*, 184.
126. V. S. D. Voet, D. Hermida-Merino, G. ten Brinke, and K. Loos, *RSC Adv.* **2013**, *3*, 7938.
127. W. Yu, M. Inam, J. R. Jones, A. P. Dove, and R. K. O'Reilly, *Polym. Chem.* **2017**, *8*, 5504.
128. H. Schmalz, J. Schmelz, M. Drechsler, J. Yuan, A Walther, K. Schweimer, and A. M. Mihut, *Macromolecules* **2008**, *41*, 3235.
129. J. Schmelz, M. Karg, T. Hellweg, and H. Schmalz, *ACS Nano* **2011**, *5*, 9523.
130. J. Schöbel, M. Burgard, C. Hils, R. Dersch, M. Dulle, K. Volk, M. Karg, A. Greiner, and H. Schmalz, *Ang. Chem., Int. Ed.* **2017**, *56*, 405.
131. A. M. Oliver, J. Gwyther, M. A. Winnik, and I. Manners, *Macromolecules* **2018**, *51*, 222.
132. H. Tsuji, *Adv. Drug Deliv. Rev.* **2016**, *107*, 97.
133. K. Wasanasuk, K. Tashiro, M. Hanesaka, T. Ohhara, K. Kurihara, R. Kuroki, T. Tamada, T. Ozeki, T. Kanamoto, *Macromolecules* **2011**, *44*, 6441.

134. C. Aleman, B. Lotz, J. Puiggali, *Macromolecules* **2001**, *34*, 4795.
135. K. Tashiro, N. Kouno, H. Wang, H. Tsuji, *Macromolecules* **2017**, *50*, 8048.
136. L. Cartier, T. Okihara, B. Lotz, *Macromolecules* **1997**, *30*, 6313.
137. D. Brizzolara, H. J. Cantow, K. Diederichs, E. Keller, A. J. Domb, *Macromolecules* **1996**, *29*, 191.
138. T. Okihara, M. Tsuji, A. Kawaguchi, K. Katayama, H. Tsuji, S. H. Hyon, Y. Ikada, *J. Macromol. Sci., Part B: Phys.* **1991**, *30*, 119.
139. Y. Ikada, K. Jamshidi, H. Tsuji, S. H. Hyon, *Macromolecules* **1987**, *20*, 904.
140. Y. Liu, J. Shao, J. Sun, X. Bian, L. Feng, S. Xiang, B. Sun, Z. Chen, G. Li, and X. Chen, *Polym. Degrad. Stab.* **2014**, *101*, 10.
141. Z. Jing, X. Shi, G. Zhang, and R. Lei, *Polym. Int.* **2015**, *64*, 1399.
142. Y. Song, D. Wang, N. Jiang, and Z. Gan, *ACS Sustainable Chem. Eng.* **2015**, *3*, 1492.
143. M. Nakajima, H. Nakajima, T. Fujiwara, Y. Kimura, and S. Sasaki, *Langmuir* **2014,** *30*, 14030.
144. M. Jikei, Y. Yamadoi, T. Suga, and K. Matsumoto *Polymer*, **2017**, *123*, 73.
145. D. Maillard and R. E. Prud'homme, *Macromolecules* **2010**, *43*, 4006.
146. X. Wang and R. E. Prud'homme, *Macromolecules* **2014**, *47*, 668.
147. D. Zhou, J. Shao, J. Sun, X. Bian, S. Xiang, G. Li, and X. Chen, *Polymer* **2017**, *123*, 49.
148. L. Han, C. Yu, J. Zhou, G. Shan, Y. Bao, X. Yun, T. Dong, and P. Pan, *Polymer* **2016**, *103*, 376.
149. M. Kakuta, M. Hirata, and Y. Kimura, *Polym. Rev.* **2009**, *49*, 107.
150. L. Gardella, D. Cavallo, S. Colonna, A. Fina, and O. Monticelli, *J. Polym. Sci. Part A: Polym. Chem.* **2014**, *52*, 3269.
151. H. Tsuji and T. Tajima, *Polym. Int.* **2015**, *64*, 54.
152. L. Han, Q. Xie, J. Bao, G. Shan, Y. Bao, and P. Pan, *Polym. Chem.* **2017**, *8*, 1006.
153. Y. Windu Widhianto, M. Yamamoto, K. Masutani, Y. Kimura, and H. Yamane, *Polym. Degrad. Stab.* **2017**, *142*, 178.
154. Y. Windu Widhianto, M. Yamamoto, K. Masutani, Y. Kimura, and H. Yamane, *Polym. Degrad. Stab.* **2017**, *142*, 188.
155. L. Han, G. Shan, Y. Bao, and P. Pan, *J. Phys. Chem. B* **2015**, *119*, 14270.
156. J. Shao, Z. Tang, J. Sun, G. Li, and X. Chen, *J. Polym. Sci. Part B: Polym. Phys.* **2014**, *52*, 1560.
157. H. Tsuji and Y. Yamashita, *Polymer* **2014**, *55*, 6444.
158. H. Tsuji, M. Ogawa, and Y. Arakawa, *J. Phys. Chem. B* **2016**, *120*, 11052.
159. H. Tsuji, M. Ogawa, and Y. Arakawa, *J. Phys. Chem. B* **2017**, *121*, 2695.
160. W. Li, Y. Ma, and Z. Fan, *Polym. Eng. Sci.* **2015**, *55*, 2534.
161. M. Nakajima, H. Nakajima, T. Fujiwara, Y. Kimura, and S. Sasaki, *Polymer* **2015**, *66*, 160.
162. L. Sun, A. Pitto-Barry, N. Kirby, T. L. Schiller, A. M. Sanchez, M. A. Dyson, J. Sloan, N. R. Wilson, R. K. O'Reilly, and A. P. Dove, *Nature Commun.* **2014**, *5*, 5746.
163. S. Masubuchi and S. Kazama *Synth. Met.* **1995**, *74*, 151.
164. A. Hirao, K. Murano, T. Oie, M. Uematsu, R. Goseki, and Y. Matsuo, *Polym. Chem.* **2011**, *2*, 1219.
165. M. Jørgensen, K, Norrman, S. A. Gevorgyan, T. Tromholt, B. Andreasen, and F. C. Krebs, *Adv. Mater.* **2012**, *24*, 580.
166. A. Operamolla and G. M. Farinola, *Eur. J. Org. Chem.* **2011**, *3*, 423.
167. J. Li, X. Li, D. Ni, J. Wang, G. Tu, and J. Zhu, *J. Appl. Polym. Sci.* **2014**, *131*, 41186.
168. L. He, S. Pan, and J. Peng, *J. Polym. Sci., Part B: Polym. Phys.* **2016**, *54*, 544.
169. S. Agbolaghi, S. Zenoozi, Z. Hosseini, and F. Abbasi, *Macromolecules* **2016**, *49*, 9531.
170. P. M. Reichstein, S. Gödrich, G. Papastavrou, and M. Thelakkat, *Macromolecules* **2016**, *59*, 5484.
171. X. Yu, H. Yang, S. Wu, L. Wang, Y. Geng, and Y. Han, *J. Polym. Sci., Part B: Polym. Phys.* **2015**, *53*, 1718.
172. H. Yang, R. Zhang, L. Wang, J. Zhang, X. Yu, Y. Geng, and Y. Han, *Polymer* **2016**, *97*, 238.

173. H. Cui, X. Yang, J. Peng, and F. Qiu, *Soft Matter* **2017**, *13*, 5261.
174. I. Lee, P. Amaldass, K. Yoon, S. Shin, Y. Kim, I. Kim, E. Lee, and T. Choi, *J. Am. Chem. Soc.* **2013**, *135*, 17695.
175. X. Yang, J. Ge, M. He, Z. Ye, X. Liu, J. Peng, and F. Qiu, *Macromolecules* **2016**, *49*, 287.
176. H. Yang, R. Zhang, L. Wang, J. Zhang, X. Yu, J. Liu, R. Xing, Y. Geng, and Y. Han, *Macromolecules* **2015**, *48*, 7557.
177. J. Ge, M. He, N. Xie, X. Yang, Z. Ye, and F. Qiu, *Macromolecules* **2014**, *48*, 279.
178. E. C. Davidson and R. A. Segalman, *Macromolecules* **2017**, *50*, 8097.
179. E. C. Davidson and R. A. Segalman, *Macromolecules* **2017**, *50*, 6128.
180. E. C. Davidson, B. S. Beckingham, V. Ho, and R. A. Segalman, *J. Polym. Sci., Part B: Polym. Phys.* **2016**, *54*, 205.
181. J. Park, H. C. Moon, C. Choi, and J. K. Kim, *Macromolecules* **2015**, *48*, 3523.
182. H. C. Moon, D. Bae, and J. K. Kim, *Macromolecules*, **2012**, *45*, 5201.
183. Y.Y. Kim, S. Jung, C. Kim, B.J. Ree, D. Kawato, N. Nishikawa, D. Suemasa, T. Isono, T. Kakuchi, T. Satoh, and M. Ree, *Macromolecules* **2014**, *47*, 7510.
184. R. Phinjaroenphan, Y. Y. Kim, B. J. Ree, T. Isono, J. Lee, S. Rugmai, H. Kim, S. Maensiri, T. Kakuchi, T. Satoh, and M. Ree, *Macromolecules* **2015**, *48*, 5816.
185. X.-B. Liu, Y.-F. Zhao, X.-H. Fan, and E. Q. Chen, *Chin J. Polym. Sci.* **2013**, *31*, 946.
186. Z. Tong, R. Zhang, P. Ma, H. Xu, H. Chen, Y. Li, W. Yu, W. Zhou, and G. Jiang, *Langmuir* **2017**, *33*, 176.
187. S. Nojima, Y. Higaki, K. Kaetsu, R. Ishige, N. Ohta, H. Masunaga, T. Hirai, K. Kojio, and A. Takahara, *Polymer* **2017**, *116*, 403.
188. S. Nojima, Y. Higaki, R. Ishige, H. Kabayama, N. Ohta, H. Masunaga, T. Hirai, K. Kojio, and A. Takahara, *Polymer* **2016**, *102*, 256.
189. J. Wang, Y. I. Odarchenko, M. Defaux, J. Lejnieks, D. V. Ahokhin, H. Keul, D. A. Ivanov, M. Möller, and A. Mourran, *Macromolecules* **2013**, *46*, 6159.
190. Z. Tong, J. Zhou, R.-Y. Wang, and J.-T. Xu, *Polymer* **2017**, *130*, 1.
191. R. M. Van Horn, J. X. Zheng, H.-J. Sun, M.-S. Hsiao, W.-B. Zhang, X.-H. Dong, J.-T. Xu, E. L. Thomas, B. Lotz, and S. Z. D. Cheng, *Macromolecules* **2010**, *43*, 6113.
192. H. Yang, L. Wang, J. D. Zhang, X. H. Yu, Y. H. Geng, and Y. C. Han, *Macromol. Chem. Phys.* **2014**, *215*, 405.
193. H. Yang, S. W. LeFevre, C. Y. Ryu, and Z. Bao, *Appl. Phys. Lett.* **2007**, *90*, 172116.
194. K. Honda, H. Yakabe, T. Koga, S. Sasaki, O. Sakata, H. Otsuka, and A. Takahara, *Chem. Lett.* **2005**, *34*, 1024.
195. K. Honda, M. Morita, H. Otsuka, and A. Takahara, *Macromolecules* **2005**, *38*, 5699.
196. M. Córdova, A. T. Lorenzo, A. J. Müller, P. Fragouli, H. Iatrou, and N. Hadjichristidis, *Macromol. Symp.* **2010**, *287*, 101.
197. Y. Ma, J. Huang, K. Sui, and G. Wang, *J. Polym. Sci. Part A: Polym. Chem.*, **2014**, *52*, 2239.
198. C. Liu, K. Lv, B. Huang, C. Hou, and G. Wang, *RSC Adv.* **2013**, *3*, 17945.
199. M. D. Ninago, A. G. O. De Freitas, V. Hanazumi, P. I. R. Muraro, V. Schmidt, C. Giacomelli, A. E. Ciolino, and M. A. Villar, *Macromol. Chem. Phys.* **2015**, *216*, 2331.
200. D. Pfefferkorn, M. Pulst, T. Naolou, K. Busse, J. Balko, and J. Kressler, *J. Polym. Sci., Part B: Polym. Phys.* **2013**, *51*, 1581.
201. Q. Gao, Y. Wang, Y. Ren, and Y. Li, *Macromol. Chem. Phys.* **2013**, *214*, 1677.
202. D. Wu, F. Xu, Y. Huang, C. Chen, C. Yu, X. Feng, D. Yan, and Y. Mai, *Macromolecules* **2018**, *51*, 161.
203. X. Leng, Y. Ren, Z. Wei, Y. Bian, and Y. Li, *Macromol. Chem. Phys.* **2017**, *218*, 1700178.
204. Y. Gai, D. Song, B. M. Yavitt, and J. J. Watkins, *Macromolecules* **2017**, *50*, 1503.
205. S. Kripotou, C. Psylla, K. Kyriakos, K. N. Raftopoulos, J. Zhao, G. Zhang, S. Pispas, C. M. Papadakis, and A. Kyritsis, *Macromolecules* **2016**, *49*, 5963.
206. H. Cong, S. Xu, and S. Zheng, *Chin. J. Polym. Sci.* **2017**, *35*, 1572.

207. T. Isono, Y. Kondo, S. Ozawa, Y. Chen, R. Sakai, S.-I. Sato, K. Tajima, T. Kakuchi, and T. Satoh, *Macromolecules* **2014**, *47*, 7118.
208. R. Klein, C. Schüll, E. Berger-Nicoletti, M. Haubs, K. Kurz, and H. Frey, *Macromolecules* **2013**, *46*, 8845.
209. M. Ju, L. Shen, F. Gong, Y. Gao, and W. Zhang, *Polym. Int.* **2012**, *61*, 1447.
210. M. V. Massa, J. L. Carvalho, and K. Dalnoki-Veress, *Phys. Rev. Lett.* **2006**, *97*, 247802.
211. Y. Song, Y. Chen, L. Su, R. Li, R. A. Letteri, and K. L. Wooley, *Polymer* **2017**, *122*, 270.
212. R. A. Pérez-Camargo, G. Saenz, S. Laurichesse, M. T. Casas, J. Puiggalí, L. Avérous, and A. J. Müller, *J. Polym. Sci., Part B: Polym. Phys.* **2015**, *53*, 1736.
213. S. Laurichesse and L. Avérous, *Polymer* **2013**, *54*, 3882.
214. C.-U. Lee, L. Lu, J. Chen, J. Garno, and D. Zhang, *ACS Macro Lett.* **2013**, *2*, 436.
215. J. Sun, A. A. Teran, X. Liao, N. P. Balsara, and R. N. Zuckerman, *J. Am. Chem. Soc.* **2014**, *136*, 2070.
216. C. Secker, A. Völkel, B. Tiersch, J. Koetz, and H. Schlaad, *Macromolecules* **2016**, *49*, 979.
217. R. Chang, G. Shan, Y. Bao, and P. Pan, *Macromolecules* **2015**, *48*, 7872.
218. C. Appiah, J. Akbarzadeh, H. Peterlik, and W. Binder, *Eur. Polym. J.* **2015**, *64*, 138.
219. Z. Jing, X. Shi, and G. Zhang, *Polym Int.* **2017**, *66*, 1487.
220. E. Ostas, T. Yan, T. Thurn-Albrecht, W. Binder, *Macromolecules* **2013**, *46*, 4481.
221. S. B. Chen and W. H. Binder, *Acct. Chem. Res.* **2016**, *49*, 1409.
222. M. N. Higley, J. M. Pollino, E. Hollembeak, and M. Weck, *Chem – Eur. J.* **2005**, *11*, 2946.
223. R. Dobrawa, and F. Würthner, *J. Polym. Sci., Part A: Polym. Chem.* **2005**, *43*, 4981.
224. J. Ruokolainen, R. Mäkinen, M. Torkkeli, T. Mäkelä, R. Serimaa, G. t. Brinke, and O. Ikkala, *Science* **1998**, *280*, 557.
225. R. N. Zuckermann, J. M. Kerr, S. B. H. Kent, and W. H. Moos, *J. Am. Chem. Soc.* **1992**, *114*, 10646.
226. J.Sun, G. M. Stone, N. P. Balsara, and R. N. Zuckermann, *Macromolecules* **2012**, *45*, 5151.
227. C.-U. Lee, T. P. Smart, L. Guo, T. H. Epps III, and D. Zhang, *Macromolecules* **2011**, *44*, 9574.
228. T. Hashimoto, H. Tanaka, and H. Hasegawa, *Macromolecules* **1990**, *23*, 4378.
229. H. Tanaka, H. Hasegawa, and T. Hashimoto, *Macromolecules* **1991**, *24*, 240.
230. S. Gondo, S. Osawa, T. Sakurai, and S. Nojima, *Polymer* **2013**, *54*, 6768.
231. S. Gondo, S. Osawa, H. Marubayashi, and S. Nojima, *Polym. J.* **2015**, *47*, 556.
232. S. Nojima, M. Kuroda, and S. Sasaki, *Polym. J.* **1997**, *29*, 642.
233. M. P. F. Pepels, W. P. Hofman, R. Kleijnen, A. B. Spoelstra, C. E. Koning, H. Goossens, and R. Duchateau, *Macromolecules* **2015**, *48*, 6909.
234. L. Li, Z. Cao, R. Bao, B. Xie, M. Yang, and W. Yang, *Eur. Polym. J.* **2017**, *97*, 272.
235. W. Li, X. Chen, Y. Ma, and Z. Fan, *Cryst. Eng. Comm.* **2016**, *18*, 1242.
236. T. Panthani and F. Bates, *Macromolecules* **2015**, *48*, 4529.
237. C. Park, J. Yoon, and E.L. Thomas, *Polymer* **2003**, *44*, 6725.
238. M. Lazzari and C. De Rosa, In Block Copolymers in Nanoscience; M. Lazzari, G. J. Liu, S. Lecommandoux, Eds.; Wiley-VCH: Weinheim, Germany, **2006**
239. R. A. Segalman, *Mater. Sci. Eng. R* **2005**, *48*, 191.
240. M. P. Stoykovich, M. Müller, S. O. Kim, H. H. Solak, E. W. Edwards, J. J. de Pablo, and P. F. Nealey, *Science* **2005**, *308*, 1442.
241. A. C. Balazs, T. Emrick, and T. P. Russell, *Science* **2006**, *314*, 1107.
242. C. J. Hawker and T. P. Russell, *MRS Bull.* **2005**, *30*, 952.
243. C. De Rosa, C. Park, E. L. Thomas, and B. Lotz, *Nature* **2000**, *405*, 433
244. C. De Rosa, R. Di Girolamo, F. Auriemma, G. Talarico, A. Malafronte, C. Scarica, and M. Scoti, *ACS Appl. Mater. Interfaces* **2017**, *9*, 31252.
245. C. Ma, P. Pan, G. Shan, Y. Bao, M. Fujita, and M. Maeda, *Langmuir* **2015**, *31*, 1527.
246. Y. Liang, X. Deng, L. Zhang, X. Peng, W. Gao, J. Cao, Z. Gu, and B. He, *Biomaterials* **2015**, *71*, 1.

247. J. Gou, S. Feng, H. Xu, G. Fang, Y. Chao, Y. Zhang, H. Xu, and X. Tang, *Biomacromolecules* **2015**, *16*, 2920.
248. W. Zhu, B. Peng, J. Wang, K. Zhang, L. Liu, and Y. Chen, *Macromol. Biosci.* **2014**, *14*, 1764.
249. D. K. Schneiderman and M. A. Hillmyer, *Macromolecules* **2017**, *50*, 3733.
250. Polymers for Energy Storage and Conversion; V. Mittal, Ed.; Wiley-Scrivener: Salem, MA, USA **2013**
251. C. Zhou, Z. Wei, X. Lei, and Y. Li, *RSC Adv.* **2016**, *6*, 63508.
252. J. Zhang, T. Li, A. Mannion, D. Schneiderman, M. Hillmyer, and F. Bates, *ACS Macro. Lett.* **2016**, *5*, 407.
253. M. Ponjavic, M. Nikolic, S. Jevtic, J. Rogan, S. Stevanovic, and J. Djonlagic, *Macromol. Res.* **2016**, *24*, 323.
254. S. Cometa, I. Barolozzi, A. Corti, F. Chiellini, E. De Giglio, and E. Chiellini *Polym. Degrad. Stab.* **2010**, *95*, 2013.
255. O. Oparaji, M. Minelli, C. Zhu, E. Schaible, A. Hexemer, and D. T. Hallinan, *Polymer* **2017**, *120*, 209.
256. O. Oparaji, X. Zhuo, and D. T. Hallinan *Polymer* **2016**, *100*, 206.
257. K. M. Beers, D. T. Wong, A. J. Jackson, X. Wang, J. A. Pople, A. Hexemer, and N. P. Balsara, *Macromolecules* **2014**, *47*, 4330.
258. Y. Huang, F. Chen, Y. Pan, C. Chen, L. Jiang, and Y. Dan *Eur. Polym. J.* **2017**, *97*, 308.
259. W.-S. Young, W.-F. Kuan, and T. H. Epps, III, *J. Polym. Sci., Part B: Polym. Phys.* **2014**, *52*, 1.
260. S.-J. Tan, X.-X. Zeng, Q. Ma, X.-W. Wu, and Y.-G. Guo, *Electrochemical Energy Reviews* **2018**, *1*, 113.
261. Z. Stoeva, I. Martin-Litas, E. Staunton, Y. G. Andreev, and P. G. Bruce, *J. Am. Chem. Soc.* **2003**, *125*, 4619.
262. M. Chintapalli, T. N. P. Le, N. R. Venkatesan, N. G. Mackay, A. A. Rojas, J. L. Thelen, X. C. Chen, D. Devaux, and N. P. Balsara, *Macromolecules* **2016**, *49*, 1770.
263. H. Y. Jung, P. Mandal, G. Jo, O. Kim, M. Kim, K. Kwak, and M. J. Park, *Macromolecules* **2017**, *50*, 3224.
264. J. L. Thelen, A. A. Wang, X. C. Chen, X, Jiang, E. Schaible, and N. P. Balsara, *Macromolecules* **2018**, *5*1, 1733.
265. R. Bouchet, S. Maria, R. Meziane, A. Aboulaich, L. Lienafa, J. Bonnet, T. N. T. Phan, D. Bertin, D. Gigmes, D. Devaux, R. Denoyel, and M. Armand, *Nat. Mater.* **2013**, *12*, 452
266. S. Inceoglu, A. A. Rojas, D. Devaux, X. C. Chen, G. M. Stone, and N. P. Balsara, *ACS Macro Lett.* **2014**, *3*, 510.
267. J. L. Thelen, S. Inceoglu, N. R. Venkatesan, N. G. Mackay, and N. P. Balsara, *Macromolecules* **2016**, *49*, 9139
268. J. L. Thelen, X. C. Chen, S. Inceoglu, and N. P. Balsara, *Macromolecules* **2017**, *50*, 4827.
269. M. Moshonov and G. Frey, *Langmuir* **2015**, *31*, 12762.
270. Y. Shi, F. Li, L. Tan, and Y. Chen, *ACS Appl. Mater. Interfaces* **2013**, *5*, 11692.
271. X. Li, P. J. Wolanin, L. R. MacFarlane, R. L. Harniman, J. Qian, O. E. C. Gould, T. G. Dane, J. Rudin, M. J. Cryan, T. Schmaltz, H. Fauenrath, M. A. Winnik, C. F. J. Faul, and I. Manners, *Nat. Comm.* **2017**, *8*, 15909.

GRAPHICAL ABSTRACT

Ryan M. Van Horn, Maxwell R. Steffen, and Dana O'Connor

Recent Progress in Block Copolymer Crystallization

New technologies are being developed that require more precise and more diverse manufacturing. Block copolymers, or plastics, provide scientists and engineers with the ability to tailor structures on multiple length scales. Crystallization in these systems is important for the materials' properties, such as strength, degradation rate, and conductivity, just to name a few. This article summarizes recent work in the area of block copolymer crystallization.

GRAPHICAL ABSTRACT FIGURE ((50 mm wide by 50 mm high))

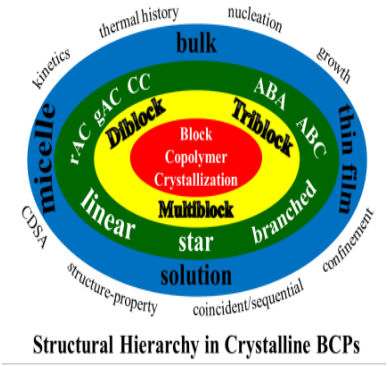

Structural Hierarchy in Crystalline BCPs